# Development of Entrained flow gasification technology for Victorian brown coals

## Final Report
## May 2016

Srikanth Chakravartula Srivatsa
Sankar Bhattacharya
**Department of Chemical Engineering**
**Monash University**

Hiromi Ishii
**Mitsubishi Heavy Industries**

BROWN COAL INNOVATION AUSTRALIA
*Positioning brown coal for a brighter future*

MONASH University

## Acknowledgement

This project is funded by the Brown Coal Innovation Australia. The project work was carried out by Monash University in collaboration with Mitsubishi Heavy Industries (MHI). Additional support was provided by Jülich Forschungszentrum in Germany. The authors acknowledge the contribution of several colleagues in MHI, Dr Michael Mueller of Jülich Forschungszentrum, and several students at Monash University – Sunaina Dayal, Humayun Khan, and Joanne Tanner.

## Disclaimer

The opinions expressed in this report do not represent the opinion of the organizations employing them.

# Contents

**Executive Summary**

This project represents a collaboration between Monash University and Mitsubishi Heavy Industries (MHI). It combines the complementary expertise in fundamental brown coal gasification research at Monash University and experience with commercial-scale coal gasifiers at MHI. Further collaboration took place with Jülich Forschungszentrum in Germany in equipment design and limited experimental work.

Gasification is a technology capable of being used as the basis for production of electricity or chemicals potentially at a lower cost and with reduced greenhouse gas emissions. Of three main technologies for gasification of coals, entrained flow gasification technology results in high carbon conversion and acceptable quality of fuel gas which is predominantly a mixture of carbon monoxide and hydrogen. However, information on gasification performance (carbon conversion and gas composition as a function of residence time) of the coal particles and the nature of slag formed (which affects gasifier operation) is largely unknown for Victorian brown coals, certainly not at the level required for the commercial development of the entrained flow gasification technology.

In order to ensure uninterrupted operation of an entrained flow gasifier, it is of utmost importance to sustain continuous slag flow out of the gasifier. Excessive build-up of slag melt on the gasifier wall reduces heat transfer in a gasifier, causing downtime or shutdown of the gasifier. It is important that the viscosity of the liquid slag is low enough so that slags flow down the gasifier walls and can be drained out from the gasifier as "molten slag". However, if the viscosity of slag is too low, an effective slag layer will not form, and therefore, will not protect the gasifier internal wall. An acceptable industry standard for the viscosity is between 100 Poise and 250 Poise that ensure the satisfactory protection of the gasifier wall and uninterrupted operation of the gasifier. Therefore, information on composition, viscosity and the change in viscosity with temperature for coal ash slags are essential for efficient operation of an entrained flow gasifier. Such information does not exist in the open literature. This project addressed this shortfall in knowledge through thermodynamic modelling and experimental and analytical work that included the following:

- Gasification experiments 1000 – 1400 °C to measure carbon conversion
- Viscosity measurements in triplicate to 1550 °C
- Differential thermo-gravimetry on ash samples
- Phase diagram study of the ash systems for the three different ash types using a commercial software
- X-ray diffraction – at Monash University and the Australian Synchrotron, and
- Trace element measurements and modelling on ash and slag samples

For the batch of three Victorian coals tested extensively in this project - Loy Yang, Morwell, and Yallourn – the information generated can be summarised as follows:

<u>Carbon conversion</u>

- 106-150 µm size air-dried particles can attain over 99% Carbon conversion in twenty-one seconds at 1000 °C or around eight seconds at 1300 °C. There was no difference among the three different brown coals, all exhibiting a similar behaviour of Carbon conversion – temperature – residence time relationship.

Viscosity

- Ash fusion temperature measurement is not a reliable predictor of slag viscosity
- None of the conventional viscosity models accurately predict the viscosity of the slags from the three tested coals
- The viscosity – temperature behaviour of the three coals is different, requiring different temperatures for an acceptable range of viscosity 100-250 Poise.
- Yallourn coal can generate a slag at acceptable viscosity range around 1450 °C.
- Loy Yang and Morwell ash require in excess of 1500 °C for an acceptable viscosity range if these are to be used on their own. This is due to the very high levels of alumino-silicates in Loy Yang ash and very high level of calcium in Morwell ash.
- Addition of CaO or Clay overburden as flux material does not reduce the temperature required for an acceptable viscosity for any of the three ash types
- For Morwell ash, a 50:50 mix with Loy Yang ash reduces the temperature requirement to 1400 °C
- For Loy Yang ash, a 50:50 mix with Yallourn ash or Morwell ash reduces the temperature requirement to 1400-1470 °C

Trace element emission

- This was limited to Zn, Mn, Ba, Cr, Ni and As – as being the elements of moderate to greatest concern related to coal gasification
- Based on both thermodynamic modelling and chemical analysis following experimental work reveal that their emission in the gas phase is not significantly dependent on temperature. Over 50% of the compounds of these elements are retained in slags at gasification temperatures, and there is no systematic influence of the flux materials on their retention.

Most gasifiers operate as a two-stage gasifier, one stage being used to devolatilize the coal and convert the carbon to fuel gas, and the second stage being used to convert the ash to a molten slag. It is expected that for all three brown coals, the first stage does not need to operate above 1300 °C. The second stage requires a higher temperature between 1400 and 1550 °C depending on the coal used.

While the project has generated substantial practical information on entrained flow gasification behaviour of Victorian brown coal for the first time, some of the reasons for viscosity behaviour of the three ash types require more fundamental investigation. This is continued at Monash University using the facilities and the expertise developed.

The training of new research staff was one objective of this project. As a means of capacity building, the project has so far trained two Ph.D. students, one Research Fellow, and four undergraduate students. Apart from the fundamentals of gasification, these researchers gained knowledge in the design, construction, commissioning and operation of high temperature-entrained flow reactor and viscometer assembly, advanced chemical analysis of fuel samples, and thermodynamic modelling.

# 1 Introduction

Gasification is a key technology for easier (at lower energy penalty and lower cost) capture of $CO_2$ and other criteria pollutants from the processing of coal or any solid fuels for producing power, fuels or chemicals. Where $CO_2$ capture is incorporated into the process, gasification power plants have been reported to be 10% cheaper than conventional coal power plants[1]. Also, gasification power plants are reported to generate 20% less $CO_2$ based on both bituminous coals [1]and brown coals[2].

For gasification, three major types of gasifiers exist:

- Fixed bed gasifiers which require coarse particles, > 10 mm
- Fluidised bed gasifiers which require particles, 1-10 mm and
- Entrained flow gasifiers which require fine particles, <200 µm

Fixed bed gasifiers are not suitable for gasification of brown coals due to their friable nature which generates fine particles due to attrition and thermal fragmentation, limiting carbon conversion and the calorific value of the fuel gas.

Fluidised bed gasifier at atmospheric and at 10 bar pressure has been used for brown coal gasification at 1.5 $MW_{th}$ scales. The work performed under the banner of the CRC for Clean Power from Lignite indicated that carbon conversion was limited to around 80% at 900 $^{o}C$ bed temperature typical of fluidised beds to minimise bed agglomeration. The low carbon conversion was due to elutriation of C-rich fine char resulting from attrition in the fluidised bed.

On the other hand, the high temperature in entrained flow gasifiers promotes carbon conversion and result in the acceptable quality of fuel gas. However, gasification performance as a function of temperature and the nature of slag formation, which affects gasifier operation, is largely unknown for Australian brown coals.

Also, to ensure satisfactory and uninterrupted operation, it is of utmost importance to sustain continuous slag flow out of an entrained flow (slagging) gasifier. Excessive build-up of slag melt on the refractory wall reduces heat transfer in a gasifier, causing downtime or shutdown of the gasifier due to ash and slag-related problems. It is important that the dynamic viscosity (henceforth termed as viscosity) of the liquid slag is low enough so that slags flow down the gasifier walls and can be drained out from the gasifier as “molten slag”. However, if the viscosity of slag is too low, an effective slag layer will not form, and, therefore, will not protect the gasifier’s internal wall. An acceptable standard for the viscosity is between 100 Poise and 250 Poise that ensures the satisfactory protection of the gasifier wall and uninterrupted operation of the gasifier. Therefore, information on composition, viscosity and the change in viscosity with temperature for coal ash slags are essential for efficient operation of an entrained flow gasifier. Such information does not exist in the open literature. Therefore,

this project funded by the Brown Coal Innovation Australia and Mitsubishi Heavy Industries was undertaken to generate the following information:

- Gasification performance (carbon conversion and gas composition) of Victorian brown coal at different temperatures under entrained flow gasification conditions
- Composition of Victorian brown coal ash
- X-ray diffraction analysis at Australian synchrotron to determine the phases in the slag at high temperature under gasification conditions
- Ash fusion tests to determine the melting behaviour of ash
- Differential thermal analysis to understand the weight loss and heat release/absorption curves in the ash at high temperatures
- Prediction of slag viscosity with the existing models in the literature and assess the suitability of the models
- Thermodynamic prediction of %-age liquid formation in the ash with temperature at varying ratios of flux addition - CaO and clay
- Prediction of different phases of the slag with temperature
- Viscosity measurements at high temperatures
- Trace element analysis of the ash samples treated at entrained flow gasification temperatures

## 2 Performance of three Victorian brown coals under entrained flow gasification conditions

A purpose-built atmospheric pressure entrained flow gasifier was used in this project. Tests were performed between 1000 C and 1400 C. A schematic, and a photograph of the gasifier system is shown in figure 1.

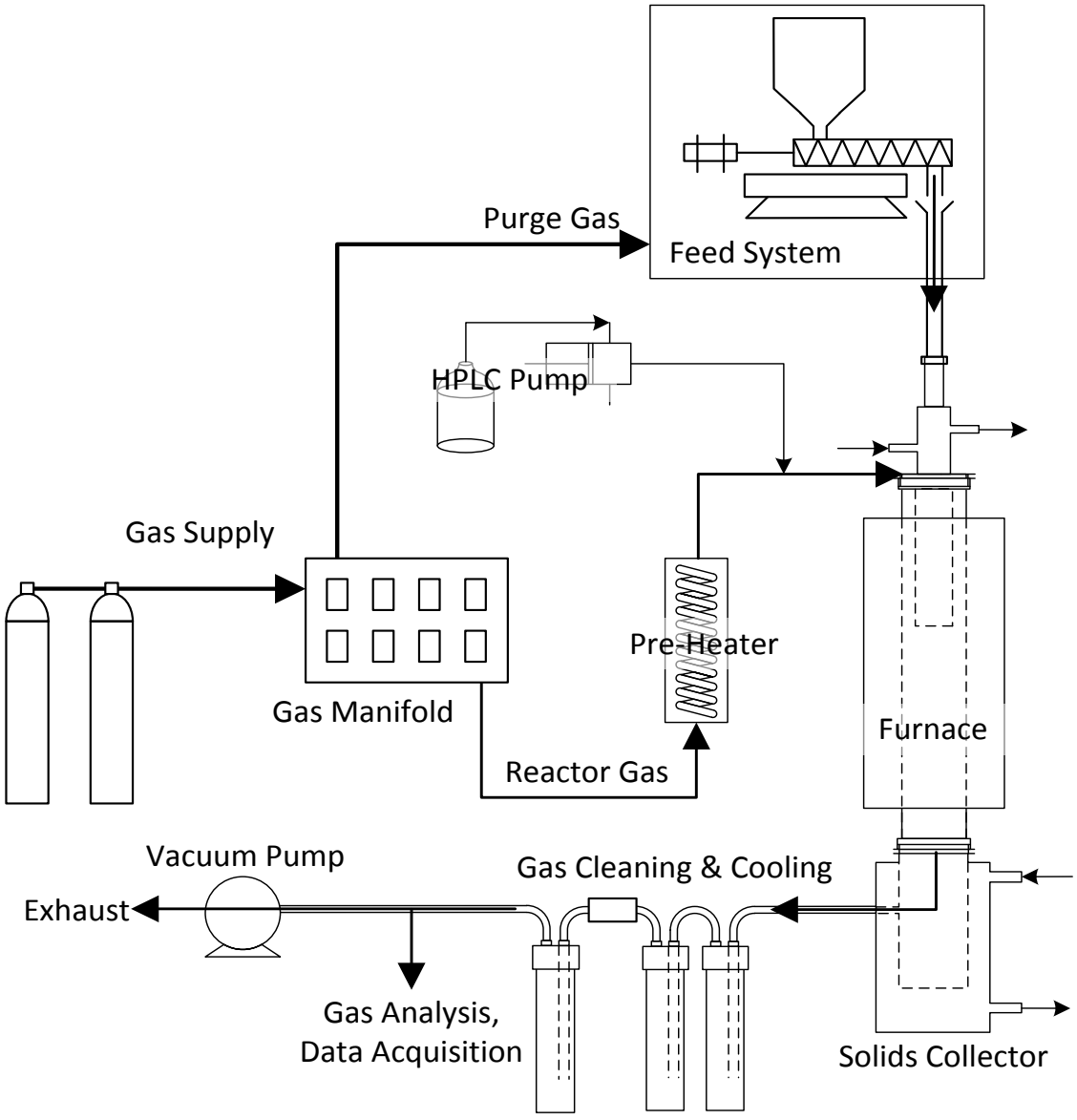


Figure 1 (a) Schematic of the gasification reactor system

The system is designed to operate at 1000 C – 1600 C, 30-180 gm/hr solid feed having 40-200 µm particle size. The residence time can be varied between 4 secs and 24 secs. Full details of this gasification system are available in a Ph.D. thesis (Tanner, 2015) which was supported by the Brown Coal Innovation Australia.

Figure 1 (b) Photograph of the gasification reactor system

Experiments were undertaken in the reactor system with several air-dried Victorian brown coals (Loy Yang, Morwell, Yallourn, Maddingley) at temperatures 1000 – 1400 C in an atmosphere consisting of 20-80% $CO_2$ and rest $N_2$ by volume. While detailed results will be made available in journal publications and another Ph.D. thesis currently under preparation, figure 2 shows the typical carbon conversion results that covers the three coals tested as part of this project – Loy Yang, Morwell, and Yallourn – with their air-dried particles of 106-150 µm particle size. The composition of these coals is presented in section 3.1.

This 106-150 µm size air-dried particles attained over 99% carbon conversion in twenty-one seconds at 1000 °C or around eight seconds at 1300 °C, at an atmosphere of 20% $CO_2$ and 80% $N_2$ by volume. There was no difference among the three different brown coals, all exhibiting a similar behaviour of Carbon conversion – temperature – residence time relationship.

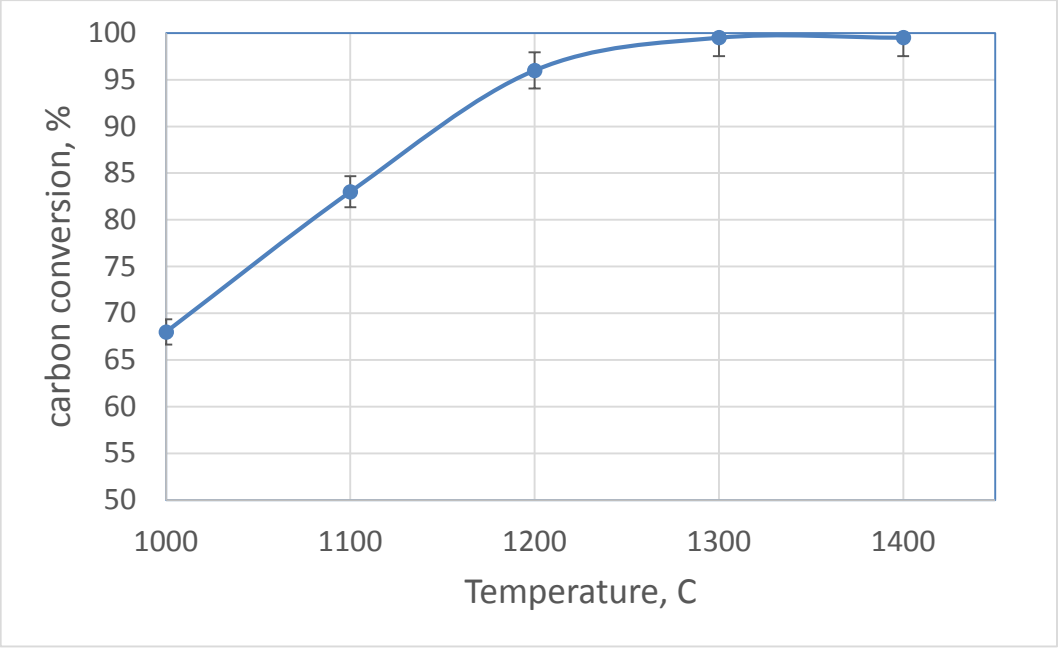


Figure 2: Typical carbon conversion for the three Victorian brown coals at 40% $CO_2$/60% $N_2$ and eight seconds residence time

## 3 Coal, ash and slag Characterization- Methods and results

This section presents a brief description of the methods used for characterization of coal, ash and slag. This is followed by results of characterization.

### 3.1 Composition of Victorian brown coals

**Table 1:** Ultimate and Proximate analysis of three Victorian brown coals

| Items | YL coal | MW coal | LY coal |
|---|---|---|---|
| ***Ultimate analysis (d.b., wt %)*** | | | |
| Carbon | 66.35 | 60.42 | 61.6 |
| Hydrogen | 4.92 | 4.59 | 4.70 |
| Nitrogen | 0.39 | 1.54 | 1.55 |
| Sulphur | 0.3 | 0.86 | 0.88 |
| Ash | 6.12 | 2.04 | 7.99 |
| Oxygen (by difference) | 21.92 | 30.55 | 23.28 |
| ***Proximate analysis (wt %)*** | | | |
| Moisture | 5.82 | 14.92 | 11.66 |
| Volatile matter (d.b.) | 48.18 | 49.31 | 48.25 |
| Fixed carbon (d.b.) | 45.7 | 48.65 | 32.1 |
| Ash (d.b.) | 6.12 | 2.04 | 7.99 |

*d.b. – dry basis*

Ultimate analysis of Victorian brown coals was performed using a Perkin Elmer (EA2400 instrument and following the AS 1038.6.1 standard. The analysis was done in triplicates. Two mg of sample was combusted at 950 $^{o}$C and the release of $CO_2$, $H_2O$, $SO_2$ and $NO_x$ were measured against the composition of the coal.

Proximate analysis of coal was performed on Netzsch thermogravimetric analyser STA-449FA. Table 1 shows the ultimate and proximate analysis of three Victorian brown coals used in the present study. Ten mg of sample was loaded in a ceramic crucible and heated from room temperature to 900 $^{o}$C in $N_2$ atmosphere and held at 900 $^{o}$C for 30 min. The weight loss until 105 $^{o}$C is considered to be the amount of moisture present in the sample, and 105-900 $^{o}$C is the temperature range for the release of volatiles. Subsequently, the gas was switched to air to burn off the fixed to measure the ash content.

### 3.2 Ash characterization

Victorian brown coals contain relatively small ash component, ~ 2%, compared to other coals which vary from 6-40%. Characterization of ash to determine the inorganic composition and their melting temperatures is important to understand the behaviour of ash in an entrained flow gasifier. The slag generated in a gasifier plays an important role in ensuring the continuous operation of the gasifier. The flow of the slag in an entrained flow gasifier depends

on the viscosity and melting temperature where the inorganic components of the ash are molten enough to flow along the walls of the gasifier. In general the presence of components like $Fe_2O_3$, CaO and $Na_2O$ are known to reduce the viscosity of the slag whereas components like $SiO_2$ and $Al_2O_3$ are known to increase the viscosity and melting temperatures of the slag. Ash samples were characterised by various techniques like Inductively Coupled Plasma-Atomic Emission Spectroscopy (ICP-AES), ash fusion tests and X-ray diffraction to gain insight into the chemical and physical properties of ash.

### 3.2.1 Ash composition

The ash used in the present study include those from three Victorian brown coals namely, Yallourn, Morwell and Loy Yang. All the ash samples were prepared by burning them in a muffle furnace at 815 $^oC$ for eight hr in air. The ash thus obtained was used to determine the composition using ICP-AES. Table 2 shows the composition of the three Victorian ash samples. The table also includes the composition clay overburden obtained from Loy Yang mine that we planned to use as a fluxing agent. Ash is considered to have the major components shown in Table 2, however, will also have other elements like V, Cr, Co, Mn, As, Ni, Zn, Ba, Sr, Cu in trace quantities.

**Table 2 The composition of ash (wt%)**

| Component | Yallourn | Morwell | Loy Yang | Clay |
|---|---|---|---|---|
| $SiO_2$ | 6.58 | 4.27 | 63.65 | 81.66 |
| $Al_20_3$ | 4.51 | 2.02 | 21.86 | 10.62 |
| $Fe_2O_3$ | 54.21 | 17.47 | 4.53 | 6.25 |
| $TiO_2$ | 0.26 | 0.26 | 2.20 | 1.05 |
| $K_2O$ | 0.21 | 0.38 | 0.65 | 0.13 |
| MgO | 21.01 | 29.45 | 3.36 | 0.16 |
| $Na_2O$ | 1.95 | 6.29 | 2.70 | 0.11 |
| CaO | 9.21 | 31.24 | 0.85 | ND |
| $SO_3$ | 0.02 | 7.57 | ND | ND |
| $P_2O_5$ | ND | ND | ND | ND |

ND-not detected

The results in Table 2 suggests that the ash composition varies with the type of coal. Yallourn ash contains high Iron, Morwell contains high CaO, and Loy Yang is dominated by $Al_2O_3$-$SiO_2$. The ash composition is shown as oxides of the individual elements for convenience. The combination in which the component elements are present in the ash does vary and have an effect on the melting behaviour of the ash.

### 3.2.2 Ash fusion tests

Ash fusion test is used to indicate the temperature at which ash starts to deform, undergo hemispherical and spherical formation and finally flow as the molten slag. This information provides a rough indication where the slag starts to flow suggesting the ideal temperature range above which the samples to be heated to measure the viscosity. Ash fusion tests were conducted in both oxidising atmospheres (in air) and reducing (40% $CO_2$ + balance CO) conditions for comparison. However, in a real gasifier since the coal gets gasified to CO, $CO_2$ and $H_2$ the atmosphere is predominantly reducing atmosphere. It is known that the ash fusion takes place at relatively lower temperatures in reducing atmosphere than in the oxidising atmosphere. The results of ash fusion analysis conducted on the ash samples are reported in Table 3. This analysis was conducted at MHI-Japan as part of their contribution to the project.

**Table 3 Ash fusion test on Victorian brown coal ash**

| Sample | AFT- Reducing atmosphere (Temp $^oC$) | | | | AFT - Oxidation atmosphere (Temp $^oC$) | | | |
|---|---|---|---|---|---|---|---|---|
| | Deformation | H-Spherical | Spherical | Flow | Deformation | H-Spherical | Spherical | Flow |
| LY | 1250 | 1400 | 1440 | >1500 | 1280 | 1500 | -- | >1500 |
| MW | 1350 | >1500 | >1500 | >1500 | >1500 | >1550 | -- | >1500 |
| YL | 1245 | 1365 | 1375 | 1480 | 1310 | 1345 | -- | 1450 |

The results in Table 3 shows that the flow temperatures for Loy Yang ash are beyond 1500 $^oC$ suggesting this sample will require very high temperature during gasification for their removal. Alternatively, fluxing agents will be required to lower the flow temperature. Morwell ash shows deformation at 1350 $^oC$ and H-spherical and spherical formation above 1500 $^oC$. The results indicate that Morwell ash will require fluxing agents. Yallourn ash also has high flow temperatures at 1480 $^oC$, however, lower than the other two coal ash samples.

**Table 4 Ash fusion test on Victorian brown coal fly ash with 4% CaO and 4% clay**

| Sample | AFT Reducing atmosphere (Temp $^oC$) | | | | AFT Oxidation atmosphere (Temp $^oC$) | | | |
|---|---|---|---|---|---|---|---|---|
| | Deformation | H-Spherical | Spherical | Flow | Deformation | H-Spherical | Spherical | Flow |
| LY | 1280 | 1380 | 1440 | 1460 | 1300 | 1390 | 1460 | 1490 |
| LY 4% CaO | 1280 | 1300 | 1340 | 1360 | 1280 | 1310 | 1350 | 1390 |
| LY 4% clay | 1260 | 1340 | 1380 | 1460 | 1310 | 1380 | 1440 | 1470 |
| MW | >1550 | >1550 | >1550 | >1550 | >1550 | >1550 | >1550 | >1550 |
| MW 4% CaO | 1220 | 1510 | >1550 | >1550 | 1340 | >1550 | >1550 | >1550 |
| MW 4% clay | 1190 | 1430 | 1490 | >1550 | 1510 | >1550 | >1550 | >1550 |
| YL | 1330 | >1550 | >1550 | >1550 | >1550 | >1550 | >1550 | >1550 |
| YL 4% CaO | >1550 | >1550 | >1550 | >1550 | >1550 | >1550 | >1550 | >1550 |
| YL 4% clay | >1550 | >1550 | >1550 | >1550 | >1550 | >1550 | >1550 | >1550 |

Further ash fusion tests were conducted at Monash University, by mixing 4% CaO or 4% clay with the ash samples to check whether the mixing of flux indeed lowers the flow temperatures. The results of AFT with flux addition are presented in Table 4. The AFT results on ash samples show slight variation compared to the results from MHI. Flow temperature of Loy Yang ash is slightly lower at 1460 $^oC$ compared to >1500 $^oC$ when measured at MHI. Morwell did not show any sign of deformation even at 1550 $^oC$, unlike the results at MHI in Table 3. On the other hand, Yallourn showed the flow temperatures to be higher than 1550 $^oC$. The results indicate the coals and corresponding ash are highly heterogeneous. The addition

of 4% CaO to Loy Yang ash sample lowered the flow temperatures by 100 $^{o}$C. However, clay did not change the flow temperature. The reason for this is that Loy Yang ash is rich in $SiO_2$ and clay is even richer in silica at 80%. Therefore, the addition of $SiO_2$ rich flux will not reduce the fusion temperatures of the Loy Yang ash. The addition of 4% CaO and 4% clay lowered the softening temperature of Morwell ash to a large extent but was not sufficient to lower the flow temperature below 1550 $^{o}$C in both cases. Increasing the amount of flux might be helpful and requires further testing. On the other hand, the addition of 4% CaO and 4% clay to Yallourn ash has no positive effect on the ash fusion temperatures.

### 3.2.3 Conclusion

The results of ash fusion analysis from MHI and Monash University show a broad variation in the melting temperature and the flow temperatures of the coal ashes. For example, Loy Yang, which did not show any flow until 1550 $^{o}$C when measured at MHI, showed a flow at 1460 $^{o}$C when measured at Monash University. On the other hand, on both measurements, Morwell did not show any sign of flow below 1500 $^{o}$C. Similarly, Yallourn sample showed flow-temperature of 1480 $^{o}$C at MHI and above 1550 $^{o}$C at Monash. Such variation may be attributed to the heterogeneity of coal and the corresponding ash. This clearly suggests that only Ash fusion temperature measurement is not a substitute for viscosity measurements.

## 3.3. Slag Characterisation

### 3.3.1 Literature review

A review of different characterization methods applied to determine the composition of ash and slag are summarised in Appendix A. The review also summarises the inherent advantages and disadvantages of the different characterization methods.

### 3.3.2 Slag Characterisation methods

The characterization methods used in this project include high-temperature X-ray diffraction at Australian Synchrotron, room temperature XRD, Differential thermal analysis (DTA), and Trace element analysis using Inductively Coupled Plasma Atomic Emission Spectrometry (ICP-AES). Using the composition determined from ICP-AES measurements, thermodynamic modelling was carried out to predict the percentage liquid formation calculations and trace element emission at varying temperatures. These data were also used to assess the different viscosity models available in the literature.

### 3.3.3 Flux addition

Coal ash has varying flow temperatures depending on composition. Some ash samples have melting temperatures over 1550 $^{o}$C. During gasification removal of the ash as molten slag at a viscosity range of 100-250 Poise is a requirement to prevent ash build-up inside the

gasifier. The ash melting temperatures can be lowered by the addition of suitable flux materials. However, the amount of flux added to the coal is also an important consideration. Excess addition of flux might have a negative effect on the final melting temperatures of the ash. In this project, two materials CaO and clay overburden from Loy Yang mine were used to study the effect on the ash fusion temperature and viscosity measurements. It is established in the literature that CaO has a positive effect in lowering the ash fusion temperatures up to certain loading. The study[2] on Mae Moh lignites (Thai lignite) showed that removal of excess CaO content from the ash samples by acid washing helped alleviate fouling problems. When CaO is present in small fractions in ash it will act as fluxing agent and lowers the AFTs. When the CaO exceeds >38% the high melting point of it dominate and have a negative effect on the AFTs of the ash. In other work[3], the effect of $CaCO_3$ on ash fusion temperatures of three unnamed coal ash showed that lowest AFT achieved at 29-33% $CaCO_3$ addition were in the temperature range of 1150-1200 $^oC$ compared to the AFT of the original ash (~40% Ca in ash) of 1400-1600 $^oC$. $CaCO_3$ beyond 800 $^oC$ decomposes to CaO and $CO_2$ resulting in CaO in the ash at high temperatures. These observations suggest that CaO can be tried as a fluxing material on Victorian brown coals depending on the Ca-content originally in the ash. Additionally, clay overburden from Loy Yang mine was also tested as flux material apart from CaO. The chemical composition of the clay overburden from Loy Yang power station is given in Table 2, which is rich in silica and alumina.

### 3.4 X-ray diffraction

X-ray diffraction (XRD) measures the crystalline phases present in the ash or slag samples and how they transform to new phases during the slagging process. Two sets of measurements were performed on the ash samples- one at Monash University at room temperature and the second set of measurement at the Australian Synchrotron in-situ at high temperatures.

#### 3.4.1 Room temperature X-ray diffraction

Figures 3-5 represent the room temperature XRD patterns of Loy Yang Yallourn and Morwell ash samples respectively. The room temperature XRD patterns suggest that Yallourn ash is dominated by diffraction peaks of Magnesioferrite $Fe_2MgO_4$, Magnetite $Fe_3O_4$, Magnesium Iron oxide $Fe_{1.6}Mg_{1.55}O_4$. Periclase MgO, Anhydrite $CaSO_4$. Loy Yang is dominated by diffraction peaks of Quartz $SiO_2$, Periclase MgO whereas Morwell is dominated with Periclase MgO, Magnesiowuestitie $Fe_{0.4}Mg_{0.6}O$, CaO and $CaSO_4$.

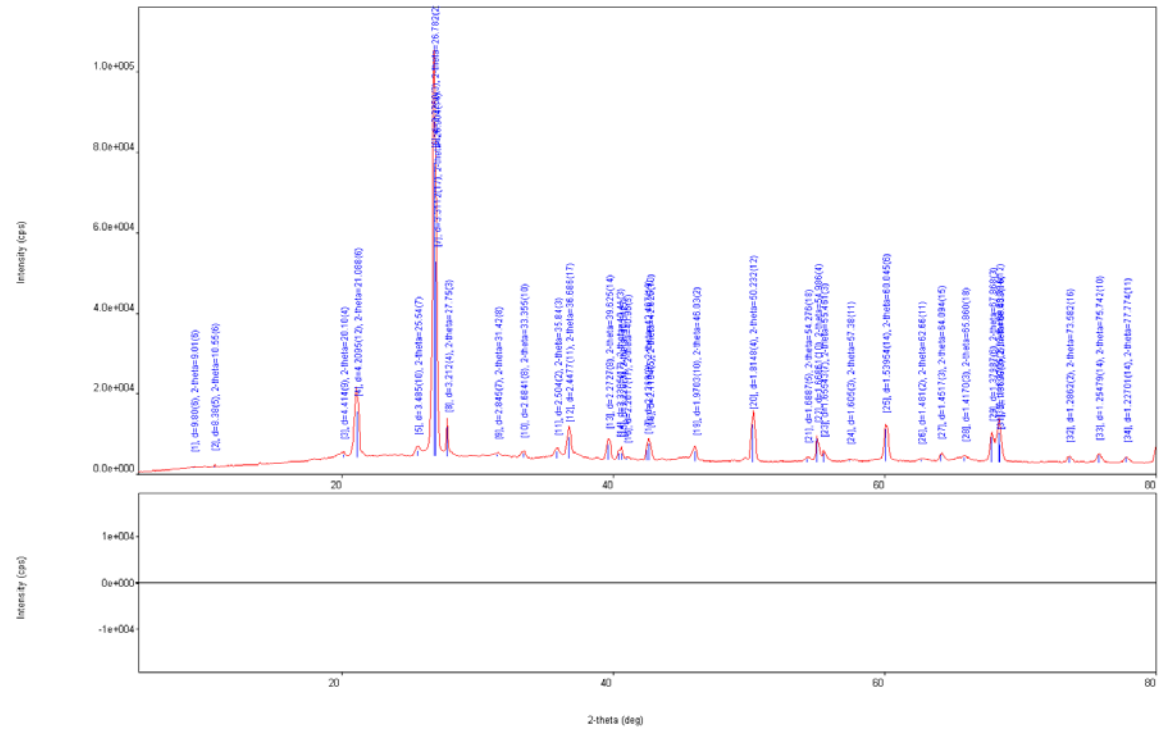


**Figure 3** Room temperature X-ray diffraction pattern of Loy Yang ash

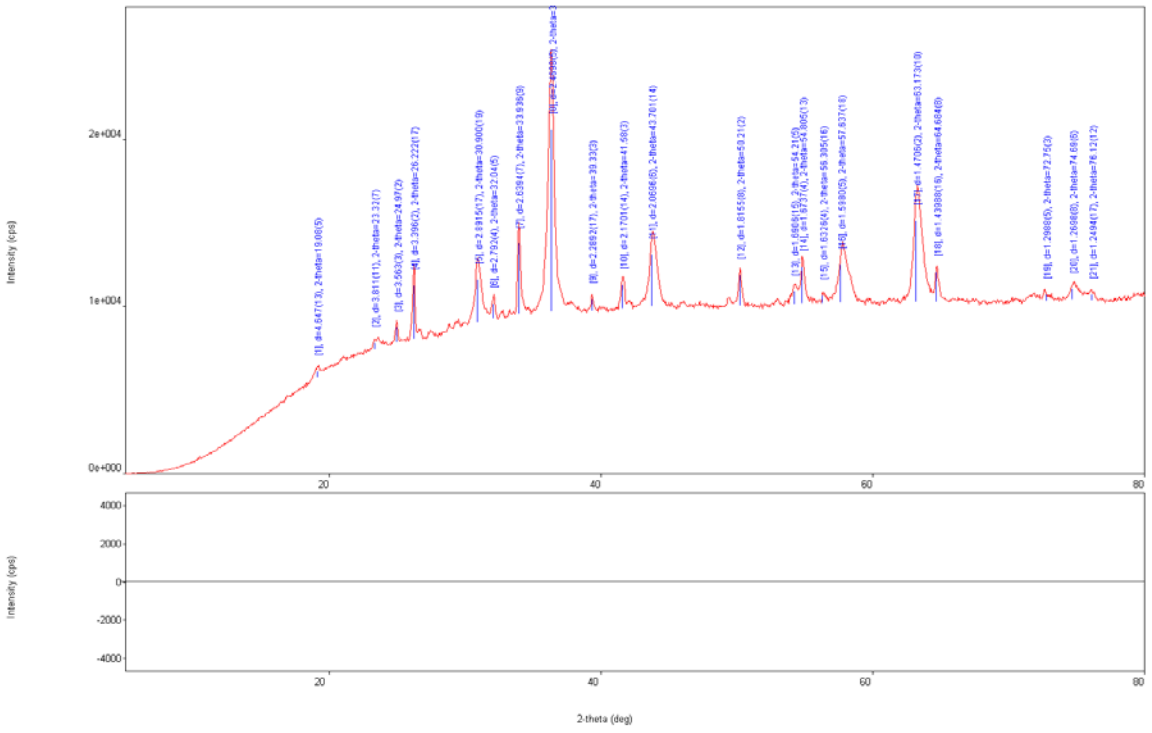


**Figure 4** Room temperature X-ray diffraction pattern of Yallourn ash

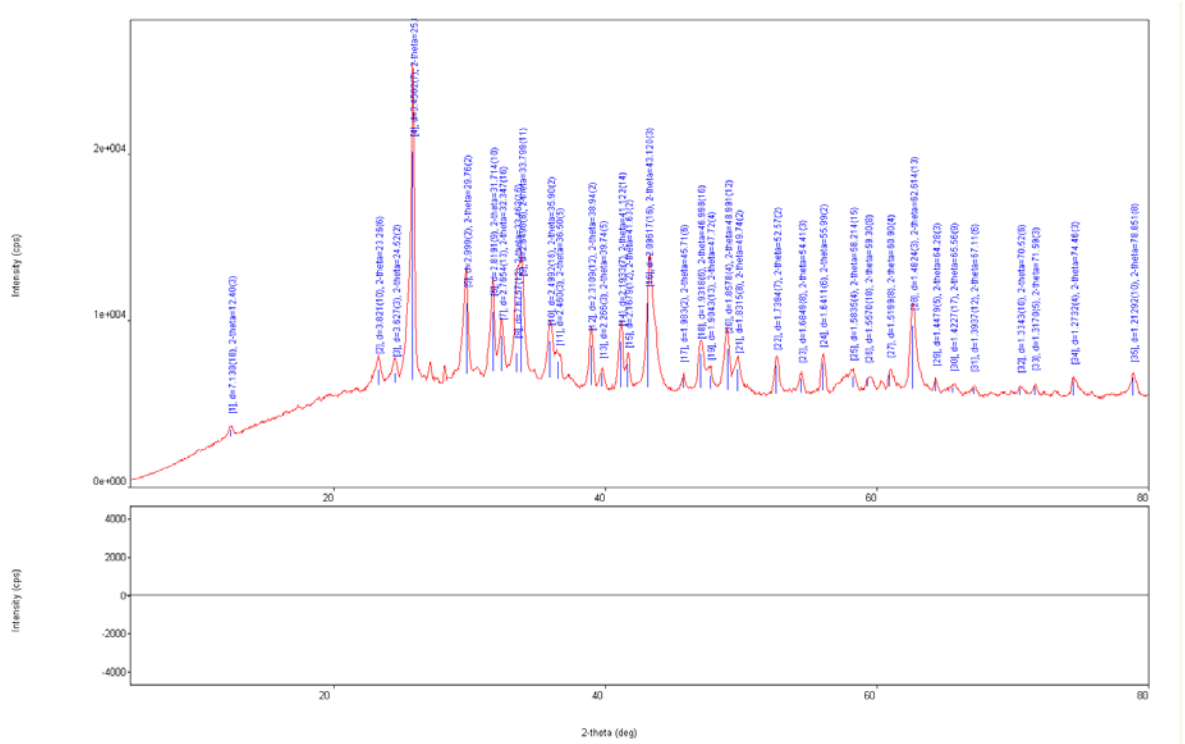


**Figure 5** Room temperature X-ray diffraction pattern of Morwell ash

To determine the phases that would be formed at gasification temperature range, the diffraction patterns should ideally be measured at that temperature range. Due to the presence of multiple components in the ash, it is also important to identify different phases present in the sample at high temperatures. These measurements were performed by using Synchrotron-based powder diffraction beamline.

### 3.4.2 In-situ high temperature XRD at Australian Synchrotron

In-situ high-temperature X-ray diffraction patterns of ash and ash mixed with the CaO samples was measured at the Australian synchrotron. The ash samples were placed on a custom made platinum heating strip 102 mm (L) x 10 mm (W) x 1 mm (T). The strip has a cavity of 20 mm (L) x 8 mm (W) and 0.2 mm (D) to hold the sample. The heating strip also has 0.35mm Pt and 10% Pt/Rh electrodes to electrically heat the sample. The heating strip was mounted inside the Australian Synchrotron X-ray diffraction beamline's Anton Parr furnace an angle of 5 degrees to the incident beam. The X-ray diffraction patterns of the ash samples were collected using Cu-Kα radiation at a wavelength of 0.61944 Å. The sample was loaded on the Pt strip by mixing the sample with acetone and coated as a thin layer. Acetone helped in preventing the formation of clumps and allowed to spread the sample evenly on the strip. The whole setup was placed inside the chamber and was continuously flushed with a pre-mixed gas consisting of 20% $CO_2$ in $N_2$. In order to monitor the phase formation, the furnace temperature was ramped at 10 °C per minute to reach each temperature of interest. The sample was held at each temperature isothermally for 1 minute for equilibration prior to the diffractogram being taken. For each measurement, data was collected for 5 minutes at two detector positions. Data

was collected at room temperature, then at 800 $^{o}$C and then onwards at 50 $^{o}$C steps until 1500 $^{o}$C.

***Insitu high-temperature XRD analysis***

Figure 6(a) shows the setup used at the Australian synchrotron to obtain the XRD profiles of the ash samples in situ at high temperatures. Figure 6(b) shows the sample holder when heated to high temperatures during the course of the experiment.

(a) 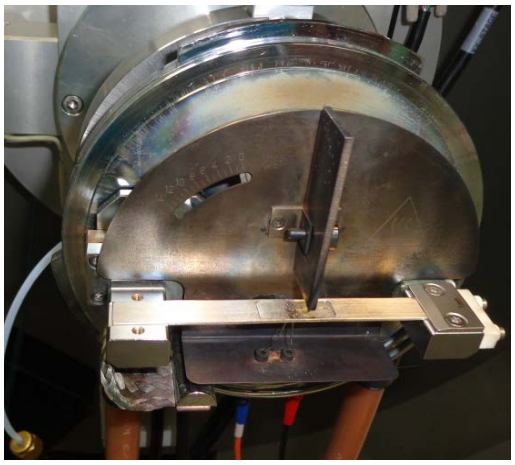 (b) 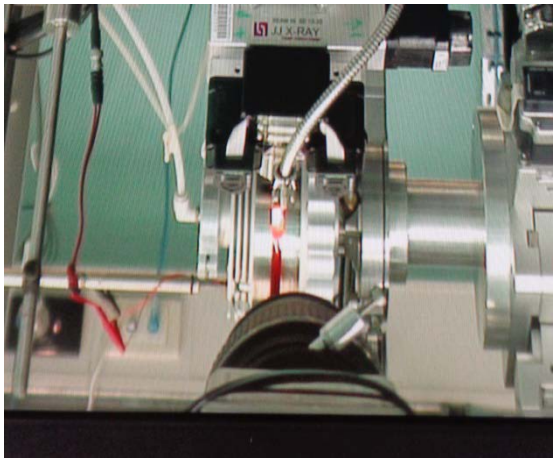

**Figure 6** Insitu synchrotron X-ray diffraction setup a) Platinum strip mounted for sample loading b) Sample above 1000 $^{o}$C during data collection.

The major phases detected for Yallourn, Loy Yang and Morwell ash samples are tabulated in Tables 5-7. The phases at each temperature are listed in decreasing order of observed dominance. The melting temperatures of the major detected phases for both the ashes are tabulated in Table 8.

***Yallourn ash***

Figure 7 shows the XRD pattern of Yallourn ash collected at a different temperature. At room temperature, the dominant phase detected is a combination Magnesioferrite spinel ($Fe_2MgO_4$), Magnetite ($Fe_3O_4$) and Magnesium Iron oxide $Fe_{1.6}Mg_{1.55}O_4$. Interestingly all the three phases have peak positions at similar locations, which indicate it is either one of these phases or combination of these phases. The ash composition shows that the major component of Yallourn ash is $Fe_2O_3$ (46.29 wt %) followed by MgO and CaO at 15.29% and 11.88% respectively. The next important phase identified in the samples is MgO (Periclase). Ca is present as either CaO or $CaSO_4$. When the sample was heated to 800 and 850 $^{o}$C, all the major peaks observed at 25 $^{o}$C were not observed and the profile is dominated with Pt peaks from the strip. This may be due to the migration or sintering of the particles on the Pt strip while heating the sample from room temperature to 800 $^{o}$C and exposing the Pt strip. However when the sample was heated to 900 $^{o}$C Magnesioferrite peaks resurface whereas Periclase (MgO) phase resurfaced at 950 $^{o}$C. At 1000 $^{o}$C the peaks started shifted to lower 2 thetas indicate phase changes in the sample and the new peak positions were identified as Magnetite but with a

mixture of various elements Fe, Mg, Al, Ca, Mn, Ti and Si with another major phase of Quandilite $Mg_2O_4Ti$.

At 1050 $^oC$, the XRD profile shows major peaks for Ulvospinel $Fe_2TiO_4$ and traces of Periclase. At 1200-1250 $^oC$ the diffractogram is dominated by Ulvospinel, Periclase and Quandilite. At 1300 and 1350 $^oC$, along with Ulvospinel a new peak of $Fe_2MnO_4$ is observed suggesting the formation of a new phase. This new phase is reflected in the DTA profile (section 3.7) as an exothermic peak. Beyond 1350 $^oC$, the peaks become broad indicating amorphous phases due to softening or slag formation of the major components present in the ash. The XRD patterns suggest that Yallourn ash starts to soften and melt beyond 1350 $^oC$ indicating the need for temperatures higher than 1350 $^oC$ to measure viscosity on the samples.

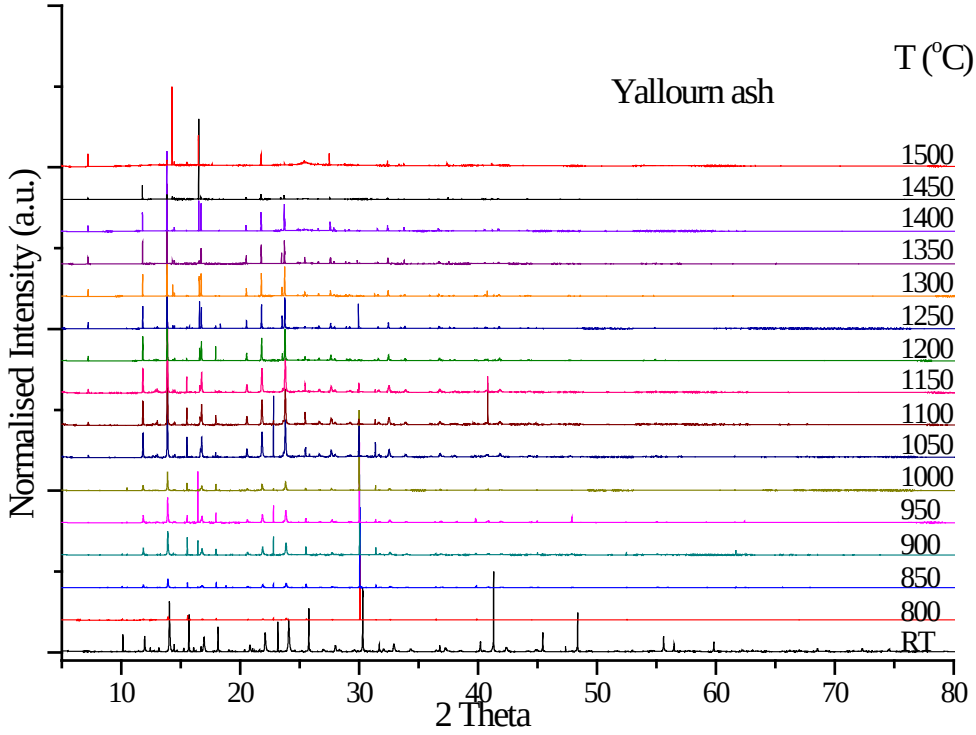


**Figure 7** Insitu synchrotron XRD patterns of Yallourn ash while heating the sample from room temperature to 1500 $^oC$.

Figure 8 shows the XRD pattern of Yallourn ash mixed with 8% CaO. At room temperature, the peaks and their positions are same as those of Yallourn ash. The major peaks are due to Magnesioferrite, Magnetite, Periclase, $CasO_4$ similar to Yallourn ash with additional peaks for CaO as it was added as a flux in this sample. However, when heated to 800 and 850 $^oC$ the spectra do not show any peaks of Periclase MgO or CaO, which can be due to the reaction of these components with other compounds of Fe, Al, Mn, and Si in the ash to form a new phase. The other major phase observed at this temperature was Ulvospinel $Fe_2TiO_4$. The pattern at 900 $^oC$ are dominated by Ulvospinel and Jacobsite - a combination of Al, Fe, Mg, Mn and Zn oxides, and at 950 $^oC$ by Quandilite $Mg_2O_4Ti$. At 1000 $^oC$, a new phase $FeMn_2O_4$ was detected which changed to $Fe_2MnO_4$ at 1050 $^oC$. Ulvospinel peak can still be seen at 1050 $^oC$ along with Magnetite, Quandilite and Jacobsite but the intensity of these peaks was low. The pattern at 1200 $^oC$ only shows peaks of Quandilite and Ulvospinel which turned to only Quandilite at

1250 $^{o}$C. The same peaks continued to show a decrease in the intensity with increase in temperature until 1350 $^{o}$C suggesting softening of the crystalline phases beyond which the pattern appears flat suggesting melting of all the phases. These observations suggest the addition of CaO as a flux to the Yallourn ash reduced the softening temperatures by 100-150 $^{o}$C.

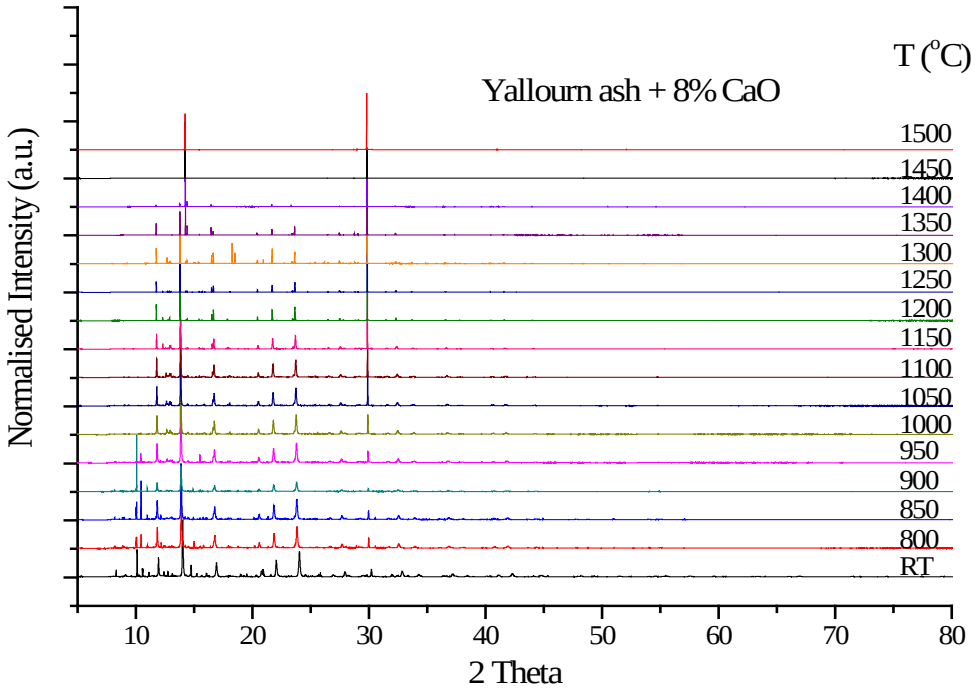


**Figure 8** Insitu synchrotron XRD patterns of Yallourn ash + 8% CaO while heating the sample from room temperature to 1500 $^{o}$C.

Figure 9 shows the XRD patterns of the Morwell ash. The room temperature diffractograms of Morwell ash is highly crystalline with peaks from Periclase MgO, Magnesiowuestitie $Fe_{0.4}Mg_{0.6}O$, CaO and $CaSO_4$. When the sample was heated to 800 $^{o}$C the spectra was dominated by MgO, calcium borosilicate and Calcite $CaCO_3$. The spectra also showed peaks for Diopside $CaMgO_6Si_2$ which is consistent with the presence of Ca and Mg as major components along with silica in the Morwell ash. The diffractogram also shows peaks for Calcite at 850 $^{o}$C along with Dolomite $Ca_{0.5}Mg_{0.5}CO_3$. The diffractograms at 900-1100 $^{o}$C show major peaks due to Magnesioferrite $FeMgO_4$, and Magnetite $Fe_3O_4$. When heated to 1150 $^{o}$C, the peaks due to $FeMgO_4$ and $Fe_3O_4$ remained and new peaks of Quandilite $Mg_2TiO_4$ were observed. The results suggest the Fe-containing components are the major constituents which prevent the ash from softening. However, when the sample was heated to 1250 $^{o}$C the major peaks disappeared with the pattern appearing flatter and with broad humps. This suggests the softening of the sample around 1200-1250 $^{o}$C and amorphous nature of the ash at higher temperatures.

***Morwell ash***

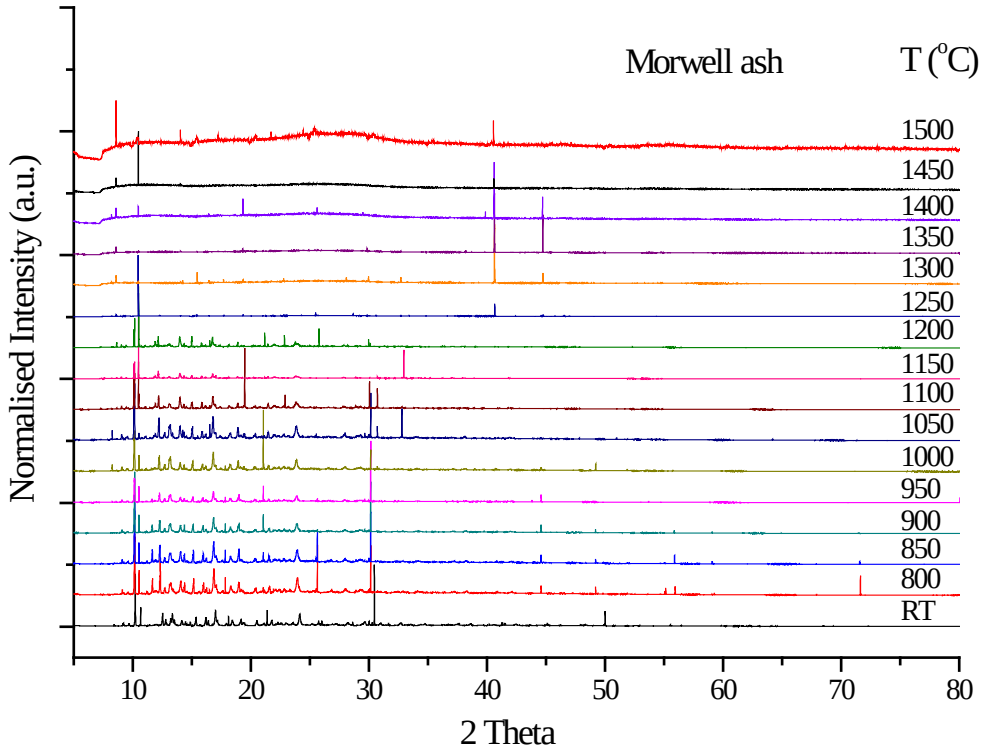


**Figure 9** Insitu synchrotron XRD pattern of Morwell ash while heating the sample from room temperature to 1500 °C

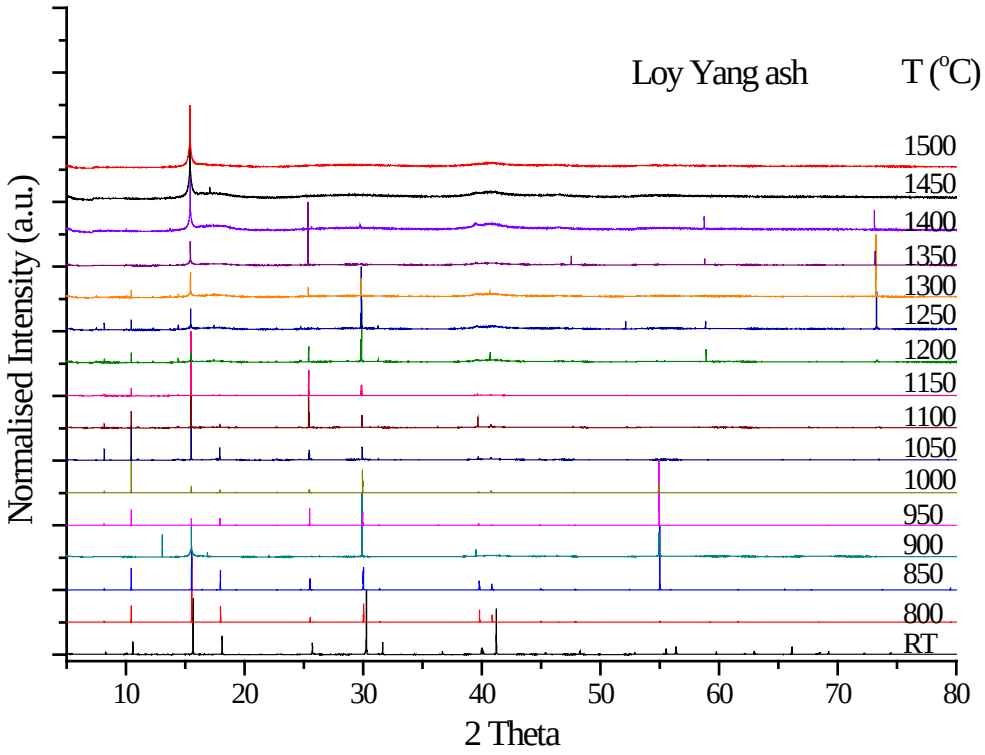


**Figure 10** Insitu synchrotron XRD pattern of Loy Yang ash while heating the sample from room temperature to 1500 °C.

***Loy Yang ash***

Figure 10 shows the XRD analysis of Loy Yang ash at room temperature. At the initial heating stages this ash is not as crystalline as the other ash sample. This may be attributed to the fact that the phases in this ash only begin to crystallise after the sample is heated to a certain temperature. At room temperature, the dominant phase detected were Periclase MgO and Silica $SiO_2$. The high dominance of $SiO_2$ peaks in the samples is consistent with the ash composition in Table 2. When heated to 800 $^oC$ the only phase detected was β-Quartz and at 900 $^oC$, the XRD pattern showed broad peaks due to softening of quartz. At 950 $^oC$, Periclase MgO resurfaced with $SiO_2$ now transforming from β-Quartz to β-Tridymite.

**Table 5** Mineral phases at different temperatures for Yallourn Ash samples

| **Temperature ($^oC$)** | **Yallourn** | **YA + 8% CaO** |
|---|---|---|
| 25 | Magnesioferrite $Fe_2MgO_4$, Magnetite $Fe_3O_4$, Magnesium Iron oxide $Fe_{1.6}Mg_{1.55}O_4$. Periclase MgO, Anhydrite $CaSO_4$ | Magnesioferrite $Fe_2MgO_4$, Magnetite $Fe_3O_4$, Magnesium Iron oxide $Fe_{1.6}Mg_{1.55}O_4$. Periclase MgO, Anhydrite $CaSO_4$, CaO lime |
| 850 | | Magnetite FeMgAlMnTiSi Oxide, Ulvospinel $Fe_2TiO_4$ |
| 850 | | Magnetite FeMgAlMnTiSi Oxide, Ulvospinel $Fe_2TiO_4$ |
| 900 | Magnesioferrite $Fe_2MgO_4$, Periclase MgO | Ulvospinel $Fe_2TiO_4$, Jacobsite AlFeMgMnZn Oxide, |
| 950 | Magnesioferrite $Fe_2MgO_4$, Periclase MgO | Quandilite $Mg_2O_4Ti$, Ulvospinel $Fe_2TiO_4$, Jacobsite AlFeMgMnZn Oxide, |
| 1000 | FeMgAlMnTiSi$O_x$ Oxide, Quandilite $Mg_2O_4Ti$ | $FeMn_2O_4$, Quandilite $Mg_2O_4Ti$, Jacobsite AlFeMgMnZn Oxide, |
| 1050 | Ulvospinel $Fe_2TiO_4$, Periclase MgO | $Fe_2MnO_4$, Ulvospinel $Fe_2TiO_4$, Quandilite $Mg_2O_4Ti$, Jacobsite AlFeMgMnZn Oxide, |
| 1100 | Ulvospinel $Fe_2TiO_4$, Quandilite $Mg_2O_4Ti$ , Periclase MgO | Ulvospinel $Fe_2TiO_4$, Quandilite $Mg_2O_4Ti$ |
| 1150 | Ulvospinel $Fe_2TiO_4$, Quandilite $Mg_2O_4Ti$ , Periclase MgO | Amorphous or no detectible peaks |
| 1200 | Ulvospinel $Fe_2TiO_4$, Quandilite $Mg_2O_4Ti$ , Periclase MgO | Amorphous or no detectible peaks |
| 1250 | Ulvospinel $Fe_2TiO_4$, $Fe_2MnO_4$ | Amorphous or no detectable peaks |
| 1300 | Ulvospinel $Fe_2TiO_4$, $Fe_2MnO_4$ | Amorphous or no detectable peaks |
| 1350 | Amorphous or no detectable peaks | Amorphous or no detectable peaks |
| 1400 | Amorphous or no detectable peaks | Amorphous or no detectable peaks |
| 1450 | Amorphous or no detectable peaks | Amorphous or no detectable peaks |
| 1500 | Amorphous or no detectable peaks | Amorphous or no detectable peaks |

Until 1200 $^oC$, only broad peaks due to amorphous $SiO_2$ were observed. This also could block the peaks from other components present in the ash. The pattern at 1200 $^oC$ also showed small peaks due to $Al_2MgO_4$ and $Al_2FeO_4$, however in minor quantities. At 1250 $^oC$, these two phases

form a solution and resulted in a new spinel phase ($AlFeMgO_4$) along with the original phases. At 1300 $^oC$ all the phases due to spinels no longer exist, leaving only very broad humps, which are assigned to amorphous $SiO_2$ and $MgSiO_3$. Beyond this temperature, the sample showed only broad humps and peaks from the Pt strip. When the XRD results are compared to the heat flow curves showed two endothermic peaks at 1275 $^oC$ followed by a peak at 1410 $^oC$. The peak at 1275 $^oC$ suggests the softening of the major components of ash $SiO_2$ and $Al_2MgO_4$ and $Al_2FeO_4$. The peak at 1400 $^oC$ is due to softening of minor quantities of other components present in the ash. From these observations, it can be concluded that Loy Yang ash does soften to some extent by 1300 $^oC$.

**Table 6** Mineral phases at different temperatures for Morwell Ash

| **Temperature ($^oC$)** | **Morwell** |
|---|---|
| 25 | Periclase MgO, Magnesiowuestitie $Fe_{0.4}Mg_{0.6}O$, CaO, $CaSO_4$ |
| 800 | Periclase Mgo, Calcium borosilicate and $CaBrSiO_3$, Calcite $CaCO_3$, Diopside $CaMgO_6Si_2$ |
| 850 | Calcite $CaCO_3$, Dolomite $Ca_{0.5}Mg_{0.5}CO_3$ |
| 900 | Magnesioferrite $FeMgO_4$, Magnetite $Fe_3O_4$ |
| 950 | Magnesioferrite $FeMgO_4$, Magnetite $Fe_3O_4$ |
| 1000 | Magnesioferrite $FeMgO_4$, Magnetite $Fe_3O_4$ |
| 1050 | Magnesioferrite $FeMgO_4$, Magnetite $Fe_3O_4$ |
| 1100 | Magnesioferrite $FeMgO_4$, Magnetite $Fe_3O_4$ |
| 1150 | $FeMgO_4$, $Fe_3O_4$, Quandilite $Mg_2TiO_4$ |
| 1200 | Amorphous or no detectable peaks |
| 1250 | Amorphous or no detectable peaks |
| 1300 | Amorphous or no detectable peaks |
| 1350 | Amorphous or no detectable peaks |
| 1400 | Amorphous or no detectable peaks |
| 1450 | Amorphous or no detectable peaks |
| 1500 | Amorphous or no detectable peaks |

**Table 7** Mineral phases at different temperatures for Loy Yang Ash

| **Temperature ($^oC$)** | **Loy Yang** |
|---|---|
| 25 | Quartz $SiO_2$, Periclase MgO |
| 800 | β-Quartz $SiO_2$ |
| 850 | β-Quartz $SiO_2$ |
| 900 | β-Quartz $SiO_2$ |
| 950 | Quartz (β-Tridymite), Periclase MgO |
| 1000 | Quartz (β-Tridymite) |
| 1050 | Quartz (β-Tridymite) |

| | |
|---|---|
| 1100 | Quartz (β-Tridymite) |
| 1150 | Quartz (β-Tridymite) |
| 1200 | Quartz (β-Tridymite), Spinel $Al_2MgO_4$, $Al_2FeO_4$ |
| 1250 | Quartz (β-Tridymite), AlFeMgO4 spinel |
| 1300 | Amorphous $SiO_2$ and $MgSiO_3$ |
| 1350 | Amorphous $SiO_2$ and $MgSiO_3$ |
| 1400 | Amorphous $SiO_2$ and $MgSiO_3$ |
| 1450 | Amorphous or no detectable peaks |
| 1500 | Amorphous or no detectable peaks |

**Table 8** Melting temperature of major mineral phases and the ashes they are present[4 5]

| **Phases** | **Melting Temperature (°C)** | **Ash** |
|---|---|---|
| Magnesioferrite $Fe_2MgO_4$ | 1750 | Yallourn |
| Periclase MgO | 2825 | Yallourn, Morwell |
| Lime CaO | 2927 | Yallourn, Loy Yang, Morwell |
| Quartz $SiO_2$ | 1670 | Loy Yang |
| Magnesium Aluminate spinel $Al_2MgO_4$ | 2135 | Loy Yang |
| Magnetite $Fe_3O_4$ | 1597 | Loy Yang |
| CaO | 2613 | Morwell |

### 3.4.3 Conclusion

Insitu synchrotron XRD on Victorian brown coals ashes shows the major peaks present in Loy Yang are periclase MgO and Quartz from its high $SiO_2$ (63.6 wt%) composition. This β-quartz phase changes to β-Tridymite above 950 °C. At temperatures above 1200 °C Spinel $Al_2MgO_4$, $Al_2FeO_4$ are observed followed by amorphous $SiO_2$ and $MgSiO_3$ phases at 1300 °C. Yallourn showed multiple phases comprising of Magnesioferrite, Magnetite, Periclase and $CaSO_4$, reflecting the high composition of Fe in the sample. At temperatures beyond 1000 °C, phases of Periclase, Ulvospinel, and Quandilite are observed. At 1250 °C, only Ulvospinel and $Fe_2MnO_4$ are observed. Beyond 1350 °C the sample showed only amorphous phases as a result of softening. Yallourn ash with 8% CaO also showed similarity as Yallourn ash at the beginning, however, showed phases of Jacobsite at 1000 °C and the sample turned amorphous around 1250 °C. This indicates that the addition of CaO reduced the softening temperatures of Yallourn ash. Finally, Morwell ash has major phases of Periclase and Magnesiowuestitie at room temperature. Morwell ash at 800 °C showed peaks due to Calcite, Diopside, and corundum. At 900 °C, the major peaks are due to Magnesioferrite and Magnetite at 1100 °C. The sample showed amorphous peaks beyond 1200 °C.

Insitu synchrotron XRD studies provided insights into the major crystalline phases present in the Victorian brown coal ash samples. The results qualitatively identified the ash

softening temperatures and the positive effects of CaO flux addition in reducing the softening temperatures of the ash. For example, 8% CaO addition to Yallourn ash showed a reduction of softening temperature by 100 $^{o}$C.

The results assist in the selection of a temperature for the measurement of viscosity of Victorian brown coal ash. The results show that the initial softening temperatures of the sample start at 1300 $^{o}$C. The results also identify the different phases formed as the ash is heated. But these do not indicate the extent of liquid or solid present in the ash as a function of temperature. This is described in the next section.

Hence, to predict the slag melting and its ability to flow, complementary modelling will be used to predict the % liquid in the slag and phase changes in the ash with temperature.

### 3.5 Phase diagrams of ash samples

FactSage software was used to predict phase changes for a $CaO$-$Al_2O_3$-$SiO_2$-$FeO$-$MgO$-$Na_2O$ system. This system was chosen as these are the major components of the three Victorian ash samples. The diagrams show the variation of phases with temperature and difference in ash composition. Phase diagrams were obtained for temperatures ranging from 1100-1600 $^oC$ to include a range where at the lowest temperature the ash is solid and at the highest temperature the ash is likely to be fully liquid.

#### 3.5.1 Phase diagrams of Yallourn ash

Figure 11 shows the change in phases with temperature for a system mimicking the Yallourn ash composition. Since Yallourn has high content of MgO (21%) which has high melting temperature of > 2850 $^oC$ the slag contains higher amounts of solid component. As the temperature increases, the solid phases present at lower temperatures gradually reduces and at 1400 $^oC$ there is a small percentage of solid components of $NaAlO_2$, MgO, and CaO. The actual composition of Yallourn coal in this system is represented by a label "YL" in Figure 11 shows it is a combination of liquid slag and solid MgO. It is seen that after a temperature of 1300 $^oC$ and by 1500 $^oC$, the ash progressively turns to liquid slag with < 5% solid content.

#### 3.5.2 Phase diagrams of Morwell ash

Figure 12 shows the phase diagrams for Morwell ash. The trend is similar to Yallourn ash, where the phases gradually reduce to liquid phase with increasing temperature with some solid content remaining at the end. The actual composition of the ash, as represented by the label "MW", eventually lies in the liquid phase with some solid MgO content at 1600 $^oC$. However, the amount of solid CaO and MgO content are relatively high compared to Yallourn ash. This can be attributed to the high melting temperatures of CaO and MgO above 2600 and 2850 $^oC$ respectively. The solid component in ash is >30 % at 1600 $^oC$. The high percentage of solid content can be a problem for the flow of slag during gasification and may require the addition of fluxing agent or coal blending to lower the slag tapping temperatures of Morwell slag.

#### 3.5.3 Phase diagrams of Loy Yang ash

Figure 13 shows the phase diagrams for Loy Yang ash. As the temperature increases, the number of phases gradually reduces and eventually at 1600 $^oC$ results in one major liquid phase, and two minor slag liquid phases with some solid content in the form of MgO and CaO even though the However, the CaO and MgO concentration of Loy Yang ash are relatively low at 3.36% and 0.85% respectively. However, Loy Yang ash contains high concentrations of alumina at 21.8%; the melting point is 2073 $^oC$, which prevents the ash from becoming completely molten. It is seen that the ash turns to liquid gradually beyond a temperature of 1200 $^oC$ and up to 1600 $^oC$. However, the solid components of ash are still present at >10% at temperatures of 1600 $^oC$, suggesting it would require high operational temperatures for the smooth removal of slag from the gasifier. The other alternative would be the addition of flux materials or coal blending to lower the slag tapping temperatures.

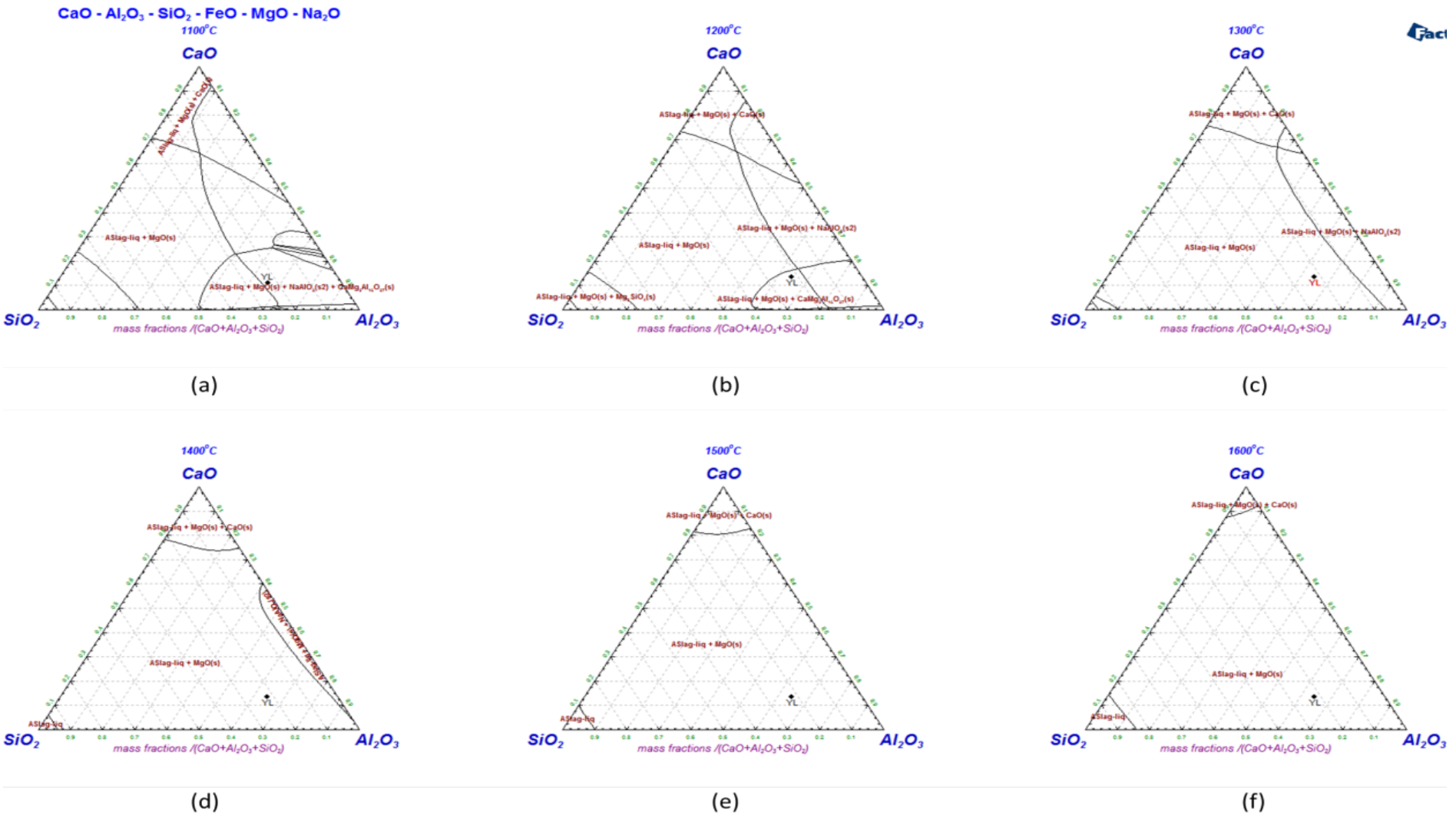


**Figure 11** Phase diagrams for $CaO$-$Al_2O_3$-$SiO_2$-FeO-MgO-$Na_2O$ system mimicking Yallourn ash composition at (a) 1100 ºC, (b) 1200 ºC (c) 1300 ºC, (d) 1400 ºC (e) 1500 ºC, (f) 1600 ºC.

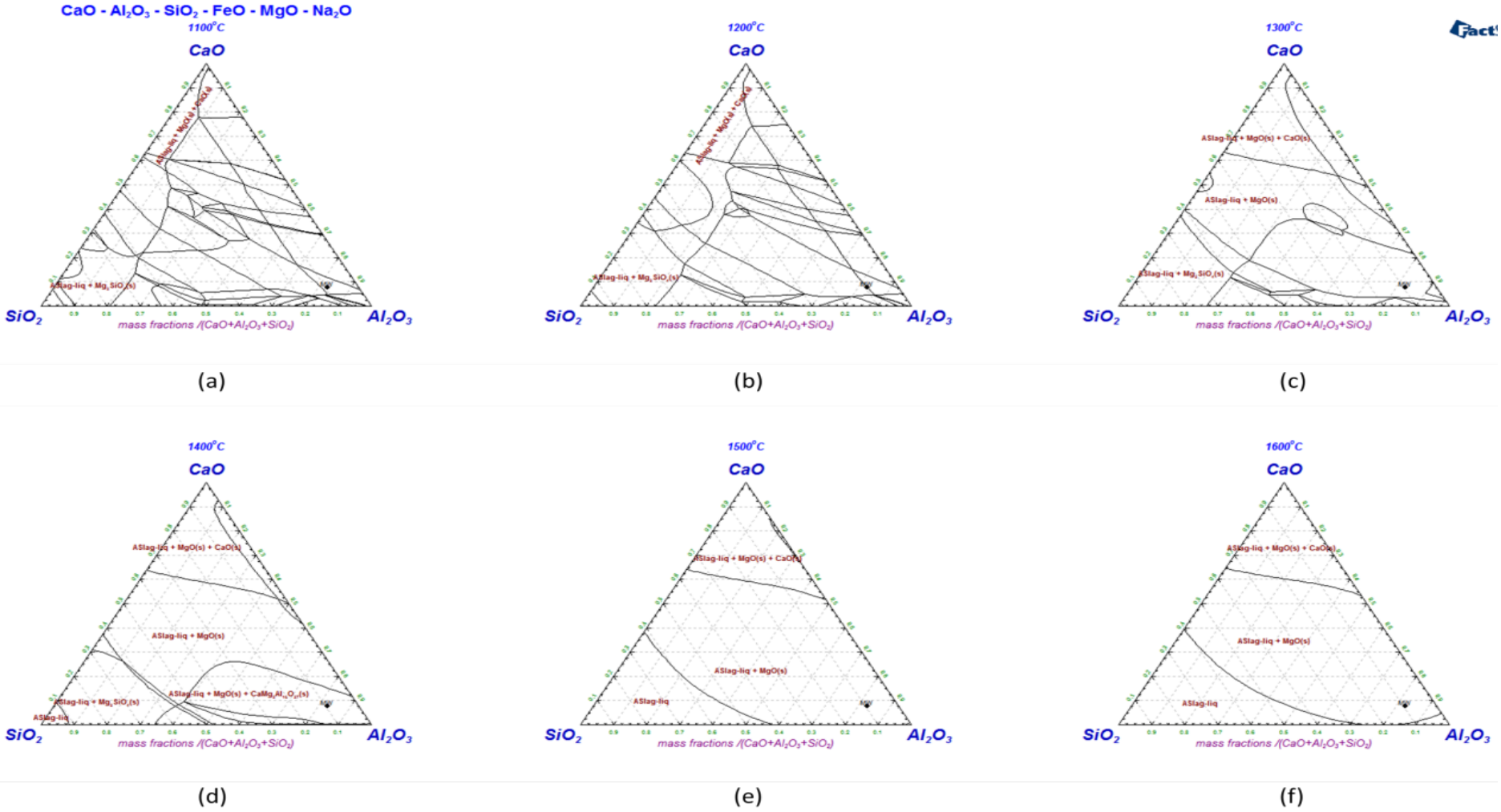


**Figure 12** Phase diagrams for $CaO$-$Al_2O_3$-$SiO_2$-FeO-MgO-$Na_2O$ system mimicking Morwell ash composition (a)1100 °C, (b) 1200 °C (c) 1300 °C, (d) 1400 °C (e) 1500 °C, (f) 1600 °C.

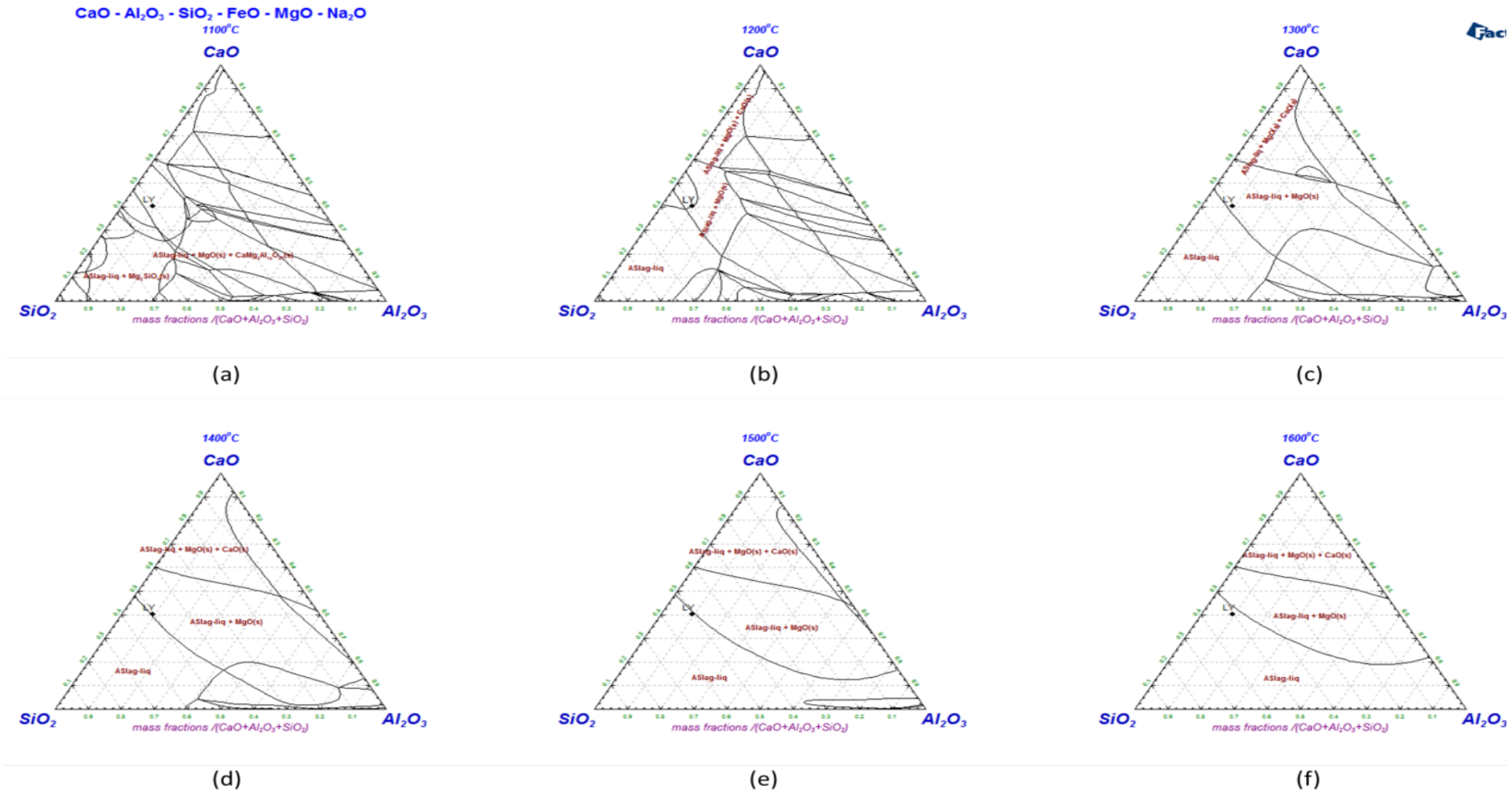


**Figure 13** Phase diagrams for $CaO-Al_2O_3-SiO_2-FeO-MgO-Na_2O$ system mimicking Loy Yang ash composition (a)1100 $^oC$, (b) 1200 $^oC$ (c) 1300 $^oC$, (d) 1400 $^oC$ (e) 1500 $^oC$, (f) 1600 $^oC$.

### 3.5.4 Conclusion

Phase diagrams for systems corresponding to the ash composition of the three ash were obtained for temperatures 1100-1600 $^{o}$C. The results indicate the following:

**Yallourn:** The solid components in Yallourn ash gradually reduced and become minimum (<5%) at 1400 $^{o}$C. The Yallourn composition at 1400 $^{o}$C showed liquid slag in combination with solid MgO. The effect of this on the viscosity needs to be verified experimentally.

**Morwell:** Morwell showed higher concentrations of solid (>30%) concentration at 16ss00 $^{o}$C suggesting it inability to achieve molten slag at these temperatures. The reason for the higher concentration of the solid component is due to the presence of CaO and MgO at 31.2% and 29.4%. These two components also have very high melting temperatures affecting the slagging temperature of Morwell ash.

**Loy Yang:** Loy Yang ash retains almost 10% solids content even above 1500 C become completely molten only above 1500 $^{o}$Cdue to its high alumina content.

The results also indicate the need for additional predictive calculation with ash and flux materials. These are shown in the next section. However, these predictions needs to be verified with actual viscosity measurements.

## 3.6 Variation of liquid fraction in ash samples with temperature - thermodynamic modelling

As indicated in the previous section, thermodynamic calculations were conducted to examine the impact of flux addition on the % liquid fraction in ash at different temperatures. The calculations were repeated for three ash compositions over a range of temperature (1000 - 1600 $^{o}$C) with two types of flux (CaO and clay) and under two environments ($N_2$ and $CO_2$). These calculations will be helpful in determining the type and quantity of flux for each coal to be used in viscosity measurement. Figures 14-16 show the variation of percentage liquid with different flux amounts and over a range of temperature.

### 3.6.1 Loy Yang ash

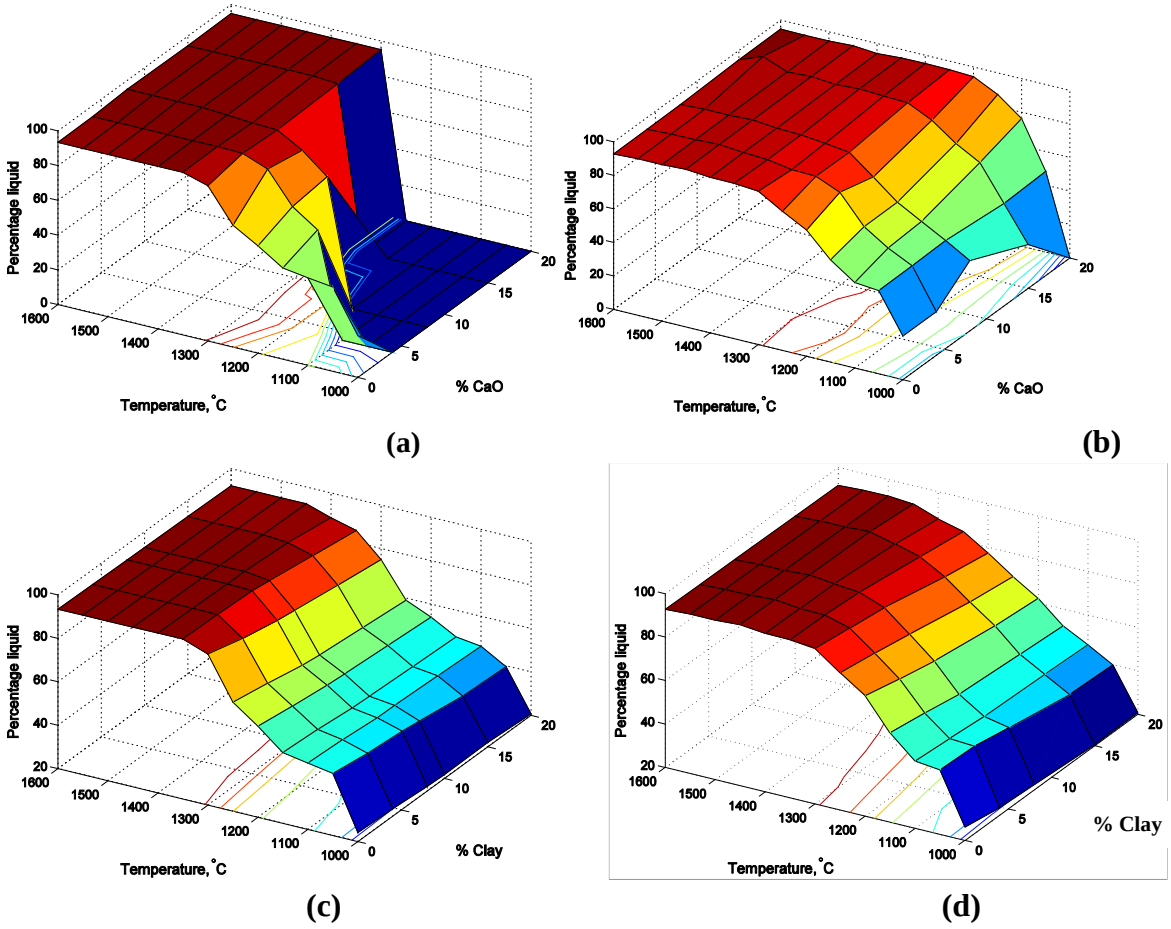


**Figure 14** Percentage Liquid variation for Loy Yang ash (a) CaO flux- Inert environment (b) CaO flux – $CO_2$ environment (c) Clay flux- Inert environment (b) Clay flux – $CO_2$ environment

Figure 14 shows the results on Loy Yang ash in the inert and $CO_2$ environment. It is apparent that Loy Yang in the inert environment will attain close to 90% liquid formation at temperatures above 1350 $^{o}$C beyond which there is no major change until 1600 $^{o}$C. The addition of CaO showed variation in the % liquid formation at the low-temperature range but did not lower the overall temperature suggesting the addition of CaO has little effect on Loy Yang ash in an inert environment. However, in $CO_2$ environment 15% CaO resulted in 95% liquid by

1550 $^{o}$C. The results suggest that large amount of CaO flux is needed to observe significant change in the % liquid formation on Loy Yang ash.

On the other hand, the effect of mixing clay was also assessed and the results are presented in Figures 14 (c) and (d). The results indicate that addition of clay as flux lowered the % liquid formation in Loy Yang ash, more compared to CaO addition. The results suggest that clay has a negative effect on enhancing the liquid formation and cannot be used as a flux material on Loy Yang ash. The negative effect of clay addition may be due to the high silica content of clay higher than the level in Loy Yang ash.

### 3.6.2 Morwell ash

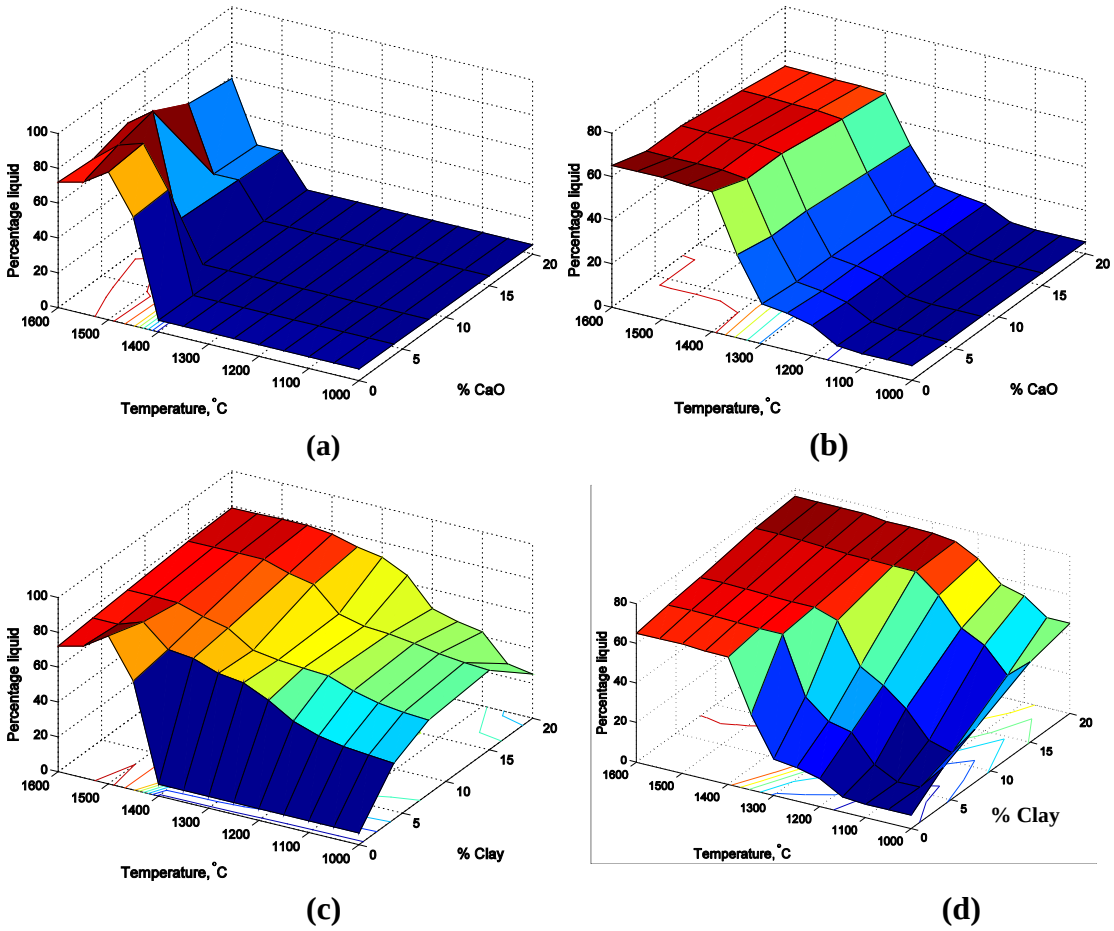


**Figure 15** Percentage Liquid variation for Morwell ash (a) CaO flux- Inert environment (b) CaO flux – $CO_2$ environment (c) Clay flux- Inert environment (b) Clay flux – $CO_2$ environment.

As evident from Figure 15(a), Morwell ash did not show any sign of liquid formation until 1400 $^{o}$C in inert conditions suggesting a high melting point of the ash. AFT measurements also indicate that the sample did not show any sign of softening until 1550 $^{o}$C; this is in accordance with the observation. However, when the temperature increased beyond 1450 $^{o}$C the liquid concentration increased by almost 75%. The addition of CaO only slightly lowered the softening temperature, but overall no major change was noticed in the % liquid formation

suggesting CaO addition would not be appropriate for slagging of Morwell ash. Similarly, in the reducing environment, the addition of CaO slightly lowered the initial melting temperatures to 1350 $^{o}$C and reached 65% liquid content at 1400 $^{o}$C. The addition of higher amounts of CaO further lowered the % liquid formation. The high inherent CaO (31.2%) in Morwell ash also works against the addition of CaO as flux. When the CaO exceeds 38% in the ash, the high melting point of it takes over and have a negative effect on the AFTs of the ash[2].

When 15% clay was added as a flux in reducing conditions the samples showed an increase in the liquid formation to 75%, suggesting the addition of clay can lower the slagging temperature of the Morwell ash. However, the highest liquid % achieved is still below 80% at 20% clay addition suggesting Morwell ash on its own or in combination with clay is unlikely to result in a flowing slag. The other alternative such as blending Morwell coal with other coals should be considered to lower the slagging temperature of mixed ash down to acceptable temperature range.

### 3.6.3 Yallourn ash

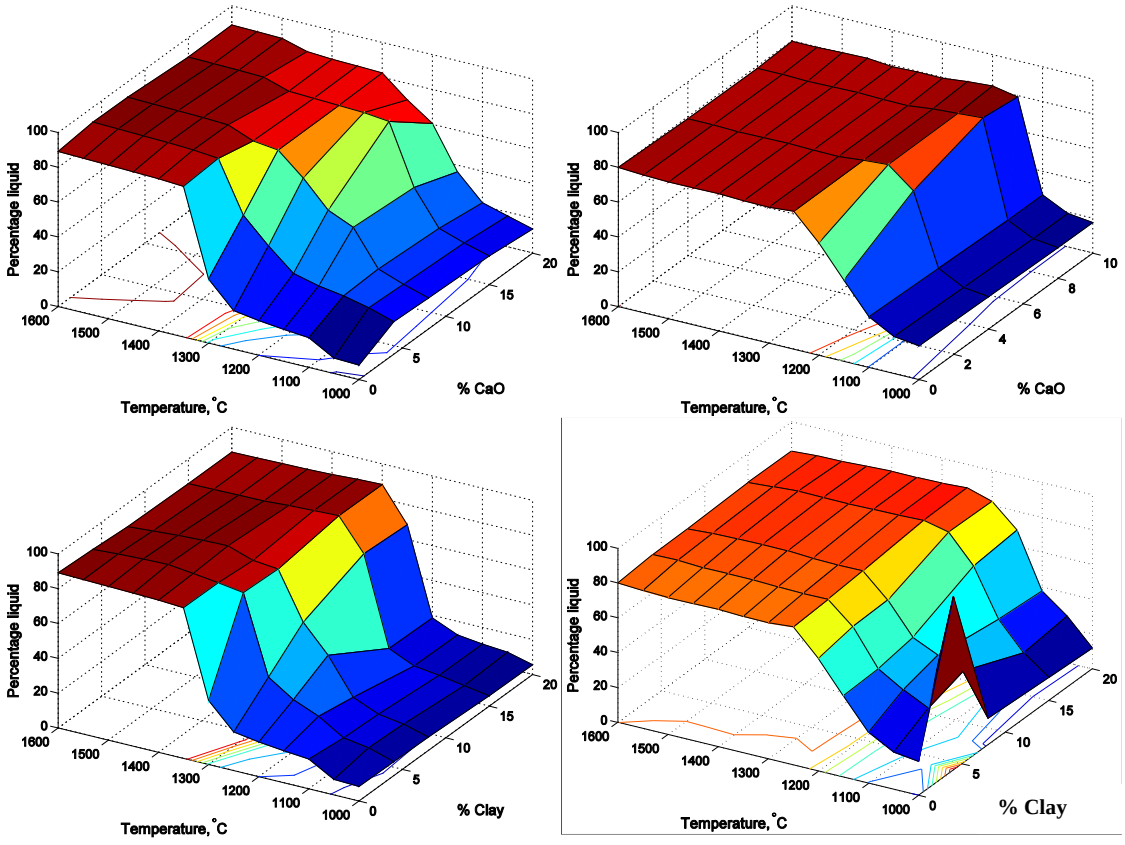


**Figure 16** Percentage Liquid variation for Yallourn ash (a) CaO flux- Inert environment (b) CaO flux – $CO_2$ environment (c) Clay flux- Inert environment (b) Clay flux – $CO_2$ environment

Yallourn ash in Figure 16 (a) show very low <20% liquid formation until 1300 $^{o}$C in an inert environment. However, there is a rapid increase to 85% liquid formation at 1350 $^{o}$C and

beyond. The addition of CaO improved the % liquid formation at lower temperature range suggesting its positive effect in melting the ash at relatively lower temperatures than Yallourn ash alone. The increase in % liquid formation trend was observed until 15% CaO addition, beyond which the %-age liquid formation decreased suggesting an optimum for CaO addition. In reducing environment the addition of CaO has no positive effect in increasing the % liquid formation as shown in Figure 16 (b). The results suggest CaO addition to Yallourn coal will not lower the ash melting temperatures under gasification conditions.

When clay is used as flux in inert environment the % liquid formation increased reaching a maximum of 90% at 8% addition. On the other hand, the % liquid formation remained at 80% in reducing environment suggesting clay will not have any positive effect on the liquid slag formation during gasification conditions.

### 3.6.4 Conclusion from thermodynamic calculations

Thermodynamic calculations were used for the prediction of % liquid formation in Victorian brown coal slag in both oxidising and reducing conditions. The effect of the addition of flux CaO and clay was also tested. The results indicate the following:

**Loy Yang ash**: Loy Yang ash can reach 90% liquid slag formation above 1350 $^{o}$C and remain almost stable beyond that temperature until 1600 $^{o}$C. The addition of CaO flux increased the % liquid formation to 95% in reducing atmosphere at 15% CaO addition. However, the results are contradictory to the ash fusion tests where the flow temperatures are measured at >1460 $^{o}$C, and phase diagram results show at least 25% solid content presence at 1600 $^{o}$C. With the addition of clay, liquid formation increased to 90% at 1450 $^{o}$C.

**Morwell ash:** Morwell ash did not show any sign of liquid formation until 1400 $^{o}$C and reached >70% liquid at 1600 $^{o}$C suggesting that it will require very high temperatures for its slagging. The addition of CaO did increase the % liquid to 75% at 1600 $^{o}$C. In reducing conditions the % liquid remained stable at 65% and CaO had no effect in improving the % liquid formation. On the other hand, clay improved % liquid formation with increased addition. However, it was around 80% suggesting that Morwell ash cannot be slagged below 1600 $^{o}$C even with the addition of flux materials. These observations are consistent with ash fusion tests and phase diagrams. The results conclude that it would be difficult to use Morwell coal alone in the gasifier and may require alternative methods such as coal blending to lower the slagging temperature of the ash.

**Yallourn ash:** Yallourn ash shows 90% liquid slag formation beyond 1400 $^{o}$C under inert conditions. Addition of CaO and clay showed a showed a slight increase in % liquid formation in inert conditions. However, in reducing condition for Yallourn ash and both CaO and clay added ash, the liquid formation did not exceed 80%.

## 3.7 Differential Thermal Analysis (DTA)

The ash samples undergo reduction, oxidation, phase transformations, decomposition, sintering or agglomeration with temperature. Differential Thermal Analysis (DTA) provides the insights of ash behaviour with heat absorption and release during different phase transformations taking place in the ash samples. The DTA graphs also shows the temperatures at which phases changes take place.

The experiments were conducted using a Perkin Elmer STA8000 simultaneous thermal analyser. Prior to the run, the system was stabilised at 50 $^{o}$C for 2min in flowing 30% $CO_2$ balanced with $N_2$ atmosphere at the rate of 100 ml/min. Once stabilised the samples were heated from 50 $^{o}$C to 1500 $^{o}$C at the rate of 20 $^{o}$C/min in the same gas flow. The effect of flux addition on the thermal behaviour of the samples was also studied by mixed different quantities of CaO (4, 6, 8, and 15%). Prior to an experiment with the sample, the crucible used for the run was treated in the same manner without the sample to obtain a background. Subtraction of the empty background from the sample run gives the actual thermal behaviour of the sample.

### 3.7.1 DTA analysis

The DTA analysis of coal ash samples in flowing $CO_2$ atmosphere, changes in the weight of the sample and also the heat flow curves during heating them from 50 $^{o}$C to 1500 $^{o}$C were recorded. Figures 17-19 show the weight loss or thermogravimetric (TG) curve, differential weight loss or differential TG curve and heat flow curves for Loy Yang (LY), Yallourn ash (YL), Morwell ash (MW) ash samples. Each ash sample is grouped with 4, 6, 8, and 15% CaO flux added to the ash prepared at 815 $^{o}$C. The discussion here is split in two sections with weight changes before 820 $^{o}$C classified as the low-temperature section and the data beyond 820 $^{o}$C as the high-temperature section.

***Low temperature range***

Thermogravimetric (TG) curve and corresponding differential thermogravimetric (DTG) on Loy Yang ash sample were shown in Figure 17. The TG curve showed a continuous but very small decrease in the weight of the sample until 800 $^{o}$C which is due to the loss of residual moisture, unburnt carbon combustion and gasification in the sample. However, when varying amounts of CaO flux was added, all the samples showed an increase in weight in the temperature range of 380 $^{o}$C to 580 $^{o}$C. This can be attributed to the formation of $CaCO_3$ by the reaction of CaO flux added to the sample and $CO_2$ present in the carrier gas. CaO is commonly used as a solid sorbent for the capture of $CO_2$ from flue gas streams as $CaCO_3$ at 500 $^{o}$C and release pure $CO_2$ at above 800 $^{o}$C[6, 7]. Loy Yang ash only contains 0.88% of CaO, and did not show any weight gain due to adsorption of $CO_2$ nor desorption of $CO_2$ at higher temperatures suggest that Ca in Loy Yang ash is not in a form that can allow capture of $CO_2$. The samples with CaO added to them showed a sharp drop in the weight of the sample at 820 $^{o}$C due to the release of $CO_2$ adsorbed on the CaO. The weight loss increased with the concentration of CaO flux added suggested the formation of $CaCO_3$.

Figure 18 shows the TG and DTG curve of Yallourn ash. The curve did not show any peaks either due to adsorption or desorption of $CO_2$ as observed in case of Loy Yang ash. This indicates that Ca (9.2%) in the ash is not present as CaO which can adsorb and desorb $CO_2$. It is present in the combination of other components present in the ash. However, with the addition of CaO, it followed a similar trend as in Loy Yang ash with adsorption of $CO_2$ between 380-500 $^oC$ and desorption at 800 $^oC$ and beyond.

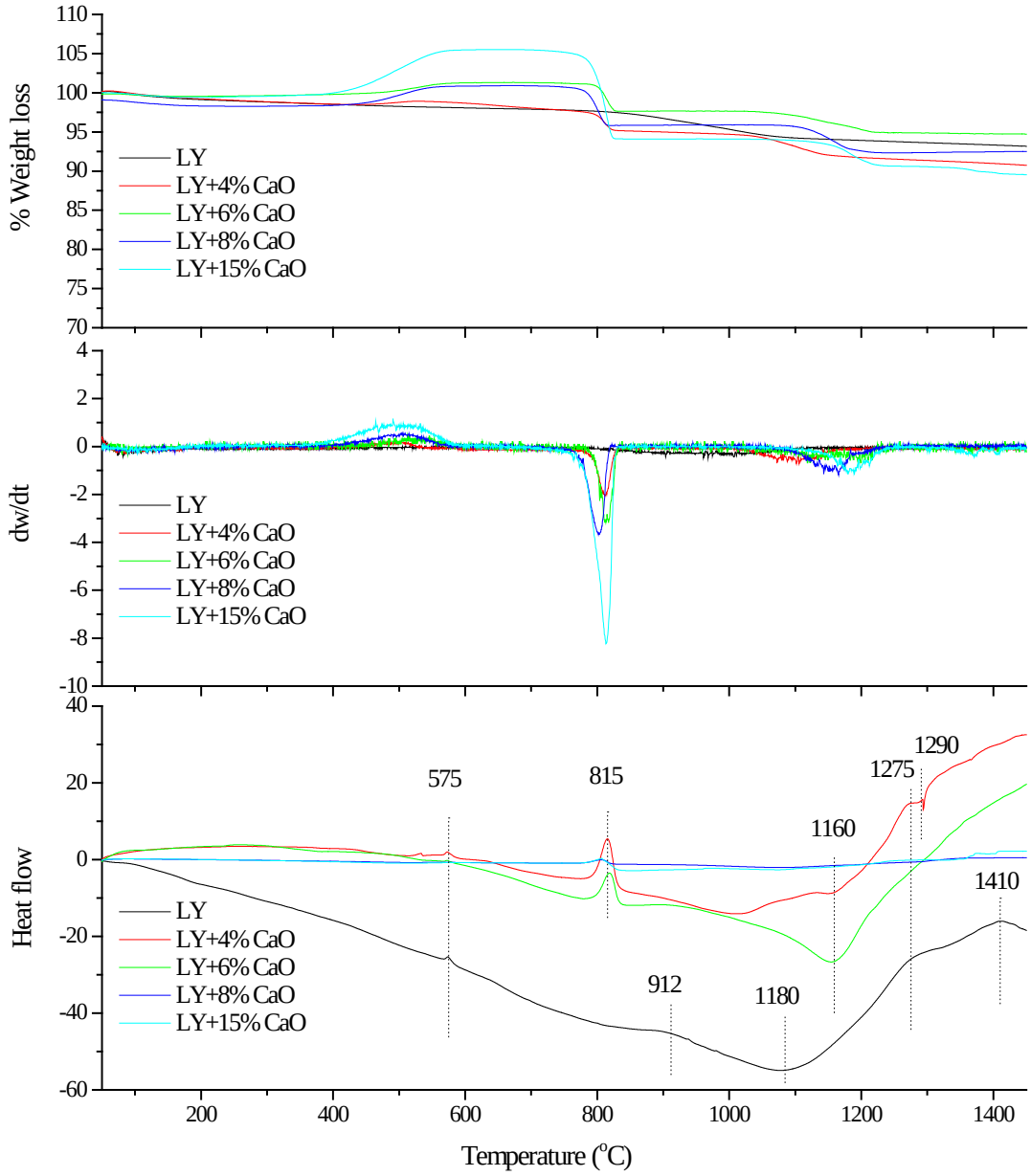


**Figure 17** TG, DTG and heat flow curves of Loy Yang ash prepared at 815 $^oC$ and the effect of 4, 6, 8, and 15 % CaO flux additions. Endothermic – positive peak (crest) and exothermic peak – negative peak (trough) in the heat flow curve.

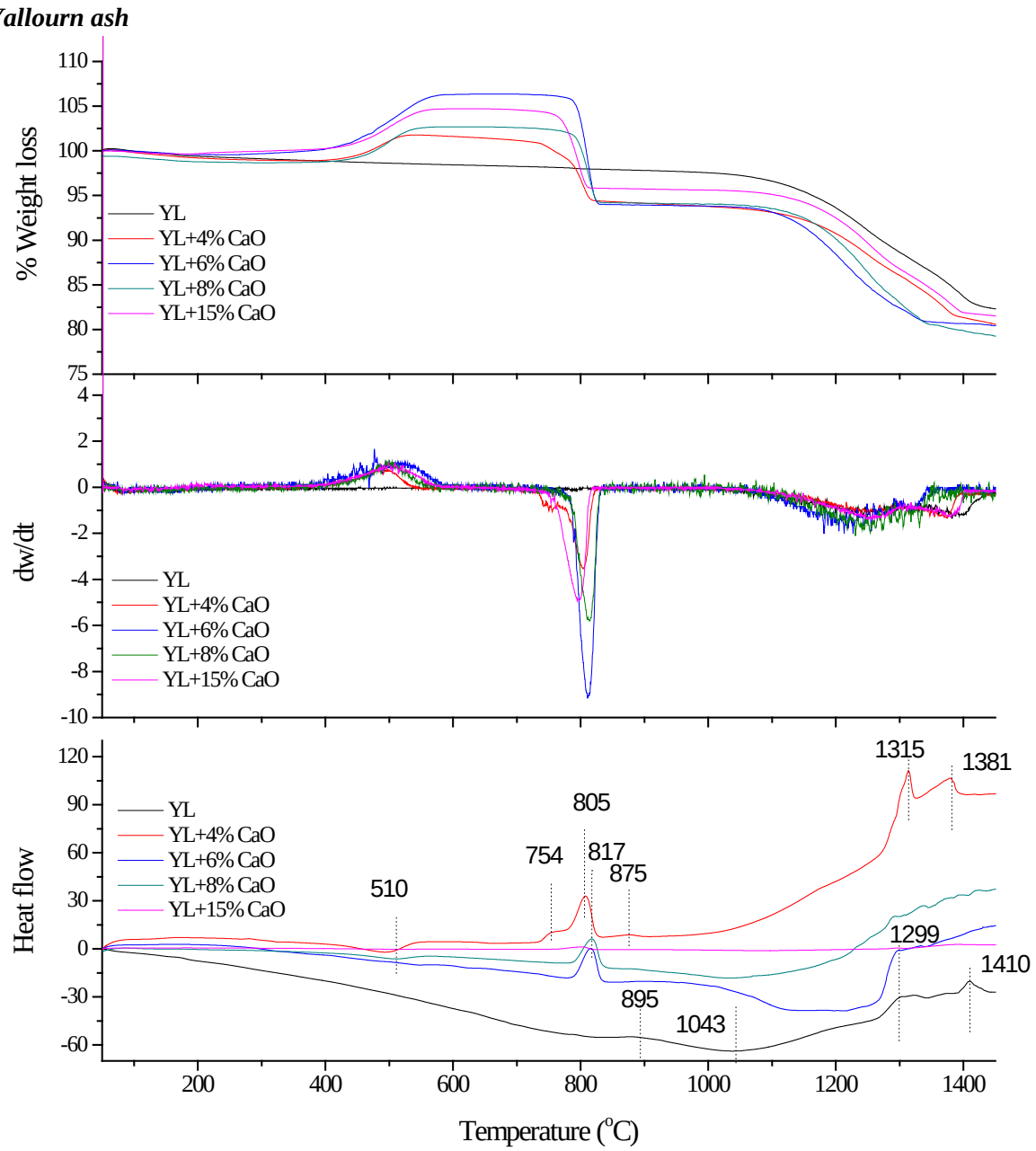


**Figure 18** TG, DTG and heat flow curves of Yallourn ash prepared at 815 °C and the effect of 4, 6, 8, and 15 % CaO flux additions. Endothermic – positive peak (crest) and exothermic peak – negative peak (trough) in the heat flow curve

The TG curve for Morwell ash (Figure 19) showed 1.6 wt% loss at 780 °C suggesting $CO_2$ release from the sample at these temperatures. The $CO_2$ adsorption/desorption in Morwell ash can be due to the presence of a minor portion of Ca present in the ash is in CaO form. A minor $CO_2$ adsorption peak compared to the amount of CaO (31.2%) present in the ash indicates that majority of Ca present in the ash is present as a mixed mineral form with a small proportion present as free CaO. Interestingly, the addition of 4% CaO to Morwell ash did not show any $CO_2$ adsorption/desorption unlike Loy Yang and Yallourn samples. This may be due to the reaction of CaO with other phases present in the ash. At higher CaO flux additions, the

samples showed $CO_2$ adsorption/desorption similar to the Loy Yang and Yallourn samples added with CaO flux.

***High temperature range***

Loy Yang ash (Figure 17) showed a continuous weight loss starting from 820 $^oC$ to 1000 $^oC$ of about 4.1%. This can be attributed to the decomposition or evaporation of sulphates, chlorides or oxides of Na and K[8, 9]. For the samples with 4% CaO flux, the starting point of the weight loss shifted to higher temperatures, 1105 $^oC$. With the addition of 6% CaO the starting position further shifted to 1200 $^oC$. However, there is no major change in the % weight loss in the sample. The DTG curves show a change in differential weight loss behaviour from a broader trough to a sharp peak with 8% CaO, with the peak centred at 1160 $^oC$. At 15% CaO the peak position shifted to 1184 $^oC$. This shift in temperature increased with the amount of CaO flux added, suggesting CaO has increased the thermal stability of the mineral composition present in the Loy Yang ash sample.

For Yallourn samples (Figure 18), the weight loss at the high-temperature zone occurred only above 1100 $^oC$ and is about 15.3%. DTG curves above 1100 $^oC$ show the Yallourn ash has two major weight losses- first one centred at 1250 $^oC$ and the second one above 1380 $^oC$. With the addition of 4% CaO the peak position at 1400 $^oC$ shifted to lower temperature. At 6 % CaO addition, the high-temperature peak shifted to lower temperature and converged with the first peak at 1250 $^oC$ forming a single peak. Increase in CaO addition until 8% CaO also shifted the first peak to slightly lower temperatures suggesting the positive effect of CaO addition in the decomposition of the mineral matter. However at 15% CaO addition the second peak re-emerged suggesting the reversal of the effect by CaO addition to the Yallourn ash.

In the case of Morwell ash (Figure 19), the weight loss of the sample started at 1080 $^oC$ and continued until 1400 $^oC$. Morwell samples exhibit high weight loss, approximately 22%, which can be attributed to the release of Na compounds. This is consistent with the ash composition of Morwell ash with $Na_2O$ (6.29%) and $SO_3$ (7.57%). With 4% CaO addition the weight loss in this temperature region was decreased which indicates the formation of some complex phases between CaO and mineral matter. However, with the addition of 8 and 15% CaO the weight loss increased and the temperature range of the weight loss shifted to lower temperature regions below 1350 $^oC$.

### 3.7.2 Heat flow curves

For the heat flow curves, upward peaks represent the endothermic process and the downward peaks represent the exothermic process. Endothermic peaks may be interpreted as indicators of reduction, vaporisation or melting; exothermic peaks indicate crystallisation and oxidation[10, 11].

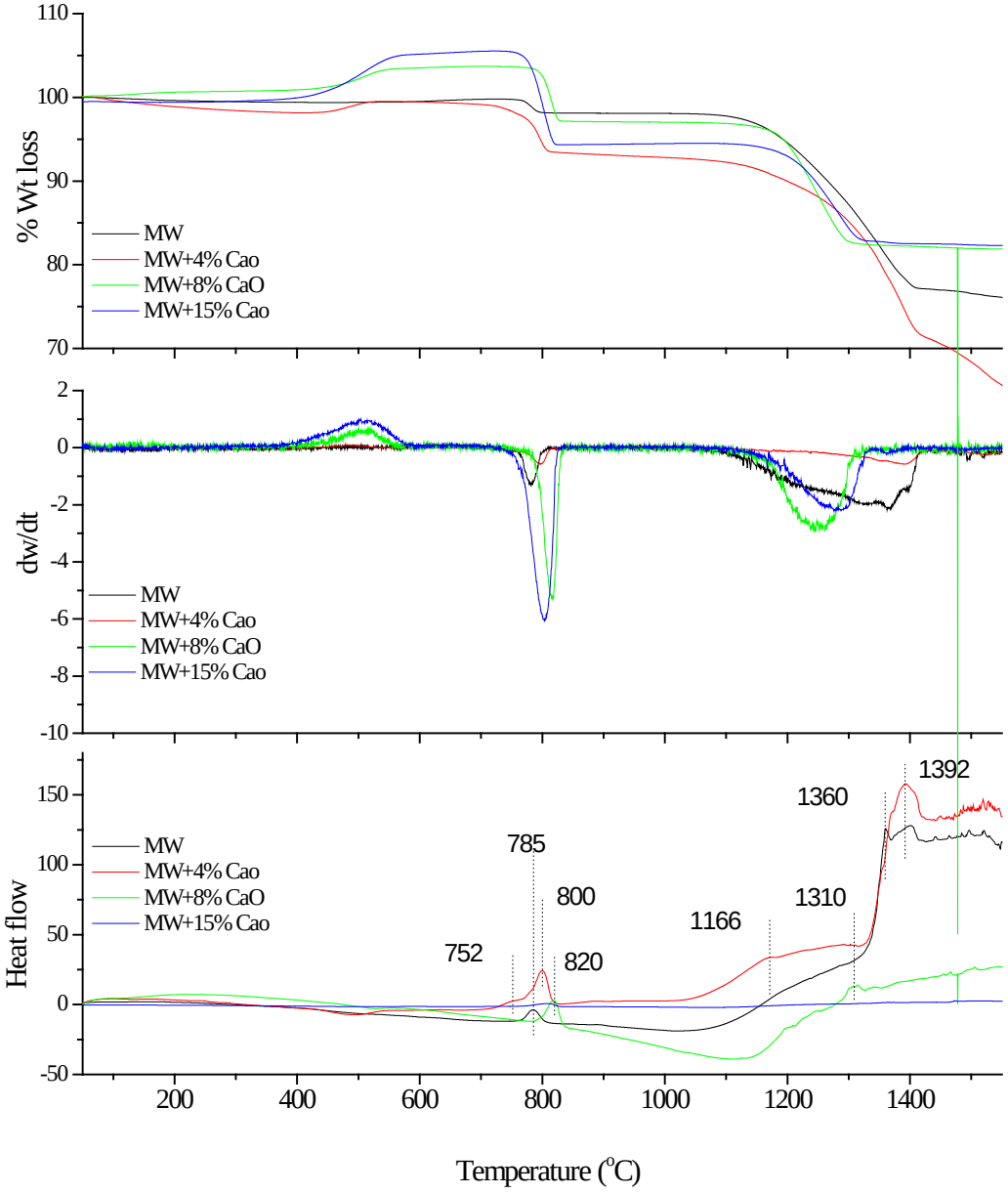


**Figure 19** TG, DTG and heat flow curves on Morwell ash prepared at 815 ºC and the effect of 4, 6, 8, and 15 % CaO flux additions. Endothermic – positive peak (crest) and exothermic peak – negative peak (trough) in the heat flow curve

***Loy Yang ash***

The heat flow curve of LY ash shows a continuous decline in the profile suggesting exothermic reactions taking place. For Loy Yang ash sample without any additional CaO, the profile shows continuous exothermic peak starting from 50 ºC to 1100 ºC indicating oxidation and crystallisation. The dip at 50-110 ºC is attributed to the loss of residual moisture and a small endothermic peak at 575 ºC represents quartz α→β transformation[12]. The exothermic heat flow profile from 50 ºC to 1100 ºC indicates crystallisation and the large size of the peak indicates a high degree of crystallisation[13]. The exothermic nature may also be due to the combustion of any unburnt carbon left in the sample. The exothermic nature in the sample can be attributed to the dehydroxylation of Fe, Al, and Ca-Mg hydroxides from 200-620 ºC, Fe

sulphate decomposition between 470-810 $^{o}$C[14, 15]. The sample also showed broad endothermic peak centred at 912 $^{o}$C which can be attributed to the clay mineral destruction and formation of mullite, spinel, and corundum. The broad exothermic dip between 900-1200 $^{o}$C can be attributed to a variety of reactions taking place in the minerals present in ash. The temperature range between 960-1000 $^{o}$C is attributed to the reactions between CaO and silicates. Above 1000 $^{o}$C the peaks are attributed due to crystallisation of amorphous silica to cristobalite, the formation of corundum (crystalline form of $Al_2O_3$) with traces of Fe, Ti and Cr[14]. This observation on Loy Yang ash is due to the high $SiO_2$ (63.65%) and $Al_2O_3$ (21.86%) concentration present in it.

Beyond 1100 $^{o}$C, the sample showed a continuous endothermic profile with two humps at 1275 $^{o}$C and 1410 $^{o}$C respectively. The endothermic profile here represents the softening and hemispherical temperature (of ash fusion tests) of slags as observed from ash fusion results which absorb heat during the process. The exothermic raise from 1100 to 1300 $^{o}$C is attributed to the initial softening of montmorillonite and illite which are the phases of combination of aluminium silicates of soda, potassium or lime. The hump at 1275 $^{o}$C is attributed to quartz softening and the peak at 1410 $^{o}$C is due to melting of or Fe-Ca-Mg silicates.

The samples with 4 and 6% CaO addition initially until 300 $^{o}$C showed endothermic profiles, beyond which an exothermic profile become evident. The exothermic dip beyond 300 $^{o}$C can be attributed to the adsorption of $CO_2$ in the gas stream by the CaO added to the sample since adsorption of $CO_2$ is an exothermic reaction. An addition of 4% CaO sample showed an endothermic peak at 533 $^{o}$C along with quartz inversion peak at 575 $^{o}$C. Further, both the samples showed endothermic peaks centred at 815 $^{o}$C due to the desorption of $CO_2$ from $CaCO_3$. Beyond this temperature though the samples show an exothermic dip in the profile; 4% CaO showed endothermic peaks at 1075 and 1125 $^{o}$C, whereas these peaks did not appear in the sample with 6% CaO addition. The peak at 1080 $^{o}$C in Loy Yang ash is shifted to 1160 $^{o}$C for both the samples. The high temperatures peaks at 1275 $^{o}$C and 1410 $^{o}$C due to melting of quartz and melting of Fe-Ca and Fe-Ca-Mg spinels converged at 1160 $^{o}$C suggesting this point as the new softening temperature of the sample. However, in samples with 8% and 15% CaO added, the profile remained almost linear to X-axis with minimal heat absorption or release, suggesting little or no effect of CaO addition beyond 6%.

Yallourn ash is rich in $Fe_2O_3$ (46.3%) followed by MgO (15.3%), and CaO (11.9%). Yallourn ash showed continuous exothermic profile which extends from the onset to 1050 $^{o}$C. This initial exothermic profile can be attributed to dehydroxylation of Fe 200-400 $^{o}$C; decomposition of Ca-Mg oxides 350-620 $^{o}$C, Fe sulphates decomposition 470-810 $^{o}$C. The samples showed endothermic peaks at 895 $^{o}$C, 1299 $^{o}$C, and 1410 $^{o}$C. The peak at 895 $^{o}$C indicates the decomposition of calcite and dolomite; corundum and cristobalite formations are observed at 1299 $^{o}$C and melting of the mineral phases was observed at 1410 $^{o}$C.

Addition of 4 and 6% CaO to Yallourn ash showed broad endothermic profile from ambient to 300 $^{o}$C which can be attributed to the dehydroxylation of Fe and dehydration of gypsum $CaSO_4$. However, the intensity of the hump is less in the sample with 6% CaO than

in the sample with 4% CaO added. Both the samples showed exothermic peaks at 495-510 $^{o}$C due to adsorption of $CO_2$ on CaO. This is followed by an endothermic peak at 810 $^{o}$C due to the release of $CO_2$. 4% CaO with a heat release at 875 $^{o}$C continued to an exponential endothermic profiles with sharp peaks at 1314 $^{o}$C and 1378 $^{o}$C. Small exothermic kinks observed at 510 $^{o}$C which is indicative of the adsorption of $CO_2$ on CaO. The samples also showed endothermic peaks centred at 800-820 $^{o}$C for the decomposition of $CaCO_3$. However, with the addition of CaO the broad exothermic profile observed in Yallourn ash was reduced. The addition of 4% CaO, the profile remained endothermic beyond 1000 $^{o}$C. With the sample also showed two sharp endothermic peaks centred at 1315 $^{o}$C and 1381 $^{o}$C consistent with a slight decrease in the final melting temperature from 1410 $^{o}$C. With the addition of 6 and 8% CaO, the profile again showed exothermic behaviour like Yallourn ash. This observation suggests the reaction of CaO with some components of ash, releasing heat. In these samples, the final endothermic peaks also shifted to 1300 $^{o}$C suggesting a positive effect of CaO in reducing the softening or melting temperatures of the ash. However, with 15% CaO addition the sample did not show a major difference in heat flow profile and remained flat throughout suggesting 15% CaO flux has made the sample very resistant to any phase changes at temperatures to 1500 $^{o}$C.

***Morwell ash***

The major inorganic components of Morwell ash are CaO (31.2%), MgO (29.45%), and $Fe_2O_3$ (17.5%). The ash composition suggests that the samples have high amounts Ca present in the sample and further addition of CaO as flux will not be beneficial in reducing the melting point of the slag. However, TG curve suggests that only 4.2% of the Ca is present as CaO and the remaining is present in either mixed oxide or silicate or sulphate form. Alternatively, the Morwell ash also contains relatively low concentrations of $SiO_2$ and $Al_2O_3$ suggesting fewer transformations/melting of glass phases. The Morwell ash showed lean exothermic profile until 1100 $^{o}$C. The ash sample shows an exothermic peak at 815 $^{o}$C for the release of $CO_2$ from $CaCO_3$ present in the samples. The profiles showed an endothermic hump from 1100 $^{o}$C to 1300 $^{o}$C which can be related to initial α-quartz softening. Further, the profile showed two sharp endothermic peaks at 1360 $^{o}$C followed by a peak at 1400 $^{o}$C. The peak at 1360 $^{o}$C is attributed to the initial melting of Fe-Ca oxides, followed by Ca-Fe-Mg silicates at 1400 $^{o}$C.[14].

Morwell ash with 4% CaO showed no change until 1050 $^{o}$C without any major transformations expect at 500 and 815 $^{o}$C for $CO_2$ adsorption and desorption due to the addition of CaO to the ash sample. Beyond 1000 $^{o}$C the profile showed broad endothermic peak centred at 1166 $^{o}$C which is likely due to the interaction of CaO, and $SiO_2$ and $Al_2O_3$ forming new phase. At 1320 $^{o}$C, the profile showed sharp endothermic rise with maxima at 1392 $^{o}$C similar to the Morwell ash alone. The strong endothermic nature beyond 1320 $^{o}$C in all the samples is accompanied with weight loss suggesting decomposition or evaporation of components present in the sample. With the increase in CaO to 8%, the exothermic nature of the profile between 800-1150 $^{o}$C is more pronounced than the Morwell ash. However, at 15% CaO, the profile stayed flat throughout suggesting flux addition has exceeded its optimum.

### 3.7.3 Conclusion

TG and DTG curves of the ash samples show weight loss of Victorian brown coal ashes during heating in $CO_2$ environment from ambient to 1500 $^oC$. Loy Yang and Yallourn sample only showed relatively lower weight loss of 4.2% and 15.3% respectively, whereas Morwell showed higher weight loss close to 25% weight loss between 1000-1350 $^oC$. The higher amount of weight loss in Morwell is in line with the ash composition with a high amount of Na, Ca and S present in it. These components of ash have low decomposition temperatures or boiling points. In case of CaO flux added samples, weight gain at 400-500 $^oC$ due to the adsorption of $CO_2$ and weight loss at 800 $^oC$ due to the desorption of $CO_2$ from $CaCO_3$. Morwell ash addition of CaO shifted the weight loss peak to lower temperatures suggesting the positive effect of CaO in decomposing or breaking down of the components of ash.

Heat flow curve of Loy Yang and Yallourn ash shows continuous exothermic peak from ambient to 1100 $^oC$ suggesting the oxidation or crystallisation of phases present in the sample. Beyond 1100 $^oC$, the samples started to show endothermic peaks relating to softening or melting of components present in the samples. With the addition of CaO, the peaks at high temperatures shifted by at least 50-100 $^oC$ lower indicating a positive effect of the addition of CaO as flux material in decreasing the softening or melting temperatures of the samples.

Although DTA data showed insights into the behaviour of ashes at high temperatures, this alone does not provide a conclusive evidence of the behaviour of different phases present in the ash.

The characterization results and predictions of ash fusion, X-ray diffraction, DTA analysis, % liquid calculations and phase diagrams showed that Morwell ash would be the most difficult ash to melt and flow at temperatures below 1500 $^oC$. Loy Yang and Yallourn with flow temperatures of >1450 $^oC$ can be molten at lower temperatures with 4-8% CaO flux addition. However, the addition of clay has a negative effect on the liquidus temperatures. The characterization results and thermodynamic predictions have shown insights on possible melting and flow behaviours of the ash samples. However, these samples need to be tested in real gasifier conditions to determine the actual temperature range with desired viscosity of 100-250 Poise.

## 4 Trace elements in slag – measurement and modelling

Coal has several trace elements (heavy metals) some of which upon gasification at high temperature may release to the atmosphere and cause environmental and health concerns. Hence, it is important to know what elements are present in the coals and predict via modelling or estimate from experiments the level of their emission into the atmosphere.

### 4.1 Measurements

Victorian brown coal ash samples were treated at varying temperatures from 800-1300 $^{o}$C in a tubular furnace in reducing ($CO_2$) environment and the samples are analysed for the trace elements Zn, Mn, Ba, Cr, Ni and As. The reducing conditions was created to mimic entrained flow environment. These are the elements of "greatest and moderate" concern related to coal gasification.[16] The ash samples were also mixed with 4% and 8% CaO with Loy Yang and Yallourn ash. Similarly, 4%, 8%, and 15% CaO were mixed with Morwell ash and treated at varying temperatures 800-1300 $^{o}$C in $CO_2$ environment.

For the trace element analysis, the samples are prepared by the following procedure; 0.2g of the sample was weighed into a Teflon coated microwave digestion vessel. Then 6ml of 65% Nitric acid ($HNO_3$), 2ml of 30% (HCl) and 2ml of 30% hydrogen peroxide ($H_2O_2$) was added into the vessel[17]. The samples were digested in the microwave oven. After the digestion, the solution was transferred to 25ml of volumetric flasks, made up to volume with distilled water. With every set of sample one blank sample was also prepared to contain the only mixture of acids and distilled water.

#### 4.1.1 Yallourn ash

The results in Table 9 and Figure 20 below show the concentration and trends of the trace elements present after treating Yallourn ash at different temperatures in $CO_2$ atmosphere. The units of results are in wt%.

**Table 9 Trace elements in Yallourn ash samples**

| Sample | Zn | Mn | Ba | Cr | Ni | As |
|---|---|---|---|---|---|---|
| **YL-800 ºC** | 0.0069 | 0.446 | 0.764 | ND | 0.012 | 0.0085 |
| **YL-900 ºC** | 0.0077 | 0.439 | 0.611 | ND | 0.011 | 0.00072 |
| **YL-1100 ºC** | 0.0072 | 0.437 | 0.762 | ND | 0.0012 | ND |
| **YL-1300 ºC** | 0.0028 | 0.136 | 0.518 | ND | 0.005 | 0.00038 |
| **4% CaO-YL-800 ºC** | 0.0057 | 0.243 | 0.654 | 0.011 | 0.011 | ND |
| **4% CaO-YL-900 ºC** | 0.0061 | 0.305 | 0.78 | 0.0059 | 0.0011 | ND |
| **4% CaO-YL-1100 ºC** | 0.0052 | 0.267 | 0.838 | 0.0013 | 0.01 | ND |
| **4% CaO-YL-1200 ºC** | 0.0044 | 0.274 | 0.739 | 0.0029 | 0.0079 | ND |
| **8% CaO-YL-800** | 0.0098 | 0.429 | 0.869 | 0.32 | 0.019 | ND |
| **8% CaO-YL-900** | 0.0094 | 0.345 | 0.834 | 0.028 | 0.02 | ND |
| **8% CaO-YL-1100** | 0.0054 | 0.183 | 0.694 | 0.014 | 0.013 | ND |
| **8% CaO-YL-1200** | 0.00209 | 0.179 | 0.359 | 0.0031 | 0.0047 | ND |

ND-not detected

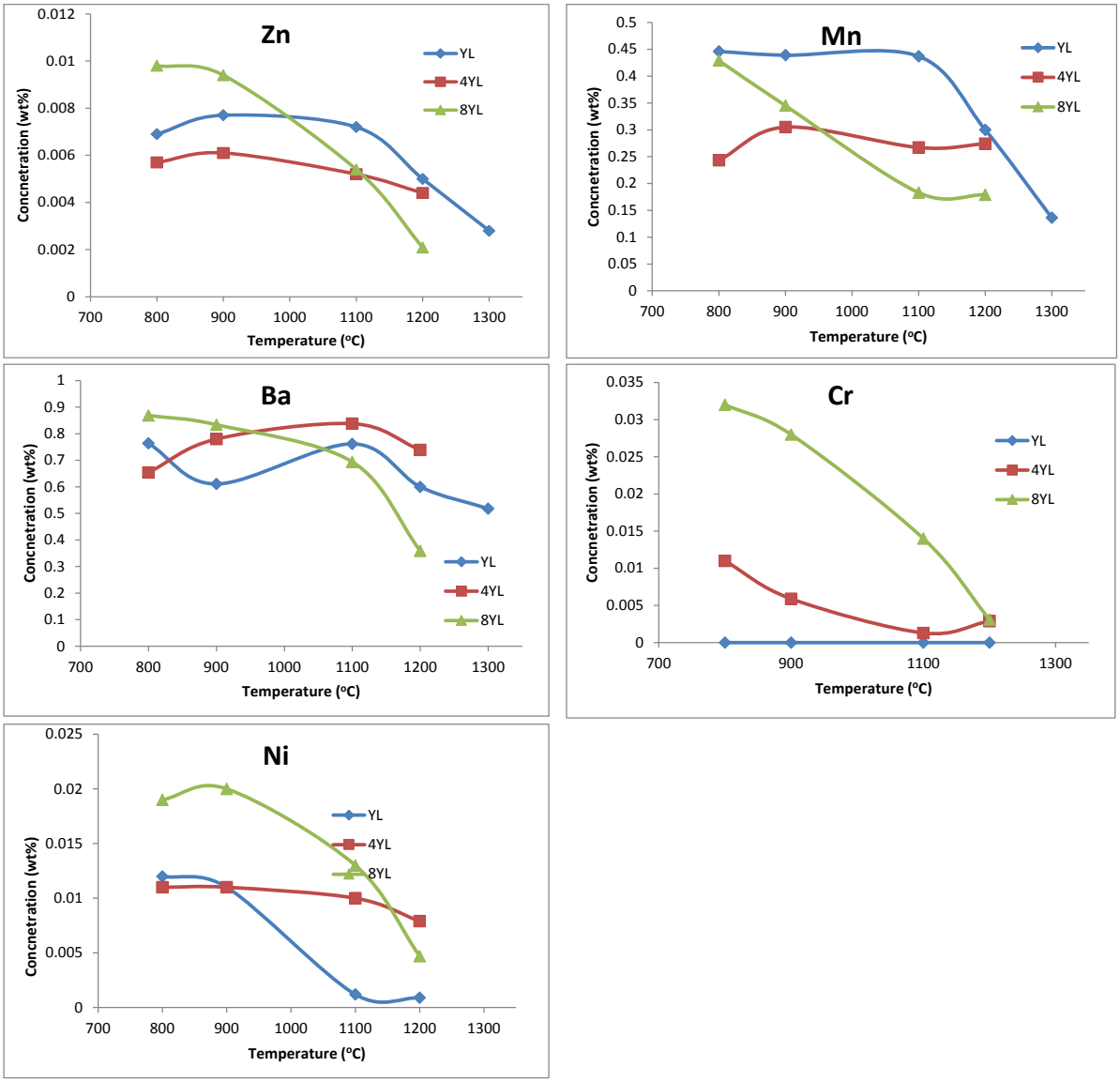


**Figure 20** Trace element concentration profiles of Yallourn ash with % CaO flux added and treated at 800-1300 °C.

- Zinc (Zn): The results indicate that the concentration of Zn in Yallourn ash decreased with temperatures suggesting its release during high-temperature gasification. With the addition of CaO, the concentration of Zn further decreased with temperature suggesting that the addition of CaO flux will increase the release of Zn during $CO_2$ gasification of the coal.
- Manganese (Mn): The sample did not show any change until 1100 °C beyond which Mn started to release from the sample. With the 4% CaO added as flux, the Mn content remains majorly unaffected, however with 8% CaO addition Mn concentration showed a decrease even at a temperature as low as 900 °C.
- Barium (Ba): The concentration of Ba remained constant until 1100 °C beyond which a slight decrease in concentration observed at 1200 °C. The addition of 4% CaO followed similar trend as Mn, a decrease in Ba concentration beyond 1100 °C. At 8%

CaO addition, the amount of Ba reduced with temperature continuously suggesting higher amounts of CaO addition tend to release Ba from the ash.

- Chromium (Cr): Interestingly the Yallourn ash did not detect any presence of Cr, which may be attributed to either non-dissolution of the Cr during digestion of the sample or being present below the detection limit . However, when CaO was added there is an increase in Cr concentration in the digested sample, indicating some fixation of Cr in the ash.
- Nickel (Ni): Ni tended to release after 900 $^{o}$C from Yallourn ash. At both 4% AND 8% CaO addition, Ni-concentration in the ash increased.
- Arsenic (As): Arsenic was only detected in Yallourn ash and tended to show a decrease in concentration with temperature suggesting its release into the atmosphere. However, As was not detected in CaO flux added samples which may be due to the fixing of As in ash or release of As during sample preparation.

### 4.1.2 Loy Yang ash

The results in Table 10 and Figure 21 below show the composition and trends of the trace elements after treatment of Loy Yang ash at different temperatures in $CO_2$ atmosphere. The samples with and without CaO flux addition have been analysed in these measurements and analysis. The units of results are in wt%.

**Table 10 Trace elements in Loy Yang ash samples**

| | | | (wt%) | | | |
|---|---|---|---|---|---|---|
| **Sample** | **Zn** | **Mn** | **Ba** | **Cr** | **Ni** | **As** |
| **LY-800** | 0.0002 | 0.26 | 0.275 | 0.0079 | 0.0057 | ND |
| **LY-900** | 0.22 | ND | 0.27 | 0.017 | 0.008 | ND |
| **LY-1100** | 0.0035 | ND | 0.016 | 0.029 | 0.013 | ND |
| **LY-1200** | 0.0036 | 0.0049 | 0.01 | 0.02 | 0.0093 | ND |
| **4% CaO-LY-800** | 0.0038 | 0.0094 | 0.027 | 0.021 | 0.0095 | 0.001 |
| **4% CaO-LY-900** | 0.0076 | ND | 0.023 | 0.019 | 0.0096 | ND |
| **4% CaO-LY-1100** | 0.0051 | ND | 0.01 | 0.011 | 0.0063 | ND |
| **8% CaO-LY-800** | 0.0066 | 0.021 | 0.029 | 0.017 | 0.0077 | 0.0023 |
| **8% CaO-LY-900** | 0.0063 | 0.012 | 0.02 | 0.015 | 0.0075 | ND |
| **8% CaO-LY-1100** | 0.0066 | ND | 0.028 | 0.022 | 0.0087 | ND |
| **8% CaO-LY-1200** | 0.0052 | ND | 0.018 | 0.03 | 0.0095 | ND |

ND- not detected

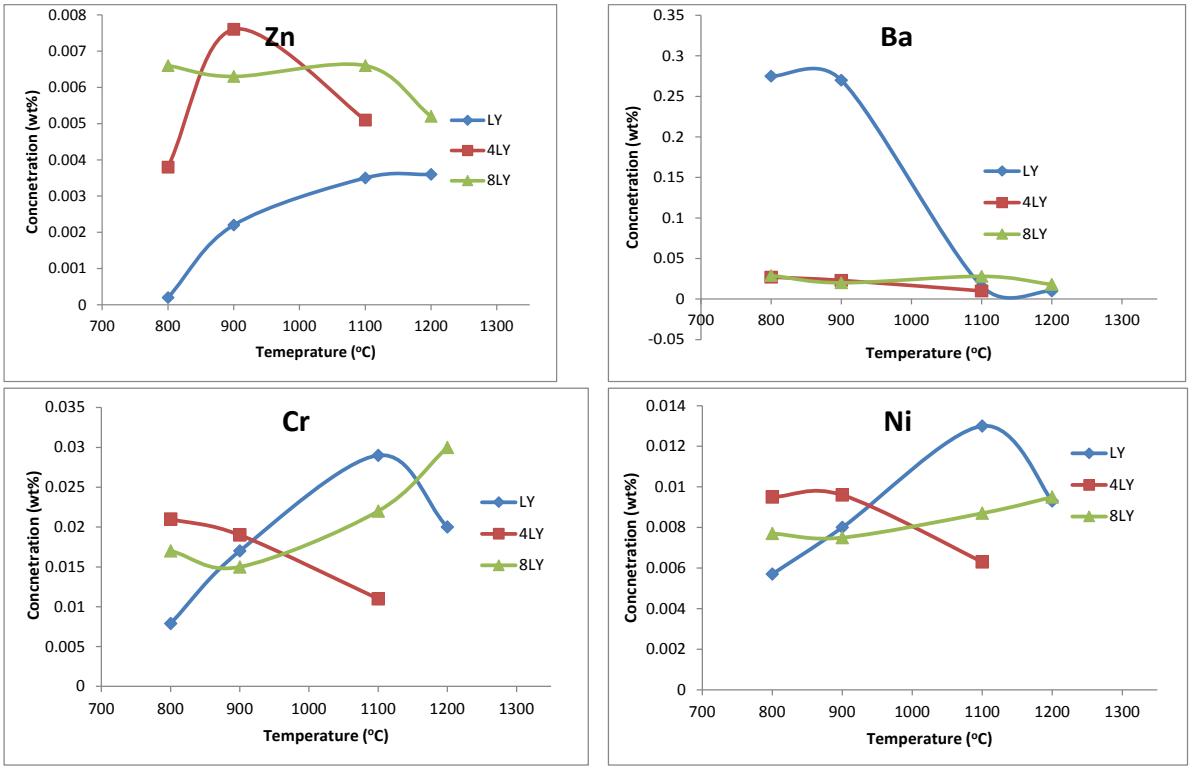


**Figure 21** Trace element concentration profiles of Loy Yang ash with %CaO flux added and treated at 800-1300 °C

- Zinc (Zn): Loy Yang ash showed very small amount of Zn in the sample at 800 °C but there is an increase in concentration with temperature suggesting high amount of Zn dissolution during digestion with the sample treated at high temperature. The addition of 4% CaO there is an increase in concentration until 900 °C and then a drop beyond 900 C suggesting that addition of CaO aids in the release of Zn into the atmosphere at higher temperatures. At 8% CaO addition the concentration of Zn remained constant until 1100 °C beyond which it showed a decline suggesting the release of the Zn into the atmosphere. The results suggest that the addition of CaO aids in capturing the Zn compounds in ash.
- Barium (Ba): Loy Yang ash showed a sharp decline in Ba content with temperature and reached close to 0 wt% at 1100 °C suggesting its release into the atmosphere. With CaO addition, there is only a minor quantity detected in the ash. This indicates only limited fixing of the Ba in the ash in presence of Ca.
- Chromium (Cr): The concentration of Cr increased with temperature in Loy Yang ash until 1100 °C beyond which a decline was noticed. The addition of 4% CaO showed a continuous decrease in concentration whereas 8% CaO addition showed an increase in Cr concentration in the ash with temperature.
- Nickel: Ni observed a trend similar to that of chromium.
- Arsenic and Manganese: Arsenic was detected in low concentrations in Loy Yang ash. On the other hand, Manganese concentration tends to decrease and reach near zero at temperatures as low as 900 °C both with and without CaO suggesting their release

during gasification. CaO addition cannot fix these elements to the ash at high-temperature gasification.

The results indicate that 4-8% CaO addition can fix elements Ni, Cr, and Ba into the Loy Yang ash, but would release Zn beyond 1100 $^{o}$C during the gasification process. Mn and As was released irrespective of CaO addition at temperatures during gasification.

### 4.1.3 Morwell ash

The results in Table 11 and Figure 22 show the concentration and trends of the trace elements after treating Morwell ash at different temperatures in $CO_2$ atmosphere. The samples with and without CaO flux addition had been prepared for these measurements and analysis. The units for the results are in wt%.

**Table 11 Trace elements in Morwell ash samples in wt%**

| | | | wt% | | | |
|---|---|---|---|---|---|---|
| **Sample** | **Zn** | **Mn** | **Ba** | **Cr** | **Ni** | **As** |
| **MW-800** | 0.011 | 0.312 | 0.126 | ND | 0.003 | 0.0023 |
| **MW-900** | 0.011 | 0.325 | 0.132 | ND | 0.0032 | 0.0021 |
| **MW-1100** | 0.0045 | 0.371 | 0.31 | ND | 0.0039 | 0.0019 |
| **MW-1200** | 0.0053 | 0.349 | 0.097 | 0.0008 | 0.0028 | 0.0005 |
| **MW-1300** | 0.0024 | 0.12 | 0.076 | ND | 0.00084 | 0.0009 |
| **4% CaO-MW-800** | 0.01 | 0.283 | 0.103 | ND | 0.0029 | ND |
| **4% CaOMW-900** | 0.014 | 0.331 | 0.136 | ND | 0.0052 | 0.014 |
| **4% CaOMW-1100** | 0.095 | 0.333 | 0.122 | ND | 0.0045 | 0.00029 |
| **8% CaO-MW-800** | 0.011 | 0.279 | 0.112 | ND | 0.0024 | ND |
| **8% CaO-MW-900** | 0.01 | 0.312 | 0.094 | ND | 0.0025 | 0.00038 |
| **8% CaO-MW-1100** | 0.0105 | 0.317 | 0.085 | ND | 0.0031 | 0.00018 |
| **8% CaO-MW-1200** | 0.131 | 0.035 | 0.444 | 0.026 | 0.021 | ND |
| **15% CaO-MW-800** | 0.0028 | 0.229 | 0.029 | 0.0014 | 0.0025 | ND |
| **15% CaO-MW-900** | 0.0061 | 0.098 | 0.075 | 0.00093 | 0.0019 | ND |
| **15% CaO-MW-1100** | 0.0051 | 0.17 | 0.048 | 0.0023 | 0.0036 | ND |
| **15% CaO-MW-1200** | 0.0026 | 0.255 | 0.051 | 0.0014 | 0.0032 | ND |
| **4Clay-MW-800** | 0.01 | 0.114 | 0.125 | 0.00076 | 0.0019 | ND |
| **4Clay-MW-900** | 0.0066 | 0.341 | 0.028 | 0.0016 | 0.0033 | ND |
| **4Clay-MW-1100** | ND | 0.381 | 0.045 | 0.0028 | 0.0036 | ND |
| **8Clay-MW-800** | 0.01 | 0.114 | 0.125 | 0.00076 | 0.0019 | ND |
| **8Clay-MW-900** | ND | 0.381 | 0.045 | 0.0028 | 0.0036 | ND |
| **8Clay-MW-1100** | ND | 0.381 | 0.045 | 0.0028 | 0.0036 | ND |

ND- not detected

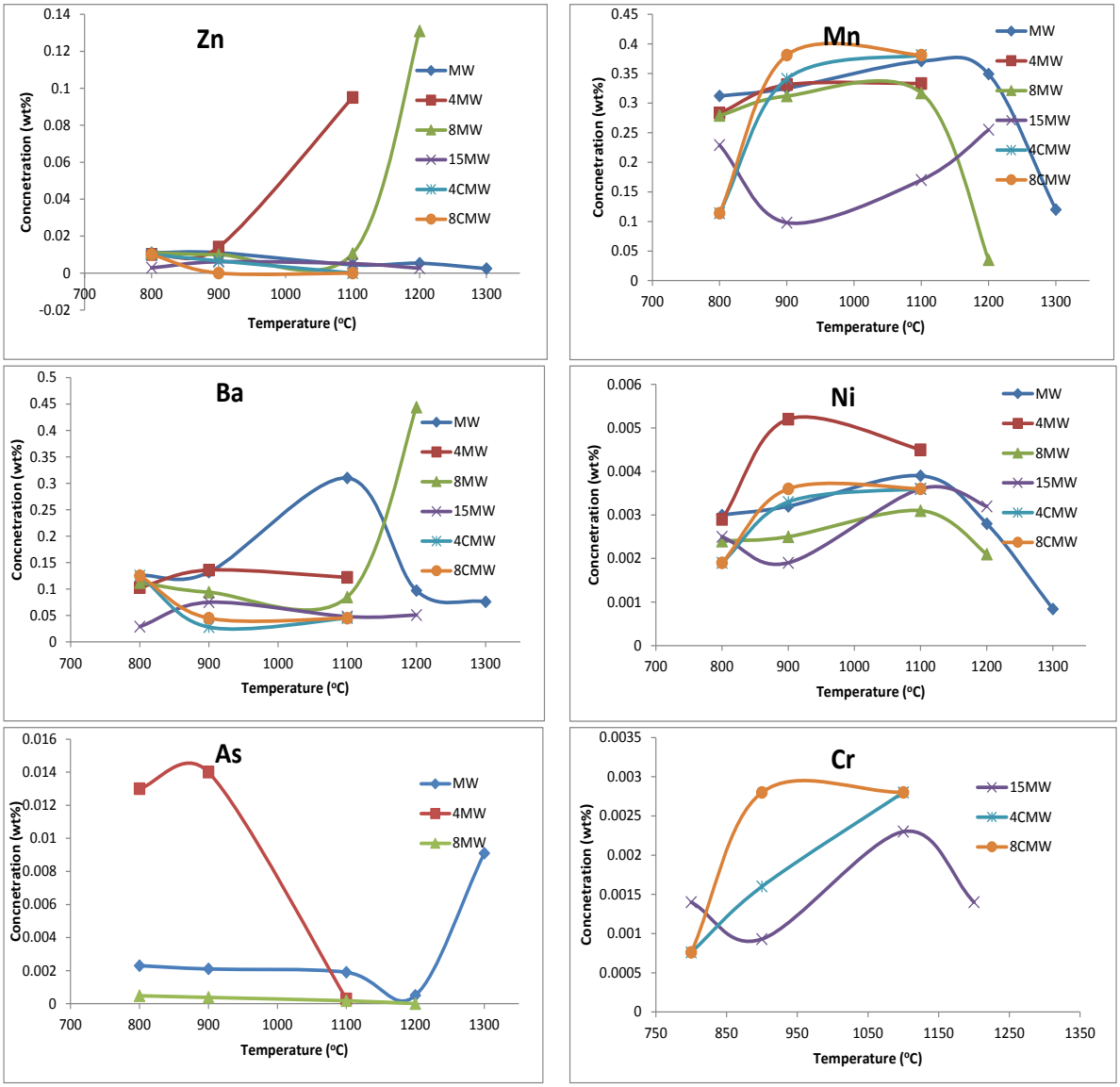


**Figure 22** Trace element concentration profiles of Morwell coal ash with %CaO and %Clay addition and treated at 800-1300 °C

- Zinc (Zn): The concentration of Zn in Morwell ash is close to zero. The addition of 4 and 8% CaO showed a sudden increase in Zn concentration beyond 900 °C, but at 15% CaO, the trend was different. The addition of clay did not show any sign of an increase in Zn concentration which remained flat throughout the temperatures tested.
- Manganese (Mn): Manganese remained stable in the ash until 1200 °C, beyond which it showed a sudden drop in concentration suggesting its release from the ash. The addition of 4 and 8% CaO showed a slight increase in the concentration of Mn until 1100 °C, beyond which the concentration decreased. 15% CaO showed a slightly different trend; initially at 900 °C the concentration decreased, beyond which it increased. With the addition of clay the concentration of Mn increased in the ash, however, the samples at higher temperatures 1200 °C and above, were not tested as these samples sintered and could not be retrieved from the crucible.

- Barium (Ba): The concentration of Ba increased with temperature until 1100 $^{o}$C, beyond which it decreased. The increase in concentration can be attributed to the evaporation other components in the ash before Barium resulting in an increase in Ba concentration in the ash. The addition of 4 and 15% CaO did not change the Ba concentration in the sample whereas 8% CaO addition showed a sudden increase of Ba concentration at 1200 $^{o}$C. This result warrants further investigation. On the other hand, during the addition of clay to the ash the concentration of Ba remained constant.
- Nickel (Ni): Morwell ash showed a decrease in Ni concentration above 1100 $^{o}$C suggesting its release during high-temperature gasification. Addition of 4 and 8% CaO slightly increased Ni concentration initially until 900 $^{o}$C and 1000 $^{o}$C respectively beyond which a decrease in concentration was observed. At 15% CaO addition, the change in concentration exhibited no particular trend. At 4% and 8% CaO addition, a slight increase in Ni concentration at 900 $^{o}$C was noted which remained stable until 1100 $^{o}$C.
- Arsenic (As): The concentration of Arsenic remained constant until 1100 $^{o}$C, beyond which a slight decrease at 1200 $^{o}$C and a sudden increase at 1300 $^{o}$C was observed, possibly due to the formation of calcium arsenate.. The reason for the increase in As concentration at 1300 $^{o}$C is not known. The addition of 4% CaO showed a higher concentration of As in the sample which tends to decrease beyond 900 $^{o}$C, whereas at 8% CaO addition the concentration of As remained low and not much variation is observed. At 15% CaO and clay addition the concentration of As was not detected at all in the sample.
- Chromium (Cr): was not detected in Morwell ash and in 4% and 8% CaO mixed samples except at 1200 $^{o}$C. When the CaO content increased to 15%, the sample showed the presence of Cr whose concentration varied without any particular trend. Addition of clay to the Morwell ash however, increased the concentration of Cr with temperature until 1100 $^{o}$C. The increase in concentration of Cr with temperature may be due to evaporation of certain components in the ash, and some fixation of Cr by CaO.

The results indicate that the trace elements in Morwell ash exhibited trend in the change in their concentration with and without flux addition. However, in general, there was some fixation of the compounds of all the elements in the ash as a result of the addition of CaO.

### 4.2 Thermodynamic modelling to predict trace element emissions

The FactSage 6.4 software was used to predict the trace element speciation during gasification of Victorian brown coal under different conditions. Three Victorian brown coals (Loy Yang, Morwell and Yallourn) were used in these calculations and the considered trace elements in the study were chromium (Cr), arsenic (As), and selenium (Se) as these are of greatest environmental and health concern. All calculations were performed using a gas mixture (90% $CO_2$ + 10% $N_2$) and 1 kg of dry coal as an input. These inputs were processed over the temperature range 800 to 1500°C at 100°C intervals and at atmospheric pressure.

The predicted possible trace elements species during gasification are listed in Table 12. For easy understanding, major toxic trace element species are shown in bold font.

**Table 12** List of species containing the four trace elements considered in this work[1]

| **Trace element** | **Species** |
|---|---|
| **Cr** | **$CrO_2(OH)_2$ (g)**, **$CrO_3$ (g)**, $CrO_2OH$ (g), $CrO(OH)_4$ (g), $CrO(OH)_3$ (g), $CrO(OH)_2$ (g), CrOOH (g), CrOH (g), $Cr(OH)_2$ (g), $Cr(OH)_3$ (g), $Cr(OH)_4$ (g), $Cr(OH)_5$ (g), $Cr(OH)_6$ (g), CrS (g), $CrO_2$ (g), CrO (g), Cr (g), $CrO_2Cl_2$ (g), $CrO_2Cl$ (g), CrOCl (g), $CrOCl_2$ (g), $CrOCl_3$ (g), $CrOCl_4$ (g), CrCl (g), $CrCl_2$ (g), $CrCl_3$ (g), $CrCl_4$ (g), $CrCl_5$ (g), $CrCl_6$ (g), CrN (g), $Cr_2O_3$ (s), $(Na_2O)(Cr_2O_3)$ (s), $CaCr_2O_4$ (s). |
| **As** | **$As_4O_6$ (g), $As_2O_3$ (slag),** AsSe (g), AsO (g), AsN, AsS (g), $As_2$ (g), $AsH_3$ (g), As (g), $As_3$ (g), $As_4$ (g), $As_2Se_2$ (g), $AsCl_3$ (g), $As_4Se_3$ (g), $As_4Se_4$ (g), $As_4S_4$ (g). |
| **Se** | **$SeO_2$ (g),** $H_2Se$ (g), AsSe (g), SeS (g), Se (g), $Se_2$ (g), SeO (g), HgSe (g), $As_2Se_2$ (g), NSe (g), CSe (g), $Se_3$ (g), $SeCl_2$ (g), $CSe_2$ (g), $Se_4$ (g), $As_4Se_3$ (g), $Se_5$ (g), AlSe (g), SiSe (g), $As_4Se_4$ (g), (g), $SiSe_2$ (g), $Se_6$ (g), TiSe (g), $Se_7$ (g), $Se_8$ (g), $Al_2Se$ (g), $Al_2Se_2$ (g). |

It was also observed from thermodynamic equilibrium calculation that the steady-state period did not have any effect on equilibrium distribution of the considered trace elements.

Equilibrium compositions of the considered trace elements at different temperatures for the three Victorian brown coals are shown in Figures 23-26. Only the species with an important proportion (more than 1% v/v) of the total species at equilibrium are considered in this study.

[1] g is the gaseous state; s is the solid state; slag is the slag-liquid compound.

### 4.2.1 Chromium

Figure 23 shows the quantity of chromium predicted to be present in the vapour phase as well as the solid phase, as a function of temperature, during carbon dioxide gasification of the considered three Victorian brown coals.

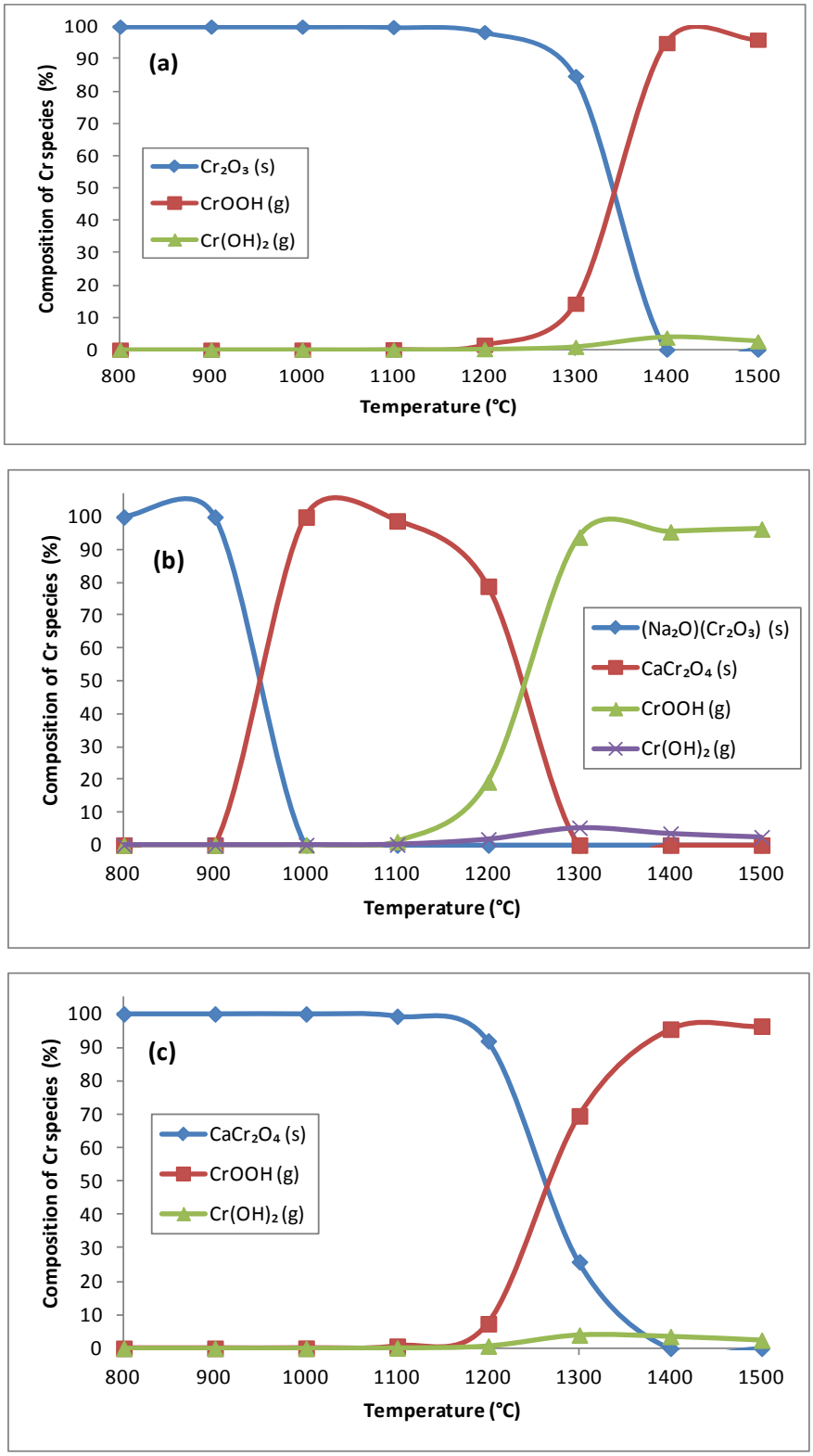


**Figure 23** Equilibrium distribution of chromium during carbon dioxide gasification of (a) Loy Yang, (b) Morwell and (c) Yallourn coals

Almost 100% of total chromium would exist up to 1200 °C in the solid phase as $Cr_2O_3$ for Loy Yang coal and as $CaCr_2O_4$ for Yallourn coal. Above 1200 °C, however, considerable amounts of gaseous CrOOH and $Cr(OH)_2$ were predicted to form, which lead to the reduction of their concentration in the solid phase.

In the case of Morwell coal, most of the Cr was predicted as solid ($Na_2O$) ($Cr_2O_3$) up to 900°C and then as solid $CaCr_2O_4$ up to 1200 °C. Above 1200 °C, however, gaseous CrOOH was the dominant Cr species with a minor contribution of $Cr(OH)_2$.

### 4.2.2 Arsenic

The quantity of arsenic compounds present in the gas phase during carbon dioxide gasification of Loy Yang coal at different temperatures is presented in Figure 24. Similar profiles are obtained in the case of Morwell and Yallourn coals and are not shown.

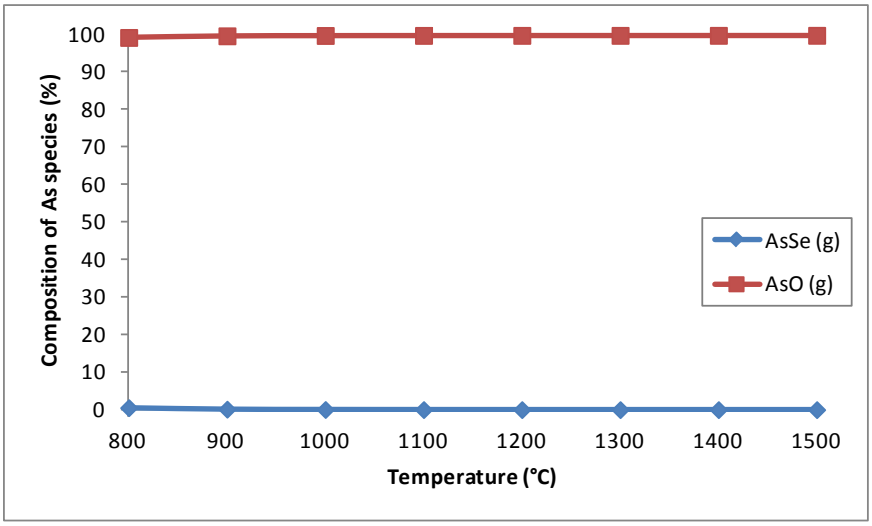


**Figure 24** Equilibrium distribution of arsenic during carbon dioxide gasification

The results indicate that arsenic selenide (AsSe) was the dominant arsenic species over the entire temperature range studied with a minor contribution of arsenic oxide (AsO).

### 4.2.3 Selenium

The equilibrium distribution of selenium during carbon dioxide gasification of three Victorian brown coals at different temperatures is shown in Figure 25.

In the case of selenium, the dominant species was $H_2Se$ (g) up to 1400 °C for Loy Yang and Yallourn coals, and up to 1300 °C for Morwell coal. At higher temperatures, substantial quantities of SeS (g) and Se (g) were predicted to form, which resulted in the drop in the $H_2Se$ (g) compound.

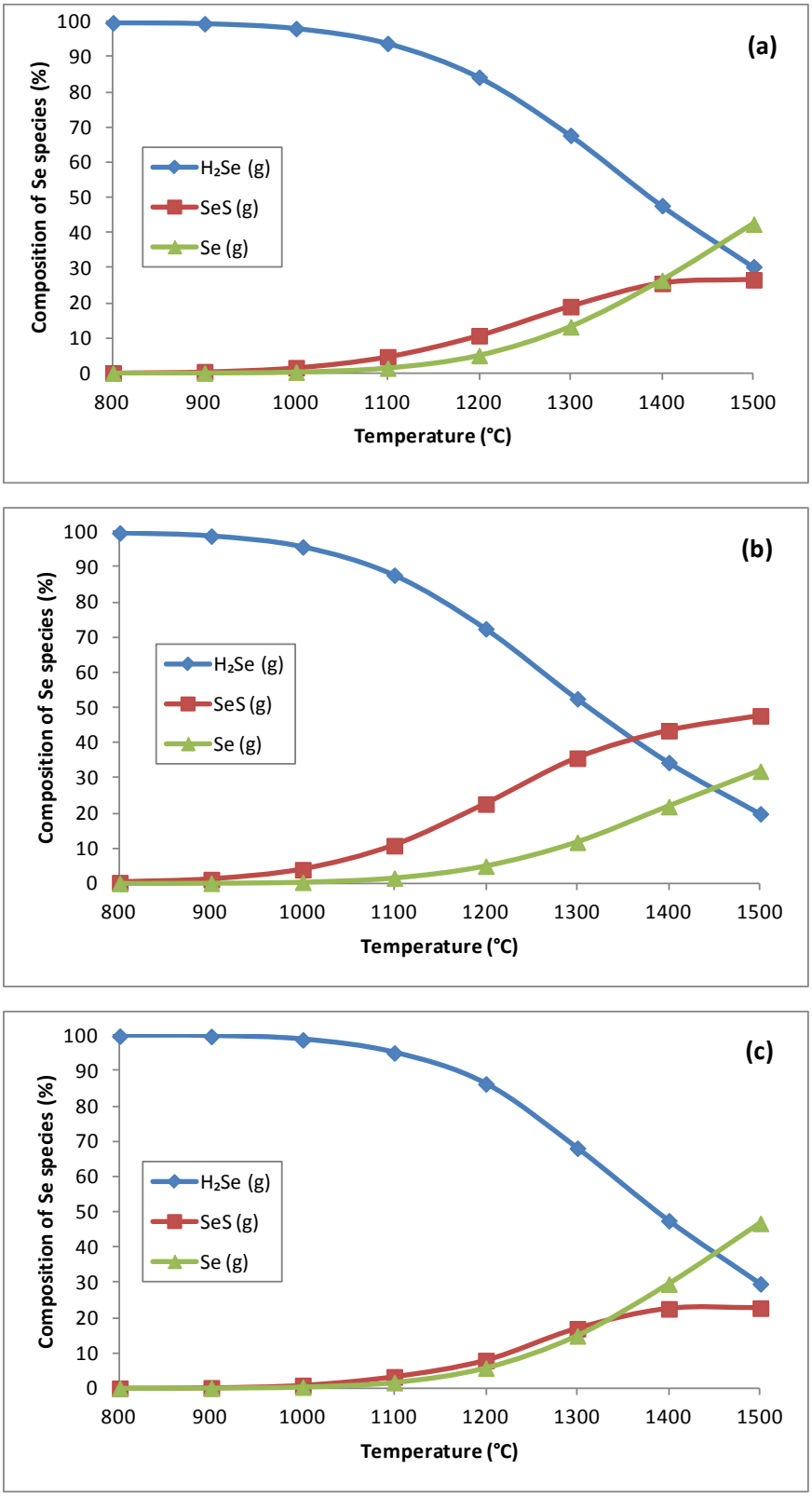


**Figure 25** Equilibrium distribution of selenium during carbon dioxide gasification of (a) Loy Yang, (b) Morwell and (c) Yallourn coals

## 4.3 Conclusion

Experimental results of trace element analysis on the release of elements like Ni, Zn, Cr, Ba, Mn, and As during gasification of coal are summarised below.

- For Yallourn ash, there is an increase in the release of elements Zn, Mn, Cr and Ni, with an increase in temperature.
- For Loy Yang ash, Ba shows full release to the gas phase by 1100 C, but other elements Zn, Cr and Ni primarily remain in the ash.
- For Morwell ash, Mn and Ni remains in ash until 1200 $^{o}$C and 1100 C respectively. The remaining elements Ba, Zn, As and Cr largely remain in the ash.

The results of thermodynamic predictions are summarised as follows:

Chromium: The amount of Cr released into gas atmosphere increase with temperature in all the three Victorian brown coals ash which contradicts the experimental results.

Arsenic: The amount of As in ash lowered with temperature in Yallourn ash suggesting its release into the atmosphere as gas phase, however, it remained undetected in Loy Yang ash. In Morwell ash, the concentration of As tends to decrease with temperature suggesting its release into the atmosphere. The predictions show that most of the As remained in gas phase even at 800 $^{o}$C.

Selenium: There is a general trend of increasing gas phase selenium with temperature from the predictions. However, selenium was not detected in Victorian brown coal ashes we tested.

In general, the thermodynamic predictions and the experimental data matches in trend for most elements except Cr. Also, even though release of some of the elements to gas phase increase with temperature, overall the absolute emission values are quite low, majority of the trace elements in coal remain fixed in the ash.

# 5 Viscosity of Slags - Existing viscosity models and their application to Victorian brown coals

Several slag viscosity models have been reported in the literature. A review of these viscosity models is provided in Appendix B. Some of these models are applied to Victorian brown coal ash. The results are presented in this section.

## 5.1 Application of select models on Victorian brown coal ash

Three Australian brown coals were used in the prediction of slag composition and viscosity during gasification in a reducing environment. The ash composition of these coals are shown in Table 2. These coals are used for power generation in Victoria. While Yallourn ash is characterised by high levels of iron, Morwell contains high levels of calcium, and Loy Yang contains high levels of silica and alumina.

The viscosity models available currently are known to be useful for predicting coal ash slag viscosity for high-rank coals. Six of the major models are discussed below and further applied to the Victorian brown coals.

### 5.1.1 Kalmanovitch modified Urbain model

The original Urbain equation (Eq. 1) can be adapted to various types of coals[18-20]. The semi-empirical Urbain model is used as the basis of viscosity modelling as it incorporates the Weyman-Frenkel equation, which includes the temperature dependency of slag viscosity[19-21].

$$\eta = aT \exp(1000b/T) \quad \text{Eq. 1}$$

Where $\eta$ is viscosity in Poise, $T$ is the temperature in Kelvin while $a$ and $b$ are model parameters as a function of slag composition[19-21]. The Kalmanovitch modified Urbain model is fairly suited for coal with high $SiO_2$ and low 'FeO' content[21, 22]. The model parameters $a$ and $b$ are given by the following Eq. 2(a)-2(g) [23, 24].

$$\ln a = -0.2812b - 11.8279 \quad \text{Eq.2 (a)}$$

$$b = b_o + b_1 N + b_2 N^2 + b_3 N^3 \quad \text{Eq.2 (b)}$$

$$b_0 = 13.8 + 39.9355\beta - 44.049\beta^2 \quad \text{Eq.2 (c)}$$

$$b_1 = 30.481 + 117.1505\beta - 129.9978\beta^2 \quad \text{Eq.2 (d)}$$

$$b_2 = -40.9429 + 234.0486\beta - 300.04\beta^2 \quad \text{Eq.2 (e)}$$

$$b_3 = 60.7619 - 153.9276\beta - 211.1616\beta^2 \quad \text{Eq.2 (f)}$$

where,

N = mole fraction of silica ($SiO_2$) Eq.2 (g)

This model takes into account the fluxing effect by the oxides (molar ratio) as shown in Eq. 2(h)

$$\beta = \frac{CaO+MgO+Na_2O+K_2O+'FeO'+TiO_2}{Al_2O_3+CaO+MgO+Na_2O+K_2O+'FeO'+TiO_2} \quad \text{Eq.2 (h)}$$

### 5.1.2 Schobert-Streeter-Diehl modified Urbain model

The original Urbain model is modified to adapt to low-rank coal slag viscosity by the addition of the term, $\Delta$ [19, 22], a linear function of temperature [25]. Here, the parameters $\Delta$, $m$, and $B$ are evaluated based on modelling of low-silica slag[19, 24, 26].

$$\ln \eta = \ln a + \ln T + \frac{1000b}{T} - \Delta \qquad \text{Eq.3 (a)}$$

$$\Delta = mT + B \qquad \text{Eq.3 (b)}$$

$$B = 01.8244(1000m) + 0.9416 \qquad \text{Eq.3 (c)}$$

$$1000\text{m} = -55.3649\text{F} + 37.9186 \qquad \text{Eq.3 (d)}$$

$$F = \frac{CaO}{CaO+MgO+Na_2O+K_2O} \qquad \text{Eq.3 (e)}$$

Where the molecular formulae in Eq.3 (e) are expressed in mole fraction.

$$\ln a = -0.2693b - 11.6725 \qquad \text{Eq.3 (f)}$$

In this model, the parameter $\alpha$ replaces the model parameter, $b$ in Schobert-Streeter-Diehl modified Urbain model. Here, $\alpha$ is given by the following equation.

$$\alpha = \frac{CaO+MgO+Na_2O+K_2O+'FeO'+2TiO_2+3SO_3}{Al_2O_3+CaO+MgO+Na_2O+K_2O+'FeO'+2TiO_2+3SO_3} \qquad \text{Eq.3 (g)}$$

### 5.1.3 $S^2$ correlation and Watt and Fereday correlation

'$S^2$ correlation' and 'Watt and Fereday correlation' are two empirical viscosity correlations developed for British coal ash slags, developed by BCURA [23, 24]. These are based on Arrhenius type equations. The simple Arrhenius type equation is given as follows.

$$\eta = A.e^{\frac{E_a}{T}} \qquad \text{Eq. 4(a)}$$

Where T is temperature, $E_a$ is activation energy, and A represents the probability of empty space before structural unit [27].

The '$S^2$ correlation' is based on coal ash slags with silicon, aluminium, iron, calcium and magnesium as the major components. It relates the viscosity-temperature characteristics of wholly liquid slags to their chemical composition. This is based on a recalculation of the compositional analysis of the slag in which all the iron present in the mixture is assumed to exist as FeO. It is most suited for slags with silica and iron oxide content less than 55% and 5% respectively [28, 29]. The viscosity is given by the following equation.

$$\log \eta = 4.468\left(\frac{S}{100}\right)^2 + 1.265\left(\frac{10000}{T}\right) - 7.44 \qquad \text{Eq.4(b)}$$

where S is expressed as percentage of silica.

The silica ratio is calculated on a weight basis. This implies that the probability coefficient depends on the silica ratio, and the activation energy is not dependent on the

composition. Therefore, the validity of this model only covers a limited compositional range [27].

The 'Watt and Fereday correlation' is given by equation 5(a), (b), and (c). It yields higher accuracy for slags with high silica content (i.e. >80%) or high iron oxide content (i.e. >15%) [28, 29] . Viscosity is predicted using the following equation.

$$\log \eta = \frac{10^7 m}{(T-150)^2} + c \qquad \text{Eq.5 (a)}$$

$$m = 0.00835SiO_2 + 0.00601Al_2O_3 - 0.109 \qquad \text{Eq.5 (b)}$$

$$c = 0.0415SiO_2 + 0.0192Al_2O_3 + \ 0.0276'FeO' + 0.0160CaO - 3.92 \qquad \text{Eq.5 (c)}$$

Where, $\eta$ is in Poise, $T$ is in Celsius, and the molecular formula is expressed in weight percentage.

### 5.1.4 Kondratiev - Jak modified Urbain model

Here, the Urbain model is modified by basing the partially crystallised molten slag viscosity, $\eta_s$ (slurry viscosity) on the effect of heterogeneous composition of molten slag and operating temperature on coal ash slag viscosity[20, 24, 30]. Viscosity of the liquid phase of coal ash slag is given by the following equation.

$$\eta_L = AT \exp\left(\frac{1000B}{T}\right) \qquad \text{Eq.6 (a)}$$

$$-\ln A = mB + n \qquad \text{Eq.6 (b)}$$

$$B = \sum_{i=0}^{3} b_i^0 X_s^i + \sum_{i=0}^{3}\sum_{j=1}^{2}\left(b_i^{c,j}\frac{X_c}{X_c+X_F} + b_i^{F,j}\frac{X_F}{X_C+X_F}\right) \times \left(\frac{X_C+X_F}{X_C+X_F+X_A}\right)^j X_S^i \qquad \text{Eq.6 (c)}$$

$$m = m_A X_A + m_C X_C + m_F X_F + m_S X_s \qquad \text{Eq.6 (d)}$$

where $X_A, X_C, X_F$ and $X_S$ are mole fractions of $Al_2O_3$, CaO, 'FeO' and $SiO_2$ respectively, and $b_i^0$, $b_i^{c,j}$, $b_i^{F,j}$, $m_A, m_C, m_F$ and $m_S$ are parameters determined through optimisation, as shown in Table 13. Viscosity of slurry $\eta_s$ is given by the following equation.

$$\eta_s = \eta_L(1 - V_s)^{-2.5} \qquad \text{Eq.6 (e)}$$

with $V_S$ being the solid volume fraction.

The major advantage of this model is that it takes into the differences in the chemistry of individual components without forgoing the importance of the Urbain assumptions [31]. However, the current study is not experimental. Therefore, due to inadequate information on solid volume fraction in brown coal slags as a function of temperature, the slurry viscosity is calculated ignoring the solid volume fraction. This will result in error, where the predicted viscosity will be overestimated at the start when the solid volume fraction is high [24].

**Table 13.** Kondratiev-Jak modified Urbain model parameters (Poise)[24]

| $j$ | | $I$ | | | | | |
|---|---|---|---|---|---|---|---|
| | | *0* | *1* | *2* | *3* | | |
| $b_i^0$ | 0 | 13.31 | 36.98 | -177.70 | 190.03 | $n$ | 9.322 |
| $b_i^{C,j}$ | *1* | 5.50 | 96.20 | 117.94 | -219.56 | $m_F$ | 0.665 |
| | *2* | -4.68 | -81.60 | -109.80 | 196.00 | $m_C$ | 0.587 |
| $b_i^{F,j}$ | *1* | 34.30 | -143.64 | 368.94 | -254.85 | $m_A$ | 0.370 |
| | *2* | -45.63 | 129.96 | -210.28 | 121.20 | $m_s$ | 0.212 |

### 5.1.5 FactSage Viscosity Module - Modified Quasichemical Model

FactSage, an integration of two computational thermochemistry software packages: FACT-Win and ChemSage, is used to calculate and predict the viscosity of different coals over a range of temperatures.[32, 33]

This software employs models for the viscosity of single-phase liquid slags and glasses. It directly relates the viscosity to the structure of the slag, and the structure, in turn, is calculated from the thermodynamic description of the melt using the Modified Quasichemical Model [34].

There are two viscosity databases. The database for melts is valid for liquid and supercooled slags with viscosities for which $\log_{10}$ (viscosity, Poise) is less than 7.5, mostly corresponding to temperatures above 900 $^{o}$C. On the other hand, the database for glasses can be used at and below the glass transition temperatures. Although this database is valid over the whole temperature range from liquid melts to glasses, but it is likely to be less accurate for liquid slags than the melts database [34].

Although the melts database is likely to provide more accurate estimations, viscosity has been predicted for the coals using both the databases as theoretically both are applicable.

Prior to applying the viscosity models to the Victorian ash samples, the actual sample was heat treated at 1350 $^{o}$C and 1400 $^{o}$C to observe the physical change due to the heat treatment. The results are presented in Figure 26. The results show that Yallourn ash did not show any sign of sintering at 1400 $^{o}$C, Morwell sintered at 1350 $^{o}$C and Loy Yang at only 1400 $^{o}$C.

**YA-1350** **YA-1400** **MW-1350** **MW-1400** **LY-1350** **LY-1400**

**Figure 26** Slag samples at different temperatures MW-Morwell, YA-Yallourn, LY-Loy Yang at 1350 and 1400 $^{o}$C

## 5.2 Discussion on the application of the models to the Victorian brown coal ash

The traditional models and FactSage databases applied to the three Victorian brown coals Yallourn, Morwell and Loy Yang are shown in Figures 27, 28 and 29 respectively. The point where the trough in the curves begins represents the temperature at which the liquid starts to flow. The slag tapping temperature is the temperature when the slag reaches a viscosity at which it can be collected from the gasifier. As accepted in the industry, this viscosity should be between 100 and 250 Poise. Viscosity above this range causes rapid refractory wear, and a viscosity below this range causes the erratic viscous flow of the slag making it difficult to collect. The slag tapping temperature under gasification conditions is generally found to be between 1400-1600 $^{o}$C [35] for high-rank coals.

### 5.2.1 Yallourn ash

Figure 27 represents results where all the models are applied to Yallourn coal. When Kalmanovitch model was applied to the ash samples were found to be molten and possess a very low viscosity which is less than 1 Poise suggesting the model cannot be applied at all for the Victorian brown coal ashes. This may be attributed to the fact that this model is suited more to coals with high $SiO_2$ and low 'FeO' content, and the three coals do not fall into that category. The Schobert model shows that the slag starts to melt around 750 $^{o}$C, which is highly unlikely as these samples are prepared at 815 $^{o}$C and did not show any sintering until 1000 $^{o}$C. The Kondratiev-Jak model (both including and excluding $SO_3$) reaches a viscosity of 250 Poise at a temperature of about 700 $^{o}$C. However, the Ash fusion test measurements show that Yallourn ash did not show any sigh of softening even at 1550 $^{o}$C, which suggests the flow temperatures will be above 1700 $^{o}$C. But FactSage melts database is expected to be more suitable for high-temperature slags than the glasses database. The FactSage model with the melts database shows a viscosity of 250 Poise at a temperature of 550 $^{o}$C. On the other hand, the model with glasses database shows a viscosity of around 250 Poise at a temperature of 840 $^{o}$C. Hence these models, FactSage melts and glasses and Kondratiev-Jak, also show the melting of the samples before 1000 $^{o}$C indicating these models cannot be applied to the Yallourn ash. However, $S^2$ correlation and Watts and Fereday correlations show that the samples melts above 1250 $^{o}$C and 1400 $^{o}$C which are relatively still far from the flow temperatures determined by ash fusion measurement.

Yallourn ash did not show any sign of sintering or melting when experimentally treated at high temperatures up to 1400 $^{o}$C shown in Figure 26.

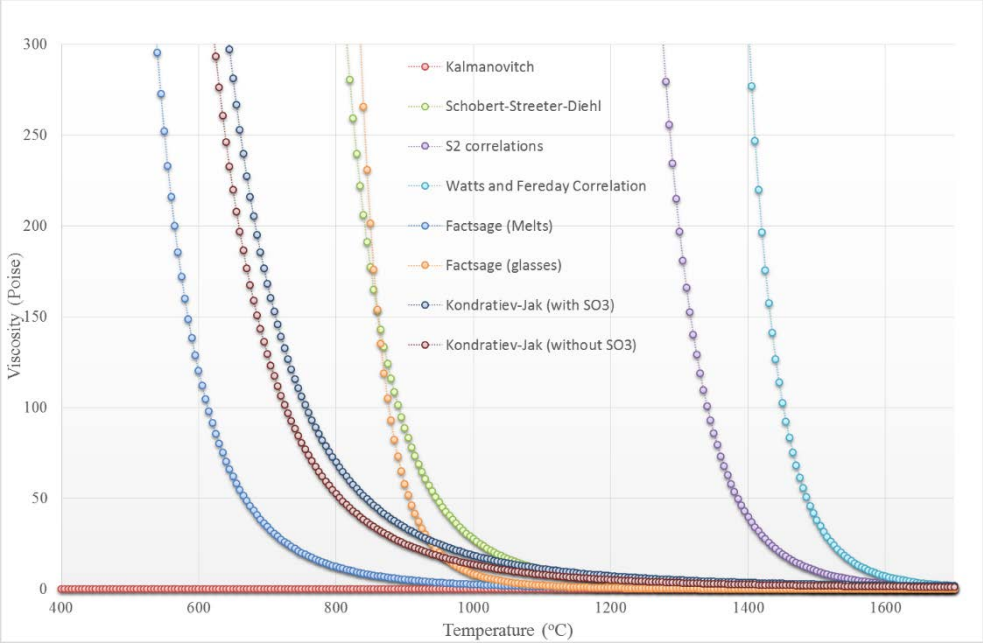


**Figure 27** Viscosity models applied with Yallourn ash

The same coal gives different curves for different models as each model is based on different criteria, such as levels of Silica and iron oxide. Moreover, other parameters such as CaO and MgO content, while accounted for in most of the models, have different coefficients attached to them.

### 5.2.2 Morwell ash

Figure 28 represents results when all the models are applied to Morwell coal ash. As observed in the case of Yallourn coal the prediction far beyond the expected values for most of the models applied. The majority of the models showed that the sample would achieve a target viscosity of 250 Poise below 1100 $^{o}$C. However, from ash fusion measurements it was determined the softening temperatures of Morwell ash starts well after 1500 $^{o}$C, which suggests the existing models cannot be applied to Morwell ash. Watts and Fereday's correlation suggest a temperature of 1400 $^{o}$C to attain 250 Poise are in the range of gasification process but, at least, 150 $^{o}$C short of possible softening temperatures as observed from ash fusion analysis. The results suggest the addition of flux materials like CaO or clay is necessary to lower the ash fusion temperature of Morwell ash.

It is interesting when the actual Morwell ash was subjected to temperatures of 1350 and 1400 $^{o}$C the sample showed initial melting as observed in Figure 26.

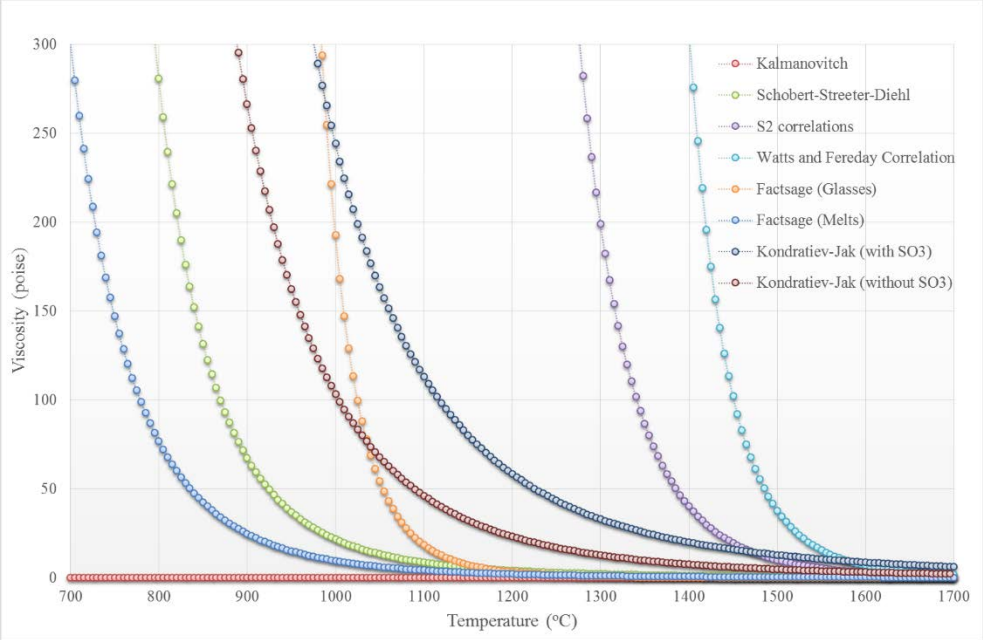


**Figure 28** Viscosity models applied with Morwell ash

### 5.2.3 Loy Yang ash

For Loy Yang coal, as shown in Figure 29, the Kalmanovitch model does not fit either. Kondratiev-Jak models show curves with a great difference to the other models, which reach a viscosity of 250 Poise at a temperature of >1850 $^{o}$C when $SO_3$ is excluded and 2010 $^{o}$C when $SO_3$ is included. The models indicate that the melting temperatures of Loy Yang ash are very high, whereas the ash fusion test shows the softening temperatures and hemispherical temperatures at 1400 and 1440 $^{o}$C suggesting flow temperatures below 1600 $^{o}$C. Hence, Kondratiev-Jak model cannot be applied to Loy Yang ash and the results were not shown in Figure 29 as the values exceed beyond 1800 $^{o}$C. However, the other models Schobert-Streeter-Diehl, $S^2$ correlation, Watts and Fereday correlation and FactSage models show that 250 Poise can be achieved between 1100-1550 $^{o}$C. Though the values vary in the range of flow temperatures determined from ash fusion analysis they are not exact. The curves for these models showed that viscosity of 250 Poise can be achieved as FactSage (melts) <1200 C, Schobert-Streeter-Diehl <1250 C and FactSage (glasses) ~ 1250 $^{o}$C which are much lower than the flow temperatures measured from ash fusion analysis and the operation range of gasification process. However, Watts and Fereday correlation and $S^2$ correlation show that 250 Poise can be achieved at 1330 and 1415 $^{o}$C respectively.

Although, the predictions are in the temperature range of gasification process they are off by at least 100 – 200 $^{o}$C when compared to ash fusion analysis on Loy Yang ash. Ash fusion analysis on the Loy Yang ash indicates the flow temperatures are beyond 1500 $^{o}$C.

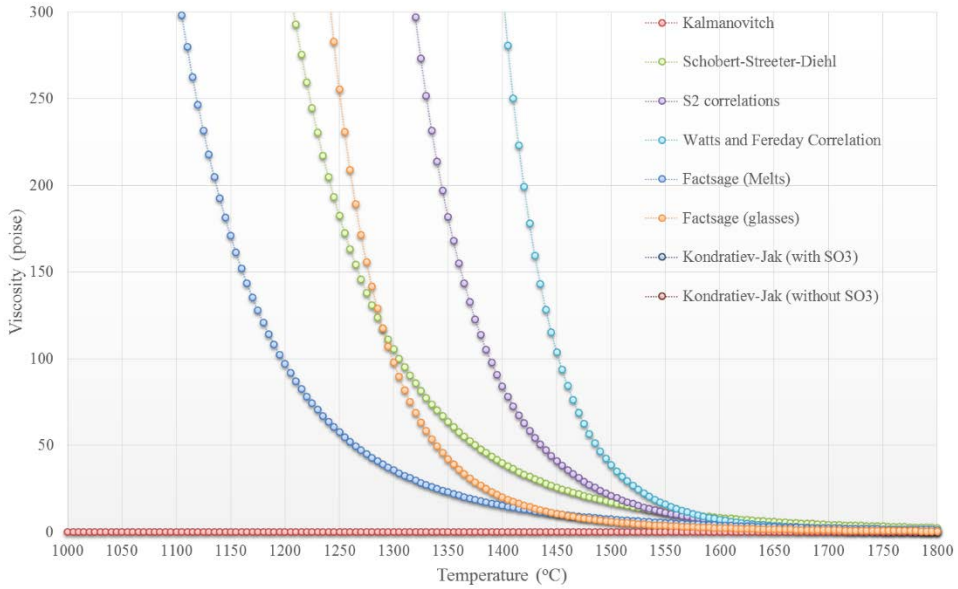


**Figure 29** Viscosity models applied with Loy Yang ash

These results may be attributed to the fact that compared to the other two coals, Loy Yang has a higher amount of Silica and lower amount of $Fe_2O_3$ while the other two coals (Yallourn and Morwell) contain a higher amount of $Fe_2O_3$ than Silica. However, the same irregularity as the other two coals appears to exist, albeit by a small value. However, the temperature still varies by around 100 ºC for each model.

### 5.2.4 Comparison of the best fit models

Theoretically, the FactSage (melts) database should provide the best fit model for the coals as it predicts the viscosity for temperatures above 900 ºC and for slags with components similar to Victorian brown coals [34]. However, when applied to the three coals, the same database gives highly varied results as shown in Figure 30. The temperature at which the viscosity for the three coals reaches 250 Poise vary within a range of 550-1150 ºC. Not only do the predictions vary largely, this range of temperature is also substantially lower than the expected operating temperature range of entrained flow gasifiers and the range of slag tapping temperature found in the literature (1400-1600 ºC)[35].

$S^2$ correlations appear to fit better than the other models for all the three coals owing to their suitability to slag with silica content lower than 55% since the three coals fall in that category. The temperature at which the viscosity reaches 250 Poise varies within a range of around 1250-1350 ºC for the three coals as shown in Figure 31. This range of temperature is also lower than the operating temperature range and the range of slag tapping temperature for entrained flow gasifiers (1400-1600 ºC [35]). The results suggest that none of the existing models in the literature or the models derived from FactSage database are suited for the viscosity prediction of Victoria brown coals slags. Hence, viscosity measurements are required to

generate data and either reassess some of these models or derive new models for Victorian brown coal ashes.

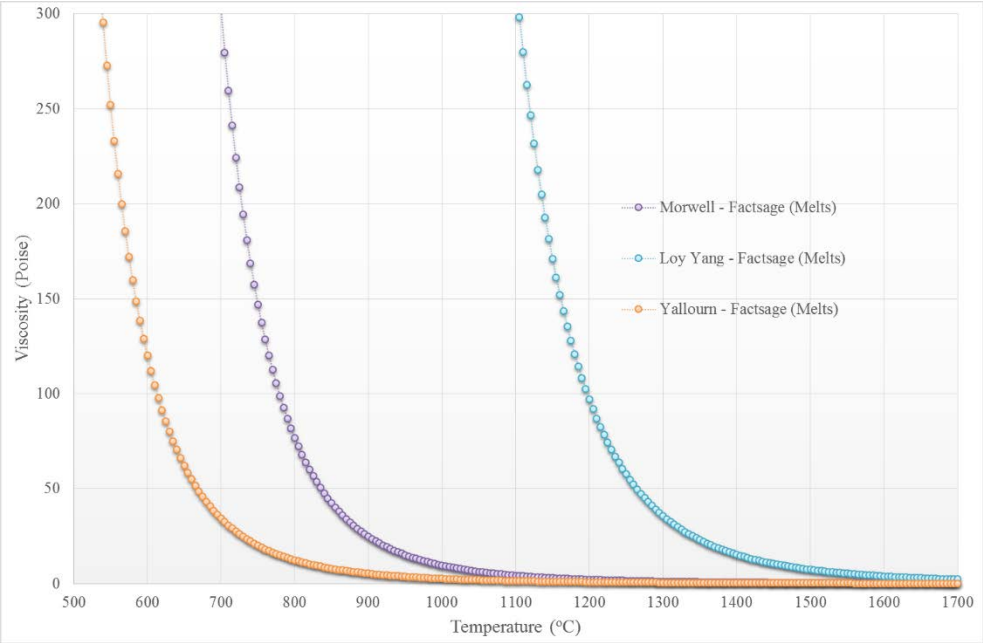


**Figure 30** FactSage (melts) database applied to the three ash samples

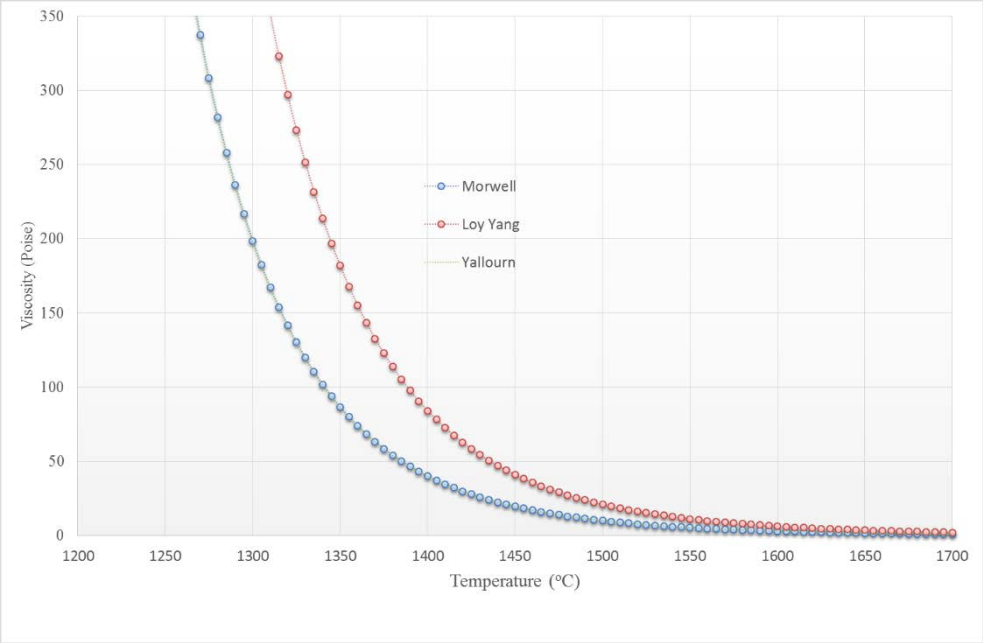


**Figure 31** $S^2$ correlation applied to the three ash samples

## 5.3 Conclusion

Slag viscosity of Victorian brown coals namely Loy Yang, Morwell and Yallourn were predicted using existing models available in the literature. The results suggest that Kalmanovitch model does not apply to any of the Victorian brown coals as this model is suited

more to coals with high $SiO_2$ and low 'FeO' content, and, therefore, fails to predict for the three coals which do not belong to this category.

The remaining models give results whose temperatures falls short of the slag tapping temperatures during gasification at 1400-1600 $^oC$. Ash fusion analysis on the Victorian brown coal ash suggests that flow temperatures of 1460 $^oC$ for Loy Yang in table 3 and Yallourn has flow temperatures of 1480 $^oC$ in table 4 whereas Morwell did not show any sign of melting below 1550 $^oC$.

The models expected to provide the best fit, $S^2$ correlation and the FactSage (melts) database, were examined closely. While the fits are better than the other models, being closer to the expected gasifier operating temperatures and literature predictions, the predictions still vary largely for the three coals. Moreover, the range of temperature for attaining 250 Poise, predicted by both these models is still significantly lower than the expected gasifier operating temperature range and slag tapping temperatures found in the literature.

The results suggest the need for experimental work to measure the viscosity of Victorian brown coal slags.

# 6 Design and construction of Viscometer assembly

The viscosity of slags is an important parameter to be measured to identify the operating conditions of a gasifier. Each coal has different ash composition and has varying ash fusion temperatures, phases, liquid slag formation temperatures as discussed in the previous sections. The results in the previous sections show that high temperatures in the range of 1300-1600 $^{o}$C are required to obtain the slags in molten form before viscosity measurements can be performed. Based on a literature review on the viscosity measured on different coals, a reactor design was conceived and is discussed in the sections below.

**Design:** A summary of high-temperature Rheometer assembly employed by other research groups are provided in Appendix C. Based on this summary, a high-temperature rheometer assembly was designed for the current project. The schematic of the Rheometer assembly designed and built for the current project is shown in Figure 32.

**Procurement:** After reviewing the existing literature on the various viscometers available Brookfield Ultra DV III with LV spring was selected.

**Calibrations:** The viscometer was calibrated with the standard liquids 12500, 30000 60,000 cP silicone liquid supplied by Thermo Fischer at room temperature and 717a NIST glass standard for high-temperature calibration to determine the Viscometer constants - Spindle multiplier constant (SMC) and Shear rate constants (SRC) with the custom made Molybdenum crucibles and spindles.

**Modifications**: The LV spring supplied by Brookfield was found unsuitable for viscometer measurements at the experimental conditions for brown coal. After many trials and discussion with the supplier, it was identified that the custom made bob and spindle assembly used in the present work was heavier (> 120 g) which was causing issues with the Viscometer procured.

Finally, it was decided to change the LV spring to RV spring which can support the heavy spindle at operation. It took four months for Thermo Fisher to procure the new RV spring causing a delay in the overall timeline of the project.

## 6.1 Drawing of the Viscometer assembly

A review of different Viscometer designs used in the literature is provided in Appendix C. Taking available literature design for the viscometer setup and keeping in mind the needs of the present project a new design for Viscometer assembly was developed. A drawing of the high-temperature Rheometer setup used in the current project is shown in Figure 32.

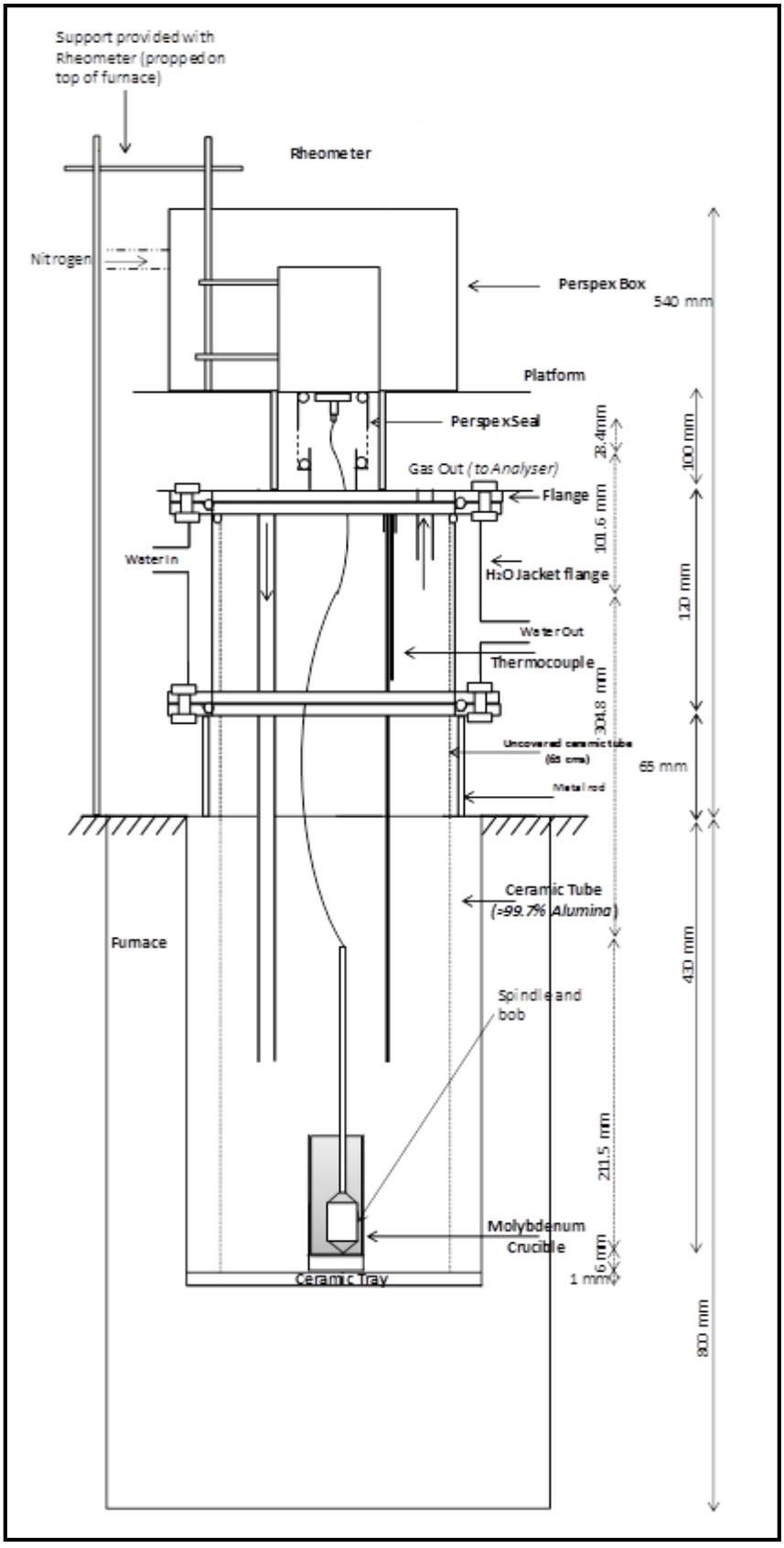


**Figure 32 Drawing of the Viscometer Assembly**

## 6.2 Viscometer assembly

This section discuss the design of the viscometer assembly used in the current project. This includes furnace selection, materials used for handling the slag, and viscometer.

### 6.2.1 Slag viscosity measurement setup

The basic construction requirements of a slag viscometer assembly include high-temperature, reducing atmosphere, easy set-up, small sample load, and easy sample loading.[36] The equipment for slag viscosity measurement mainly consists of a high-temperature furnace and a viscometer. The viscometer is mounted on top of the furnace and the samples are placed inside Molybdenum crucibles in the furnace. The measurements are taken while the sample is kept at a constant high temperature and given atmosphere.[33, 37-39] However since the experiments are conducted at very high temperatures it is important to shield the electronic hardware of the viscometer from the high temperature. The viscometer is supposed to be maintained at temperatures below 200 $^{o}$C for correct operations. Hence, the ceramic tube used in the setup should be long and extended outside the furnace above which the viscometer head can be mounted. As the ceramic tube will experience very high temperatures, the top part of the ceramic tube is water jacketed to maintain the temperature well below 200 $^{o}$C. As a further precaution, a Perspex seal was designed which is placed between the water jacket and viscometer. The viscometer head is constantly purged with the $N_2$ flow to cool it down further.

***High-temperature furnace***

A front load silicon carbide furnace by Tetlow was purchased for the current project. The dimensions of the internal work chamber are 200mm W x 200mm H x 250 mm D and the outer dimensions are 500 mm W x 665 mm H x 580 mm D. The maximum temperature of the furnace is 1650 $^{o}$C as the majority of the experiments are expected to be conducted within the temperature range of 1400-1600 $^{o}$C.

A vertical alumina tube of 5mm thickness is placed inside the work chamber. This thickness allows sufficient strength to the tube to prevent it from cracking under high temperature, due to its height or the weight of other equipment items partially supported by it. This thickness was determined by heat transfer calculations as the temperature drop between the chamber and the inside of the tube was calculated to be approximately 30 $^{o}$C which was deemed acceptable. This tube extends through the top of the furnace through an opening as shown in Figure 32.

***Viscometer- different types***

The primary equipment item in the viscosity measurement assembly is a Viscometer. In order to obtain viscosity measurements at a given temperature, slag samples are required to be sustained in molten form at that temperature before and during the measurements period. The major types of viscometers, along with the corresponding experimental conditions, used previously in similar studies for black coals and some lower rank coals, are tabulated in Table

14. The viscometers are broadly classified as Capillary, Falling-Body, Oscillation Cylinder or Plate, and Rotational viscometer.

A Capillary Viscometer operates on the principle of draining a liquid through a capillary. The viscosity is then determined from the measured flow, applied pressure, and tube dimensions. The Hagen-Poiseuille equation governs this process. These viscometers have a well-developed design and have been used for high-temperature viscosity measurements for the longest time [40]. However, these have been observed to provide imprecise data. Furthermore, the use of this viscometer at temperatures above 1200 $^{o}$C is difficult as a material selection of the parts becomes complicated [27].

A Falling-body viscometer is based on the Stokes law for a sphere where the body can either be falling or dragging upwards within a given sample [27]. This technique is most suited to transparent or translucent samples, and samples of large volume [41]. With a small sample size, such as that expected to be used in this project, the body will not be able to fall freely [42]. This leads to the need for wall corrections and results in measurements that are not absolute [43].
In an oscillation cylinder or cone and plate viscometer, the principle of operation is the swinging of a pendulum oscillating in the sample. The viscosity is calculated by observing the logarithmic decrements of the pendulum swings. This method is used for high-temperature measurements of materials of low viscosities lying in the mPa s region [27].

In a rotational viscometer employing a spindle and bob arrangement, the principle of operation involves rotating a spindle through the sample through a calibrated spring. The rotational speed, size and shape of the spindle, the dimensions of crucible govern the measurement range [37]. In this type of arrangement, the rotational flow is well defined, the crucible and spindle involve fairly simple construction, and the sample loading technique is well established. However, the sample amount required for a run is much higher than that required in a cone and plate arrangement [36]. Nevertheless, this type of viscometer covers viscosities from high to low, giving best results within 1000 to 10 Pas. It has been suggested as the most accurate method for high-temperature viscosity measurement [27, 40].

.

**Table 14: Summary of Viscometers used under various conditions in literature**

| | Viscometer | Type | Crucible | Temperature (°C) | Viscosity range | Environment |
|---|---|---|---|---|---|---|
| 1[44] | Brookfield HB-DVIII | Rotational | High-density alumina/platinum lined | 1600 | | $N_2$/CO: 80/20(vol%) |
| 2 [45] | Brookfield RVG | Rotational | | 1400-1800 | | |
| 3 [38] | Brookfield DVIII | Rotational | | | | Reducing atmosphere of 60/40 molar ratio mix of $CO/CO_2$ |
| 4 [36] | Brookfield HB-DVIII | Rotational | | 1600 | 5500 Poise | |
| 5[39] | Brookfield DV-III ultra | Rotational | High-density alumina | 500-1550 | up to 300 Pas | Oxidising |
| 6[33] | Brookfield DV-III | Rotational | High-density alumina | 800 | up to 120 Pas | Reducing: CO or $H_2$, Neutral: air, Oxidising: Air |
| 7[46] | Brookfield DV-III ultra | Rotational | | 500-1570 | up to 300 PaS. | |
| 8[47] | Brookfield DV | Cone and plate | | 600-1300 | | |
| 9[37] | Brookfield LVDVII+ | rotating bob (Rotational) | Molybdenum | 1580-1740 | 8-60 cPas | Argon+5%CO |
| 10[48] | Brookfield HB-DVIII | Rotational | High-density alumina | | | 80/20(vol%) mix of $CO_2$/CO or $N_2$/CO |
| 11[49] | Haake 1700 | Rotational | Molybdenum | 1300 | | Reducing (measured $O_2$ partial pressure) |
| 12[18] | Haake 1700 | Rotational | Molybdenum | | | $N_2$ |
| 13 [50] | Haake RV-2 Rotovisco | Rotating bob (Rotational) | High purity alumina | above 1500 | | Air, Air +10% water, reducing atmosphere |
| 14[51] | Haake RV-2 Rotovisco | rotating bob (Rotational) | High purity alumina | 1500 | | 20 H2:80 $N_2$ for reducing, pure $N_2$ for neutral, and air for oxidising conditions |
| 15[52] | Haake Rotovisco RV20 | Rotational | Platinum-Rhodium alloy 80/20 | 1700 | | |
| 16[53] | Haake Rotovisco RV-100 | Rotational | High-density alumina | 1430 | up to 3000 Poise | $CO/CO_2$:60/40 |
| 17[54] | Haake Rotovisco RV-100 | Rotational | | 1230-1380 | 1500-4000 Poise | 60/40(molar ratio) mix of $CO/CO_2$ |

***Spindle and Bob in a Rotational Viscometer***

The materials used for spindle and crucible construction commonly include alumina, platinum, carbon, tungsten, and molybdenum. Advantages of alumina are high-temperature strength and low thermal expansion coefficient. However, alumina crucibles get attacked by the slag and result in thinning of the crucible walls [55]. Furthermore, the alumina is known to contaminate the coal ash slags, by fitting into the silicate chains, specifically in the case of lower rank coals, thereby greatly affecting the slag viscosity.[26, 40] Carbon crucibles have been found to result in a reduction of slag and lead to the formation of metallic iron within the slag. Platinum is a good option for high-temperature measurements due to its high melting point and is also known to be non-contaminating. However, it is found to react with the iron present in some slags under reducing conditions. Therefore, it is not suitable for coal ash slags [27, 55].

Molybdenum and tungsten are known to cause the negligible contamination of sample.[26, 27] These are also found to be stable at high temperatures under gasification conditions due to high melting point [27, 40]. However, Molybdenum is easier to machine relative to tungsten[27, 40]. Therefore, Molybdenum crucible was used to hold the slag as shown in Figure 33 due to its low reactivity with the slags and its ability to withstand high temperatures in oxygen-free atmospheres. The dimensions of the crucible are 42 mm OD, 24.5 mm ID, 56 mm outer length and 50 mm inner length.

**Figure 33 Molybdenum crucible**

The bob and the spindle shaft is made of five parts which can be threaded to one another as shown in Figure 34. Molybdenum was the chosen material as it can withstand high temperatures without contaminating the slag samples.

**Figure 34 Custom-made Molybdenum Spindle and bob**

Two extension link of varying size 100 mm and 300 mm are used to suspend the spindle and bob as shown in Figure 35.

**Figure 35 Example of extension link**

***Rheometer***

Brookfield LVDV-III Ultra Programmable Rheometer will be used as shown in Figure 36. The rheometer operates on the principle of driving a spindle immersed in the sample through a calibrated spring. The spring torque of this model is 673.7 dyne.cm. The viscosity measurement range of this model is 0.47-11710 Poise and the measurements are made through RHEOLOADER Software. This model was chosen as it the viscosities expected to be measured fall within its measurement range.


**Figure 36 DV-III Ultra Rheometer [56]**

The viscometer is placed inside a Perspex box with a provision for nitrogen purge to prevent it from contamination by the furnace exhaust and further ensure that the temperature near the viscometer is near ambient. Further, a Perspex seal is placed such that it encloses the pivot cup of the viscometer. This extends on top of the stainless steel over the opening for the spindle platform ensuring a complete seal.

This viscometer employs a spindle and bob arrangement. The spindle and bob used for the experiments are custom-made to the required dimensions out of Molybdenum material. Since, the melting point of molybdenum, 2623 $^{o}$C, is much higher than the temperatures at which the experiments are conducted, this was the material of choice [57]. However, since it is prone to oxidation, the design of the assembly has to be such that the furnace chamber and the areas where the spindle and bob pass through are completely sealed. The advantages of Molybdenum over other materials are described in the section on spindle and bob in the rotational viscometer. The dimensions were based on the Brookfield spindle and bob and were increased proportionally. The upper limit for the dimensions was provided by the weight of the spindle and bob. The estimated weight was based on the studies related to the density of $CaO$-$Al_2O_3$-$SiO_2$ slags by Luckman and Seetha Raman [58]. The weight of the bob used in those studies for measurement of density was 178 g. The ash compositions of our coals are comparable to an extent to that of the slags used in these studies, therefore, the densities are assumed to be similar for the purpose of making an initial estimate. Furthermore, they reported that the density of the slag decreased as the temperature increased. Therefore, a conservative initial estimate of the weight of the spindle and bob to be used in the project was decided as 100 g.

Exceeding the 100g limit by more than 30g may cause discrepancies in the measurements and wearing out of the viscometer spring, as advised by the technical experts at Brookfield. The actual custom-made spindle and bob weigh 115g. The final dimensions of the custom-made spindle and bob are total length 210 mm, Diameter of spindle 5 mm, the diameter of bob 14 mm, the length of bob 30 mm. A means to control the weight of the arrangement was to use extension links (See Figure 34) as opposed to extending the shaft of the spindle itself. Extension links made from molybdenum for the area close to the furnace, and stainless steel for the area closer to the viscometer, will be used to immerse the spindle and bob into the furnace.

***Reaction chamber***

The chamber where the sample needs to be placed should be able to withstand high temperatures used in the reaction. Since the operating temperatures are close to 1500 $^{o}$C alumina tube of 90 mm outer diameter, 5 mm thickness and 620 mm length was obtained. The bottom of the alumina tube was placed on a flat alumina plate with 5 mm thickness and sealed with cement which can withstand high temperatures used in the current setup. This also prevents leak of air into the reaction chamber.

***Water jacket assembly***

As mentioned earlier, the viscometer needs to be protected from the high heat from the reaction chamber to prevent the malfunction of the unit. The alumina tube is to extend 180 mm above the furnace. A gap of 65 mm is left above the furnace to allow cooling at the top of the ceramic tube from ambient air convection. A water cooling jacket of 100 mm height is placed around the ceramic tube. The water jacket assembly has a bottom flange, water tubes, and top flange with O-rings around the alumina tube to hold the assembly in place. There is another top lid with a gasket with the provision of gas inlets-outlets, and thermocouple into the reaction chamber. It also has a hole at the centre of the lid which allows suspending the spindle from the viscometer. The continuous flow of tap water is maintained through the assembly during the course of the experiment when the temperature of the furnace is above 100 $^{o}$C. High purity argon was continuously purged during the course of the reaction to prevent any oxygen leaks inside the system.

***Perspex seal***

Perspex seal is used to connect the bottom mount of viscometer where the spindle and bob will be suspended into the reaction chamber and top of the water jacket. The seal was made of clear acrylic materials with can withstand temperatures up to 180 $^{o}$C. It has two parts matching the dimensions of the bottom of the viscometer and top of the water jacket. It can also be moved up and down so that the spindle height can be adjusted if required. The seal is provided with O-rings at the top and bottom preventing leaks in to the reaction chamber.

***Reaction Atmosphere***

The main reaction atmosphere under gasification conditions particularly entrained flow gasification is expected to be reducing, with a high CO: $CO_2$ ratio. Slag containing iron has been found to be sensitive to oxidising conditions, resulting in changing the iron from its ferrous to ferric state, thereby increasing the viscosity by a large value[27, 40]. Therefore, it should be aimed to conduct the experiments for this project under neutral or reducing atmospheres. Several gas environments used while measuring the viscosity of slags are summarised in Table 14.

## 6.3 Testing and Commissioning

All parts discussed in the previous sections are assembled as shown in Figure 32. An empty molybdenum crucible is placed inside the chamber. Prior to heating up the furnace, the chamber is purged with Ar flow overnight to scavenge and prevent any oxygen leaks into the system. Water flow is maintained through the water jacket to prevent excess heat reaching the Viscometer. The bottom of the viscometer and the top of water jacket was connected with the perspex seal. The furnace is heated up at 2 $^{o}$C/min up to maximum temperature up to 1500 $^{o}$C and held at the

maximum temperature for 2 h and cooled down. The commissioning of the viscometer assembly and the furnace was generally successful. However, few inherent problems were found which required modifications as described in the section below. The problems include a leak of oxygen into the chamber, the heavy weight of the spindle assembly and the OH&S requirement of having a suction hood over the viscometer furnace.

### 6.4 Modifications as required and associated delay

The modifications required for the Viscometer assembly include provisions for a water cooled jacket, special construction of spindle and bob, extensions for the viscometer spindle, and sealing of the pivot cup of the viscometer.

Gas suction hood over the Viscometer: Since the system is operated at high temperature with a continuous flow of inert gas like Ar, the safety officer of the department asked to ensure the gases released from the outlet will not reduce the ambient oxygen content in the vicinity of the viscometer assembly. After protracted deliberations, the safety officer asked to have a suction hood to exhaust all the gases coming out of the furnace to prevent Ar gas filling the lab and potentially causing asphyxiation. The arrangement of the suction hood by the facilities department was made after 4 months

The materials used in the system Mo crucible and extension links are sensitive to oxygen leaks into the system which will oxidise Mo resulting in contamination, the release of Molybdenum oxide powder, and breaking of the Mo extension links and failure of the experiment. In order to scavenge the oxygen leaked into the system, we identified that Graphite sleeves to the Mo crucible are required. However, the use of Graphite sleeves was not feasible instead graphite cubes of 1 $cm^3$ were placed around the crucible inside the reactor and performed a number of trial runs with acceptable results.

## 7 Slag viscosity and associated measurements

As mentioned in the previous section the slags produced in a gasifier must have a viscosity of range 100-250 Poise for efficient operation of the gasifier.[59] However, the viscosity of the coal ashes depends on the composition of the ash. The ash used in the present study- Loy Yang, Morwell and Yallourn can be classified as high $SiO_2$, high CaO and high $Fe_2O_3$ containing ashes respectively. Prediction of slag viscosity with the existing models suggests that these samples require high temperatures to have a viscosity in the prescribed range. Further, the ash samples also require flux addition to adjusting the temperatures for ash melting and viscosity.[60] It was established addition of foreign materials like CaO and clay can lower the temperatures of the slag melting. Complementary measurements were undertaken at Forschungszentrum Jülich GmbH, Germany and Mitsubishi heavy industries (MHI) Japan.

### 7.1 Work done at Forschungszentrum Jülich GmbH

This section briefly describes some of the work was undertaken at Forschungszentrum Jülich GmbH, Group of Thermochemistry. The work involved substantial measurements on emissions from Victorian brown coals at high temperatures typical of entrained flow gasification and measurements on ash and slags from Victorian and German lignites. Only ash and slag related work are reported here.

#### 7.1.1 Viscometer

A Rheotec RC1 system connected to a magnetic coupling with a coaxial cylinder sensor system was used to examine the evolution of viscosity of sub-liquid melts. The sensor system, stationary cup and rotating bob are made of pure molybdenum. The cup, which contains the specimen, is placed in the middle of the oven and separated by a dense alumina tube from the environment. Three $MoSi_2$ heating elements surround the tube. The temperature of the specimen is controlled by a thermocouple, placed directly below the cup. This enables a temperature measurement as close as possible to the fluid. To create a reducing atmosphere, a mixture containing Ar / $H_2$ is passed into the inner tube.

$$\eta = K\frac{T}{n} \qquad (7a)$$

Due to wide gap sensor geometry ($or/r_i > 1.1$), the viscometer needs to be calibrated. According to Eq. (7a)( a standard fluid was used to determine the calibration factor *K*. The standard glass G3 (HVG, Germany) was used. After calibration, the factor *K* was validated by two additional standard glasses, DGG1 (PTB, Germany) and G3 (HVG, Germany) and the results are shown in Figure 37. The maximal deviation between experimental viscosities and reference values in literature was about 30 %.

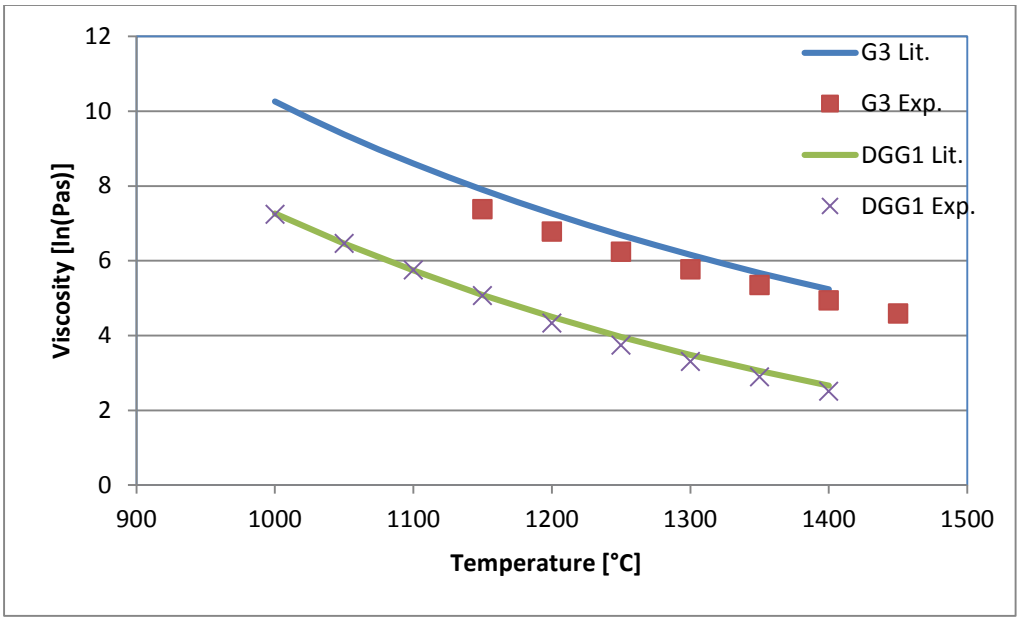


**Figure 37** Viscosity measurement on standard glasses, DGG1 (PTB, Germany) and G3 ash (HVG, Germany).

### 7.1.2 Ash Fusion Test

The melting behaviour of the samples was characterised according to ash fusion test (AFT). The ash sample was pressed to a cone according to ASTM D-1857 [61] and placed on an alumina substrate. They were exposed afterwards to temperatures up to 1500 °C under reducing gas atmosphere in using a hot stage microscope. While the specimen is heated up with a constant heating rate of 5 °C/min, every temperature step of one °C the specimen is recorded by a CCD-camera. Changes of the shape can be directly linked to technical and thermophysical properties of a fuel's ash during heating. In detail, initial deformation temperature or sintering temperature (IDT), softening temperature (ST), hemispherical temperature (HT), and fluid temperature (FT) describe the melting of the ash starting with sintering. Figure 39 shows the typical profile of Ash melting behaviour.

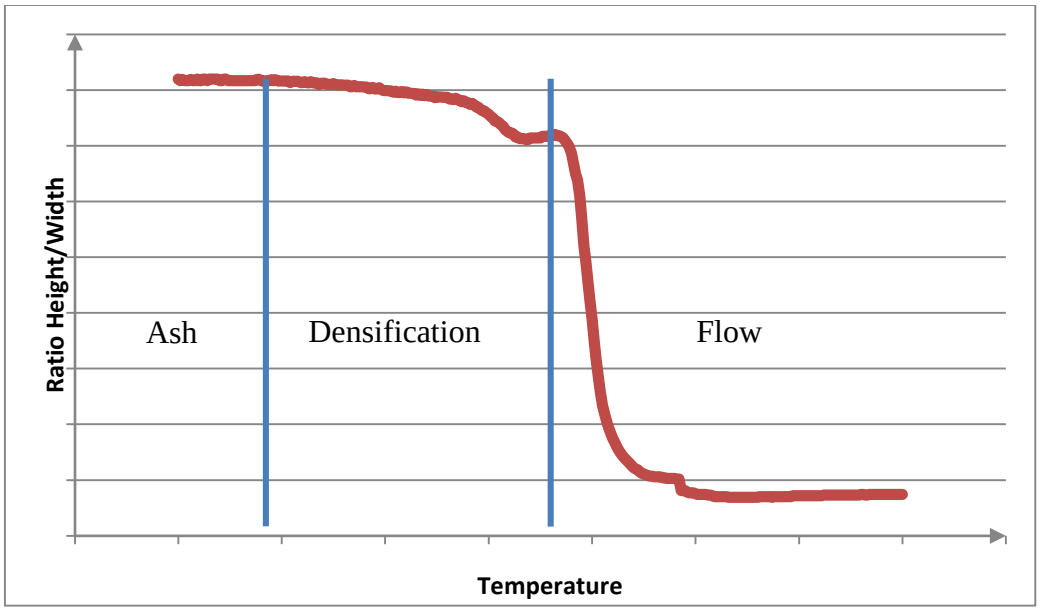


**Figure 38** Scheme of ash fusion behaviour of samples

The resulting images were automatically analysed by a Matlab algorithm (Vers. R2008a). Firstly, the images were converted to a black-and-white format. This allows the conversion into a Mat lab matrix equivalent to the size of the image. Using a spline the outer shape of the ash in each image is detected. Comparing the maximum width and height delivers a detailed insight into the melting and sintering behaviour. In Figure 38 typical change of the ratio of height to width is shown. The change of this ratio can be linked to physical changes in the ash. At first, no influence of the high temperature of the ash is observed until the densification starts. The densification is accompanied by shrinkage of the specimen. The melting itself changes the geometric ratio rapidly.

## 7.2 Results

Four lignites were investigated at Forschungszentrum Jülich GmbH, Germany. The German lignite HKT, and the three Australian lignites Loy-Yang, Morwell and Yallourn.

### 7.2.1 HKT German lignite ash

Table 15 shows the ash composition of German lignite HKT which is rich in $SiO_2$ similar to Loy Yang ash of Victoria.

**Table 15** Ash composition of HKT German lignite

| | $Al_2O_3$ | BaO | CaO | $Fe_2O_3$ | $K_2O$ | MgO | $Mn_2O_3$ | $Na_2O$ | $SiO_2$ | $TiO_2$ |
|---|---|---|---|---|---|---|---|---|---|---|
| HKT | 20.04 | 0.14 | 14.18 | 2.53 | 0.73 | 5.88 | 0.05 | 2.70 | 52.45 | 1.29 |

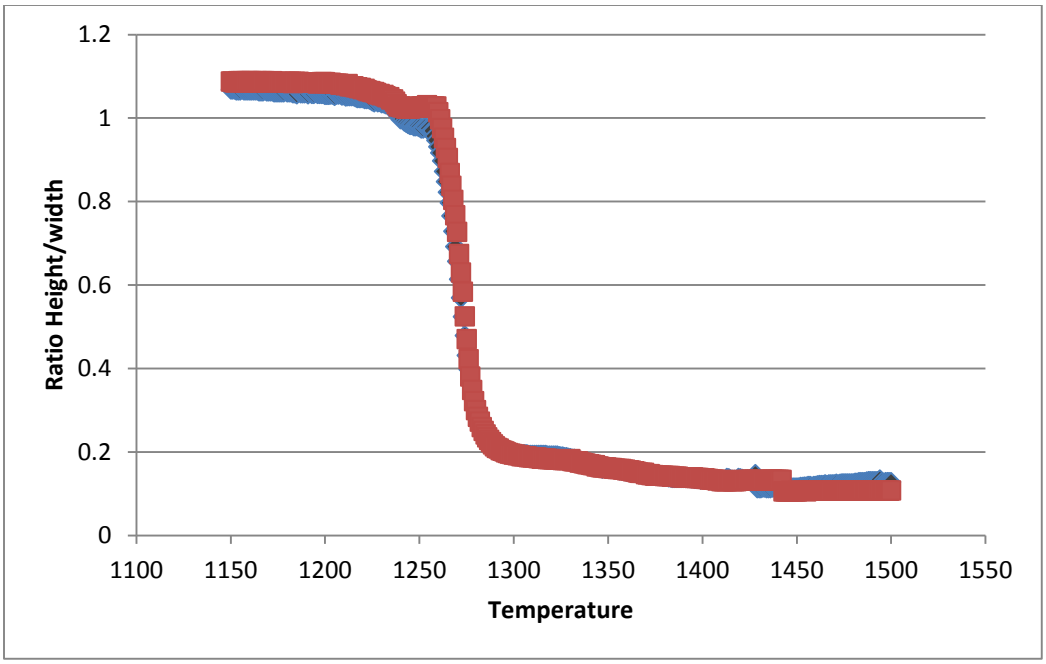


**Figure 39** Ash fusion behaviour of German Lignite HKT

Figure 39 shows the ash fusion behaviour on HKT lignite ash indicate that sintering takes place in the temperature range between 1200 – 1250 °C. It starts to melt at about 1260 °C and started to flow at 1280 $^{o}$C. Figure 40 shows the viscosity data of HKT ash. As mentioned earlier the typical viscosity in the gasifier should be around 10-25 Pa. S i.e. 100-250 Poise. The data shows that the HKT sample possesses this viscosity range between 1260-1280 $^{o}$C. Hence, it would be beneficial to operate the gasifier at 1300 $^{o}$C depending on the carbon conversion that can be achieved with this coal.

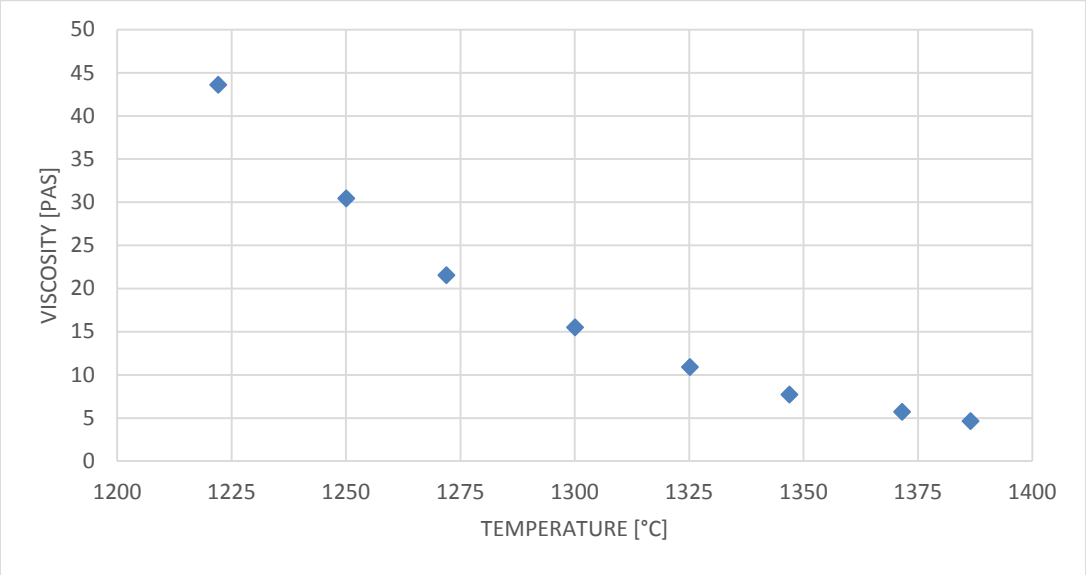


**Figure 40** Viscosity measurements on German lignite HKT.

Figure 41 shows that HKT has non-Newtonian flow for temperature lower than 1225 °C, resulting in a shear thinning flow. This change of flow is a result of crystallization of the slag during the measurement.

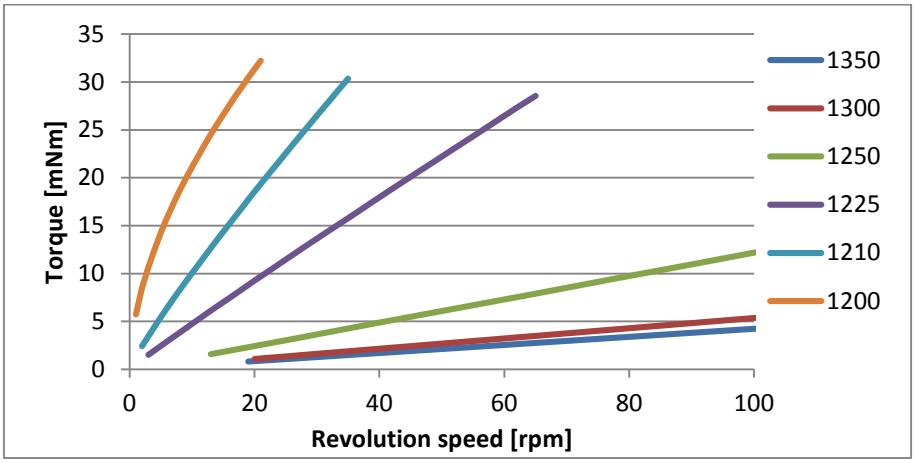


**Figure 41** Viscosity on HKT German lignite at different temperature sand torques

### 7.2.2 Loy Yang, Morwell, and Yallourn ash

Figure 42 shows AFT with a strong expand in the range between 1225°C – 1450 °C for Loy Yang. It starts to melt beyond 1400 °C. However, when compared to HKT lignite the flow behaviour is rather broad from 1400-1475 °C suggesting the ash has multiple phases which are

still crystalline and have melted in this temperature range. At temperatures beyond 1480 $^{o}$C, the sample showed a sudden drop in the graph suggesting completely molten stage. When the viscosity on the Loy Yang ash was measured, non-Newtonian behaviour with a very high viscosity above 25 PaS was noticeable. The results suggest that the Loy Yang requires the addition of flux materials to reduce the flow temperatures.

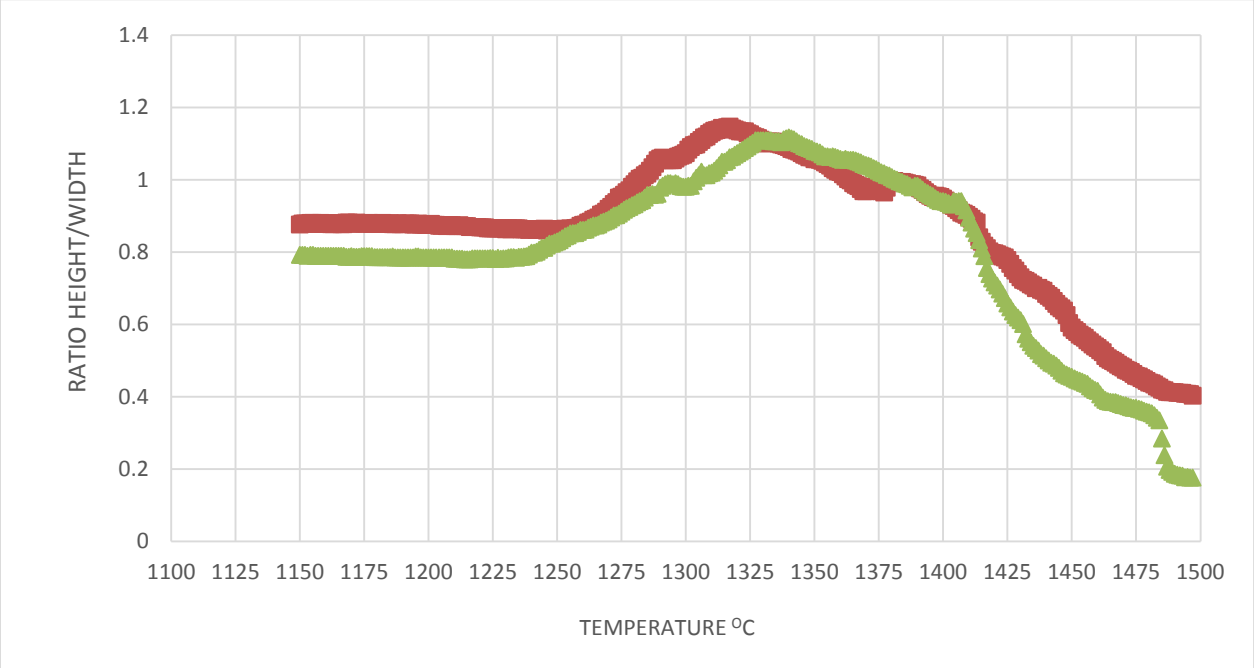


**Figure 42** AFT measurement of Loy Yang ash.

### 7.2.3 Morwell ash

Figure 43 shows AFT results of Morwell ash. Similar to Loy Yang ash, Morwell ash fusion tests suggest that the sample only starts to sinter at 1380 $^{o}$C suggesting very high melting temperatures. The slag started to flow only at 1470 $^{o}$C. The results also suggest that Morwell will require fluxing materials to reduce those temperatures in order to have a measurable viscosity.

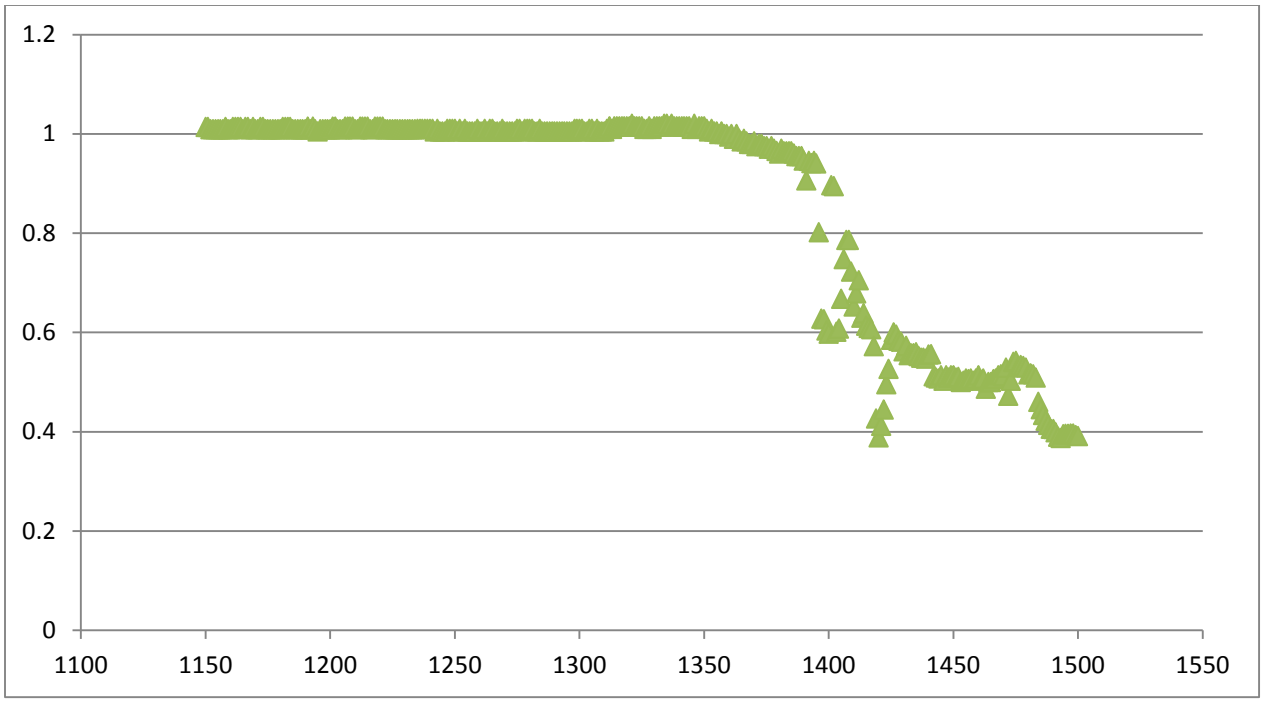


**Figure 43** AFT profile of Morwell ash

### 7.2.4 Yallourn ash

Interestingly Yallourn ash did not show any sign of sintering or melting until 1400 $^{o}$C in Figure 44. This is contrary to the AFT measurements performed at Monash University.

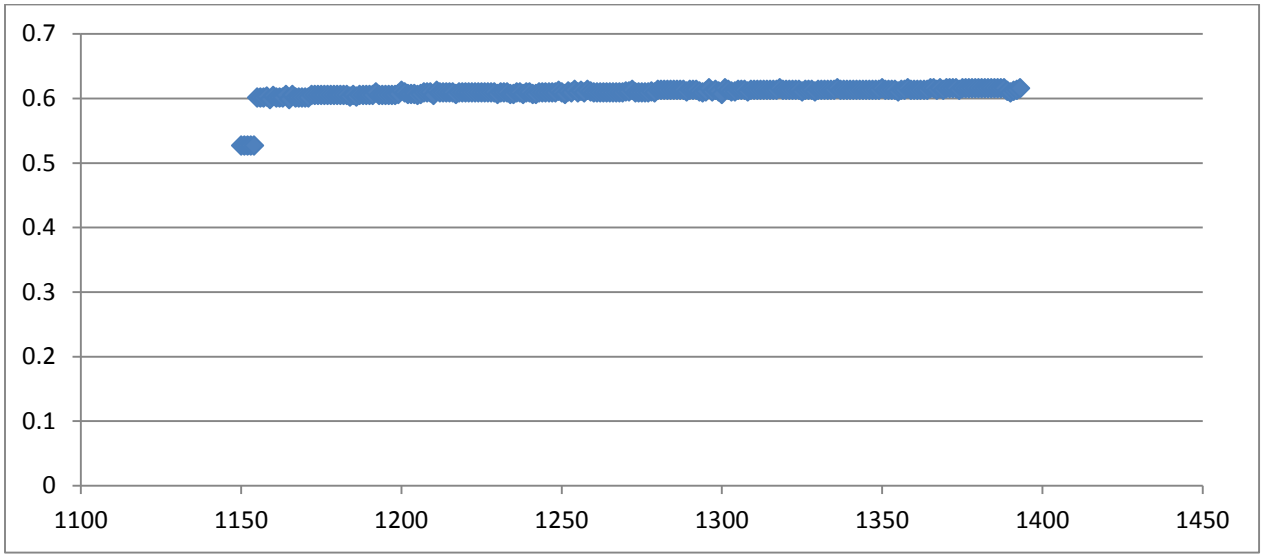


**Figure 44** AFT profile on Yallourn ash.

The viscosity measurements conducted at Forschungszentrum Jülich GmbH indicated that for all the three ashes viscosity was much higher than 250 Poise at 1450 $^{o}$C.

### 7.2.5 Conclusion

The work at Julich Germany shows that German lignite HKT has a relatively low melting temperature and can achieve the viscosity range of 100-250 Poise between 1260-1350 $^{o}$C. On the other hand Victorian brown coal ash samples have relatively high flow temperatures beyond 1450 $^{o}$C within which a measurable viscosity to 250 Poise could not be obtained.

Two alternatives can be suggested for the use of Victorian brown coal ashes to be used in a gasifier at a typical temperature range of 1200-1450 $^{o}$C.

- Mixing a flux CaO or clay to lower the flow temperature.
- The second alternative can be using a two stage gasifier where the gasification of the coal can be achieved at relatively lower temperatures in the first stage of the gasifier and higher temperature molten ash can be formed at the second stage in the required viscosity range.

### 7.3 Work done at Mitsubishi Heavy Industries (MHI), Japan

As part of the collaboration and in-kind contribution, MHI, Japan performed characterisation and viscosity measurements on one Victorian coal and Shenhua coal of Chinese origin.

#### 7.3.1 Results of characterization and viscosity on Yallourn ash.

Table 16 shows the composition of Yallourn ash measured at MHI, Japan. The results show the ash composition of sample 1 varies a lot with sample 2 suggesting heterogeneous nature of the coal. This ash is from a different batch from the one tested at Monash. The samples are also tested for ash fusion temperature as shown in Table 17. The results show a large variation in the flow temperature of the ash samples.

**Table 16: Composition of Yallourn ash**

| Element | Sample 1 | Sample 2 |
|---|---|---|
| $SiO_2$ | 3.78-50.6 | 2.48 |
| $Al_20_3$ | 2.07-13.3 | 4.03 |
| $Fe_2O_3$ | 41.2-8.91 | 46.29 |
| $TiO_2$ | 0.08-0.62 | 0.14 |
| $K_2O$ | 0.80-0.90 | 0.57 |
| MgO | 18.5-9.51 | 15.29 |
| $Na_2O$ | 3.83-2.96 | 6.2 |
| CaO | 7.58-4.19 | 11.88 |
| $SO_3$ | 17.2-7.24 | 0.57 |

**Table 17 Ash Fusion test of Yallourn coal ash**

| | Temperature ($^oC$) | | |
|---|---|---|---|
| Sample | Deformation | H-Spherical | Flow |
| Sample 1 | 1390-1190 | 1500-1250 | 1500-1280 |
| Sample 2 | 1245 | 1365 | 1480 |

### 7.3.2 Viscosity measurement on Yallourn ash

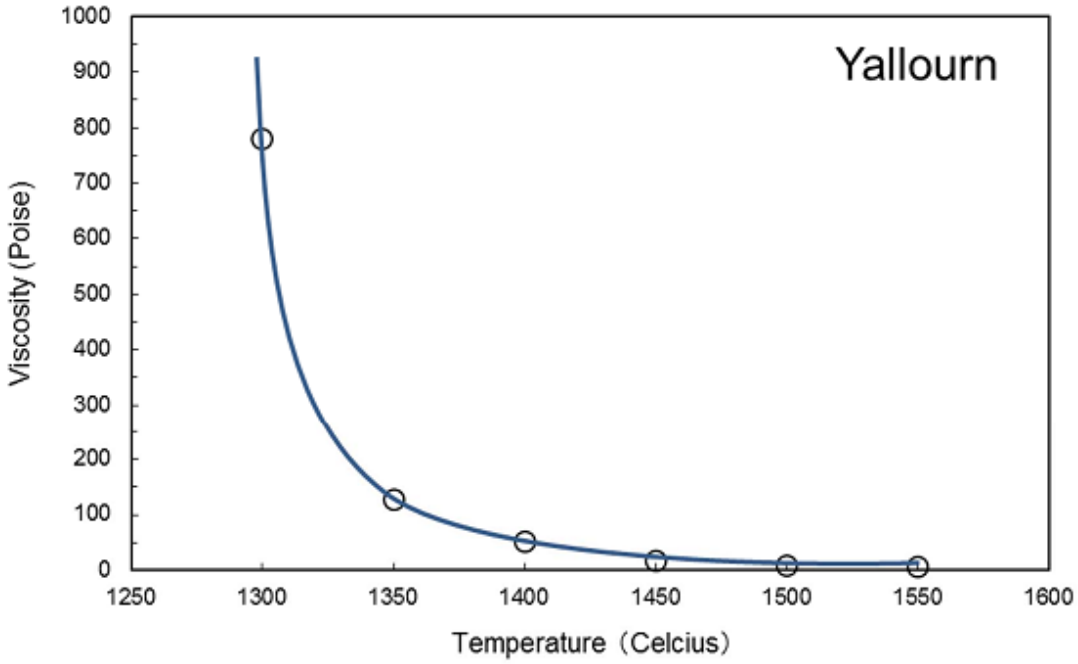


**Figure 45** Viscosity measurement on Yallourn ash

The viscosity measurement on Yallourn ash performed at MHI is shown in Figure 45. The results indicate that a desirable viscosity range of 100-250 Poise is achieved in the temperature range of 1325-1360 $^{o}$C. Test at MHI indicates that the ash composition of Yallourn varies largely resulting in variation of melting temperature of the ash. But, the viscosity data indicate a temperature range of 1325-1360 $^{o}$C.

### 7.3.3 Conclusion

Ash composition on Yallourn ash determined at MHI indicate heterogeneous nature of the coal. Ash fusion test on Yallourn ash shows 250 $^{o}$C variation in the flow temperatures of the slag. The viscosity data showed that the Yallourn ash has a viscosity of 100-250 Poise at 1325-1360 $^{o}$C.

## 7.4 Viscosity experiments performed at Monash University

### 7.4.1 Slag Preparation

Ash samples of three Victorian coals - Morwell, Yallourn, and Loy Yang were prepared in a muffle furnace at 815 $^{o}$C in air. During the sample preparation, the coal was spread in thin layers as spreading them in thick layers would result in combustion of top layers leaving the bottom layers unburnt. Victorian brown coals have very low concentrations of ash, ~ 2%, on a dry basis. Due to the low concentration of ash, large amounts of coal need to be burned to produce sufficient amount of ash required for viscosity measurements. It was determined that, for each viscosity measurement of a particular coal, at least 200 gm of ash is required *ie* approximately 10 kg of dry coal is needed to burn to produce enough ash for one viscosity measurement.

Considering the difficulty in producing the quantity of ash required for the project, a large furnace where the large quantities of coal can be combusted in a single campaign were tried at CSIRO. However, the tests performed to produce ash was not successful. Hence, we continued to produce ash in the muffle furnace which took a very long time.

It is also designed in the experimental plan to add flux materials like CaO or clay from Loy Yang mine at different ratios (minimum 3) to the three coal ash samples. Basing on this calculations, it was estimated that 3 kg ash of each type of coal was required for the completion of the measurements.

The ash is placed in a Molybdenum crucible to be used in the viscosity measurement. The crucible is then placed inside the ceramic tube as shown in Figure 32. The system was purged with Ar gas overnight to minimise the oxygen concentration in the system. Then the furnace was heated to its highest temperature. When the ash was heated to higher temperatures, as expected the sample started to shrink, sinter, and finally become molten. During the slagging process, certain amount of the ash evaporate, resulting in the overall reduction in the mass and volume of the sample. The sample size shrunk to $1/4^{th}$ - $1/5^{th}$ of the initial amount of ash loaded in the crucible. Hence, each crucible needs to be refilled 4-5 times and subjected to heating to the maximum temperature to obtain one full crucible of slag sufficient for one viscosity measurement. Preparation of one sample for viscosity measurement required almost two weeks of slagging in the Mo crucible.

Slag viscosity measurements were performed within a furnace with SiC heating elements and a Brookfield DV-III Ultra rheometer with an RV spring. The rheometer is connected to a PC for external control. The crucible is placed in a custom-built alumina chamber within the furnace for gas atmosphere control and spill protection. The sample temperature was measured by placing a pre-calibrated external thermocouple in the slag prior to the experiments. Argon purge was started overnight and maintained in the furnace at 500 $cm^3$/min to prevent any oxygen leak into

the system along with graphite blocks around the molybdenum crucible to consume any oxygen leak. A molybdenum spindle, attached to the rheometer, reaches inside the slag sample and is rotated to measure the torque.

Where CaO and clay were used as flux material, the same procedure was adopted for slag preparation inside the Molybdenum crucible.

### 7.4.2 Calibration of viscometer

Prior to measuring the viscosity of the ash, the viscometer has to be calibrated. This was done at both room and high temperature. At room temperature, calibration was conducted with with standard liquids (12500 cP, 30,000 cP), which is supplied by Thermofischer scientific. At a high-temperature viscosity of glass standard 717a from NIST was tested at a higher temperature range at 1300-1460 $^{o}$C. However, in our experimental setup, we used custom made spindles, crucibles, and extension links. Therefore, it is necessary to determine the viscometer constants - Shear rate constant (SRC) and Spindle multiplier constant (SMC) which depend on the dimensions of the crucible and the bob used to spin in the fluid.

Initially, the SMC and SRC values were kept at zero and using a standard liquid with 12,500 cP the spindle was rotated at varying rotation speeds ranging from 1 to 5 RPM and the corresponding torques were measured. These torque values against chosen viscosity of 12,500 cP and the dimensions of the spindle and crucibles used the SMC and SRC values were determined to be 26.099 and 0.3049 respectively. These values are used as input and measurements are repeated to obtain an actual viscosity of the liquid. The viscosity values obtained matched that of the liquid

Later, the viscometer is calibrated against another sample with high viscosity 32000 cP to ensure that the numbers obtained were in the range.

Viscosity calculation involved the following equations:

Shear rate ($sec^{-1}$) $\gamma = 2\omega R_c^2 R_b^2 / X^2(R_c^2 - R_b^2)$ (7b)

Where $\omega$ is angular velocity of spindle (rad/sec) = $(2\pi/60) * N$, where N=RPM

$R_c$= Radius of container (cm)

$R_b$= Radius of spindle (cm)

X= Radius at which shear rate is measured i.e. at the interface of liquid and spindle.

Shear stress (dynes/$cm^2$) $\tau = M/(2\pi R_b^2 L)$ (7c)

M= torque input by the instrument (dyne-cm)

L= effective length of the spindle

Viscosity $\eta = \tau / \gamma$ (7d)

The calculations are based on the custom made spindles and crucible used in our experiments. These equations help in determining the SRC and SMC values which were given as inputs to the instrument for the calculation of viscosity of the liquid to be measured.

### 7.4.3 Results

***Ash fusion test***

Ash fusion tests conducted on ash samples at HRL and MHI in 40% CO/60% $CO_2$ show all the Victorian ash samples have relatively very high flow temperatures; Loy Yang – 1480 $^oC$, Yallourn >1500 $^oC$ and Morwell >1500 $^oC$ as stated in earlier sections. The ash fusion results are in line with the results obtained at Julich confirming high flow temperatures. The results indicate the requirement of the addition of flux materials.

***Viscosity results using 717a standard***

Figure 46 shows the viscosity calibration measurements on NIST standard glass 717a on the viscometer along with listed values from the supplier of the standard company at corresponding high temperatures. This is the standard used in all high-temperature viscosity measurements reported in the literature. The measurement reported here are repeated three times at each temperature. In addition, such measurements were repeated at the beginning and end of the measurement campaign. The results indicate acceptable calibration at all measurement temperatures.

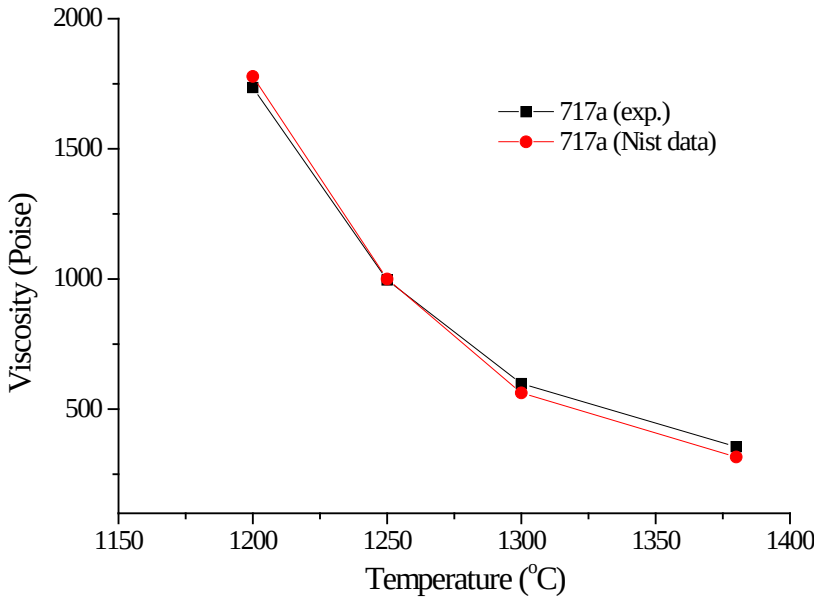


**Figure 46** Viscometer calibration with NIST glass standard 717a.

In the following sections, the viscosity measured on different ash samples are presented. The results represent the average of at least three measurements at each point.

***Loy Yang ash***

During the ash fusion test, Loy Yang ash achieved flow temperatures at 1460 $^{o}$C. However, at this temperature the viscosity was so high that it did not allow spinning of the spindle at low and high rotational speeds of 0.1 and 5 RPM.

This indicated that Loy Yang ash required the addition of flux material to lower the melting temperatures further. From ash analysis, Loy Yang ash is rich in $SiO_2$ (63.65%) and CaO (9.8%). The addition of 4% CaO to ash lowered the viscosity and measurable viscosity was achieved on Loy Yang ash.

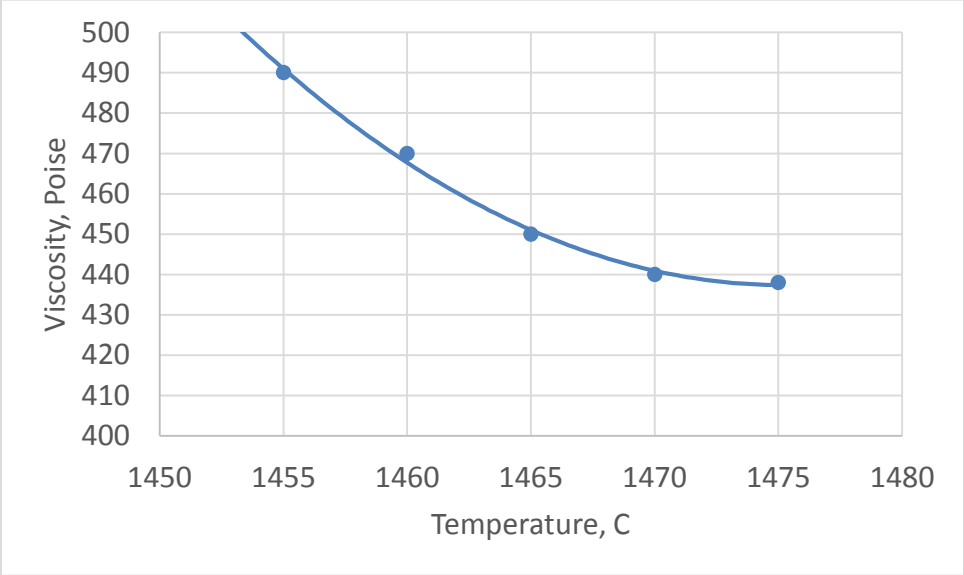


**Figure 47** Viscosity measurement - Loy Yang ash + 4% CaO

Figure 47 shows the viscosity measurements on Loy Yang ash with 4% CaO added to the ash. The ash fusion test results (table 4) show that the melting temperature of Loy Yang ash is reduced with the addition of 4% CaO by 100 C. However, the viscosity of the sample when measured is high, around 450 Poise at 1465 $^{o}$C. This suggested that further addition of CaO might be required to lower the viscosity. Literature data showed that small amount of CaO or $CaCO_3$ addition as flux to the ash would lower the ash melting temperatures[2]. However, at higher concentrations of CaO the high melting temperatures of CaO will dominate and will have negative effect on the melting behaviour of the ash. Hence, it is important to optimise the amount of CaO required to achieve viscosity in the range of 100-250 Poise.

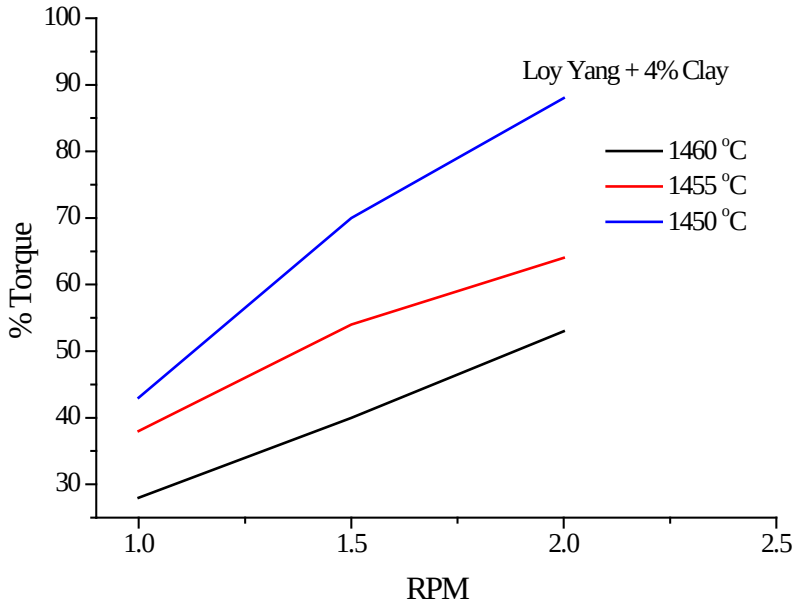


**Figure 48** Torque vs RPM - Loy Yang + 4% CaO

Figure 48 shows that Loy Yang + 4% CaO has non-Newtonian flow at temperature below 1445 °C, resulting in a shear thinning flow. This change of flow is a result of crystallization of the slag during the measurement. This figure also indicates that a temperature higher than 1460 °C is required to effectively use Loy Yang ash in a gasifier for smooth flow of slag. When the CaO content mixed with Loy Yang ash was increased to 8% the sample did not show any measurable viscosity suggesting the CaO composition has exceeded the optimum composition that could be beneficial in lowering the melting temperatures of Loy Yang ash.

Extrapolation between 1510 C and 1550 C of the viscosity measurements at 1460 °C indicate that a sample temperature in excess of 1500 °C will be required for a viscosity between 250 and 100 Poise for Loy Yang ash mixed with CaO as flux.

In further measurements, Loy Yang ash was also mixed with 4% clay rich in $SiO_2$. This only slightly lowered the viscosity compared to Loy Yang ash but showed higher viscosity than the Ly sample with 4% CaO addition.

The results in Figure 49 indicated that further addition of clay would not lower the viscosity of Loy Yang ash. This is due to the high silica content in clay combined with high silica content in Loy Yang ash makes the resultant slag difficult to melt.

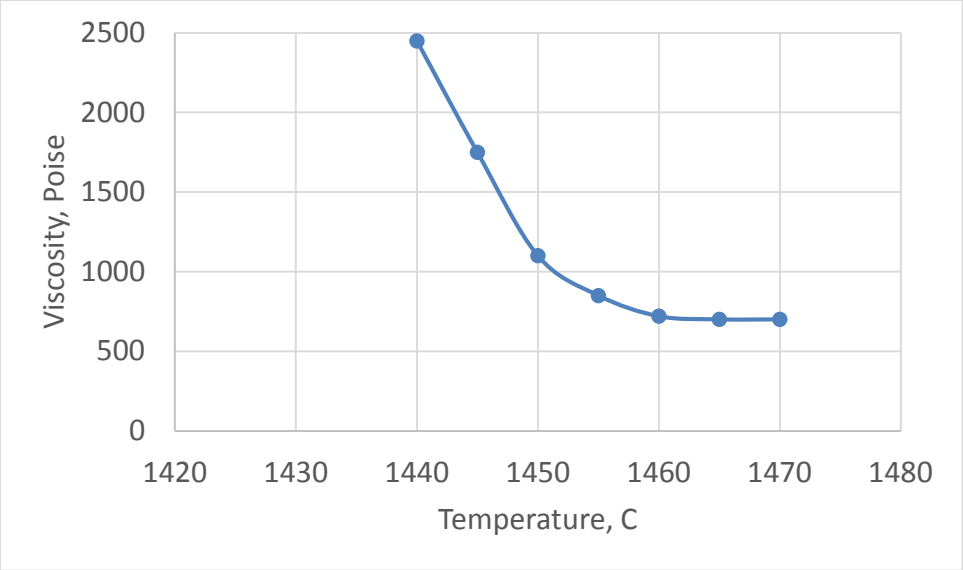


**Figure 49** Viscosity data - Loy Yang ash + 4% clay.

The viscosity measurements results reflect the results of the ash fusion tests (Table 4) performed on Loy Yang ash with flux addition, where CaO addition lowered the flow temperatures below 1460 $^{o}$C whereas clay did not alter the flow temperature. Viscosity measurements also show that the values are still above the desirable viscosity range of 100-250 Poise suitable for smooth removal of the slag from the gasifier.

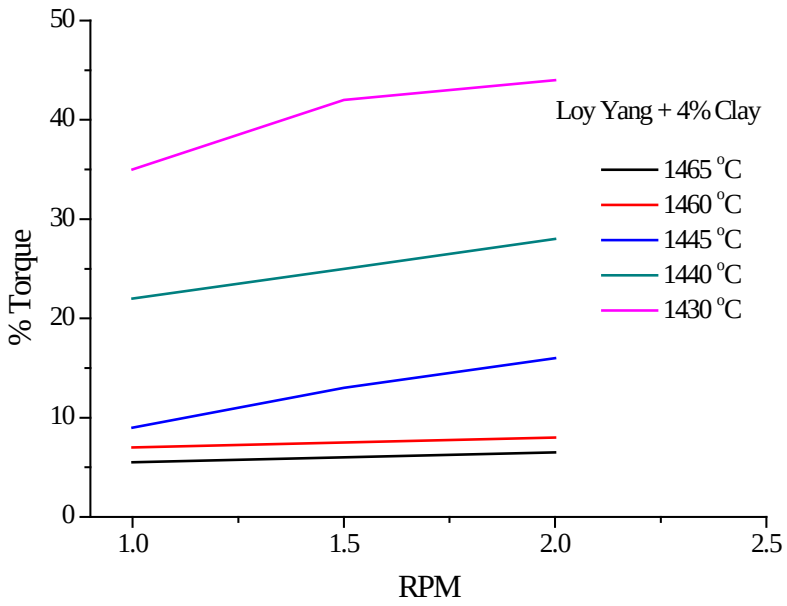


**Figure 50** Torque vs RPM - Loy Yang + 4% clay

The results in Figure 50 show the non–Newtonian behaviour of Loy Yang + 4% clay until 1460 $^{o}$C suggesting even high temperatures are required for the slag to have a smooth flow along the walls of the gasifier. The increase in torque with RPM suggest that the samples still have a large crystalline fraction of ash present in the slag.

***Comments on the viscosity of Loy Yang slag***

It is clear from the above measurements that clay addition will not lower the viscosity of Loy Yang slag. Use of the Loy Yang ash alone will require temperature in excess of 1500 $^{o}$C for viscosity to be under 250 Poise. Therefore, other measures will be required to use Loy Yang ash in a gasifier. This is discussed in section 7.6.2.

***Yallourn ash***

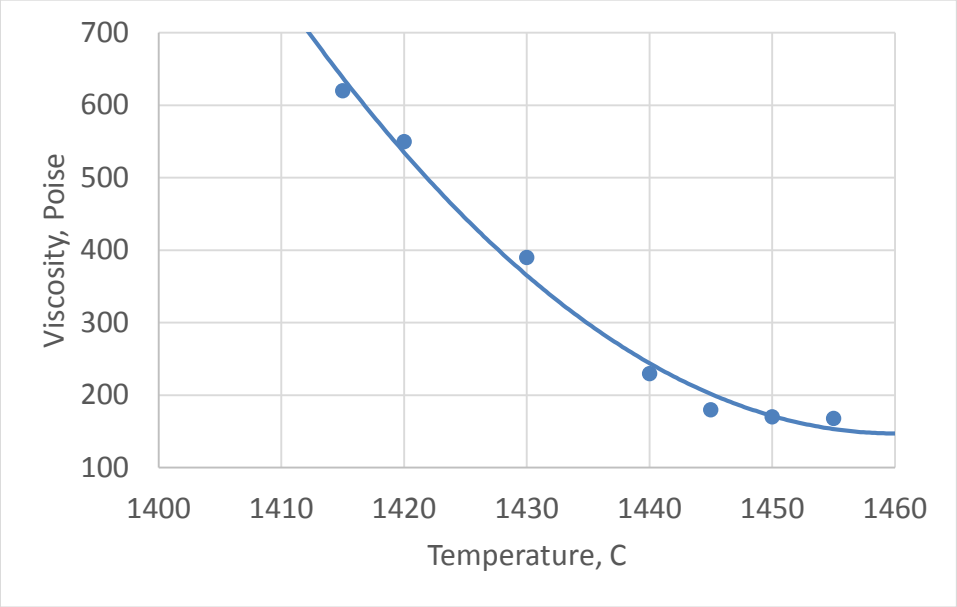


**Figure 51** Viscosity measurements - Yallourn ash

Ash fusion test on Yallourn ash showed very high melting temperatures beyond 1500 $^{o}$C. Similar results were observed during the ash fusion tests in Julich Germany. However, experiments conducted on the Yallourn ash (which has high Fe content) showed measurable viscosity at the temperatures between 1410-1450 $^{o}$C as shown in Figure 51. The viscosity range of 100-250 Poise is achieved between 1440-1450 $^{o}$C. These results contradict the ash fusion results which consistently showed melting temperatures above 1500 $^{o}$C. It is clear that ash fusion test is not a reliable predictor of slag viscosity.

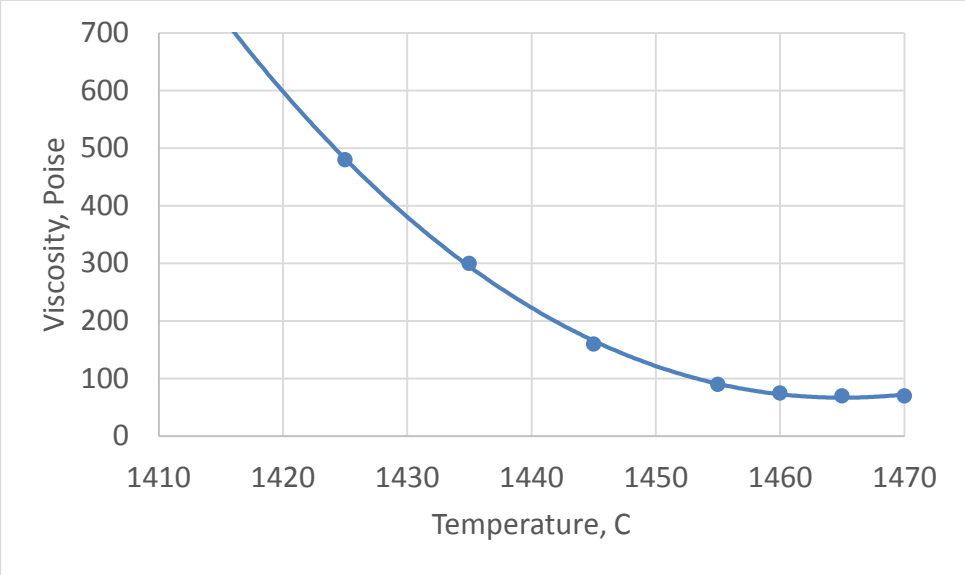


**Figure 52** Viscosity measurement on Yallourn + 4% CaO

To further test the effect of flux addition 4% CaO and 4% clay were separately added to the Yallourn ash and tested for viscosity measurements. The results are shown in Figures 52 and 53 respectively.

Yallourn with 4% CaO sample in Figure 52 showed viscosity similar to Yallourn ash as shown in Figure 51. However, the viscosity of the slag is slightly reduced compared to the Yallourn ash alone. The temperature ranges to achieve a viscosity in the range of 100-250 Poise is around 1440 $^{o}$C irrespective of whether 4% CaO is used as a flux.

Results of viscosity measurements using Yallourn ash mixed with clay are presented in Figure 53. The lowest viscosity measurable was 390 Poise at 1465 $^{o}$C. The results indicate an increase in viscosity of the slag with the addition of clay compared to Yallourn ash. Addition of clay appears to be not suitable for lowering the viscosity of Yallourn ash as was the case with Loy Yang ash.

***Morwell ash***

In the ash fusion tests, Morwell ash did not show any sign of melting until 1500 $^{o}$C. The high melting point of ash can be attributed to the high concentration of CaO (36%) in the ash. DTA results suggested that addition of 4% CaO did not have any major effect, however when 8% and 15% CaO was added the samples experienced large weight loss suggesting that the CaO promoted the evaporation of some of the components of the ash. Physically, the molten sample shrunk to 1/5$^{th}$ of its size suggesting large evaporation of certain components of the ash. However when the sample was tested for viscosity, it did not show any measurable viscosity.

The torque was reaching above 100% both at two spindle rotations speeds of 0.1 RPM and 5 RPM. The results indicate that addition of CaO could have helped some of the components of ash to evaporate but did not lower the melting temperature of the remaining components. Similarly, when the sample was mixed with clay overburden rich in $SiO_2$ (80%) at 4% and 8% concentrations the samples only sintered but did not melt.

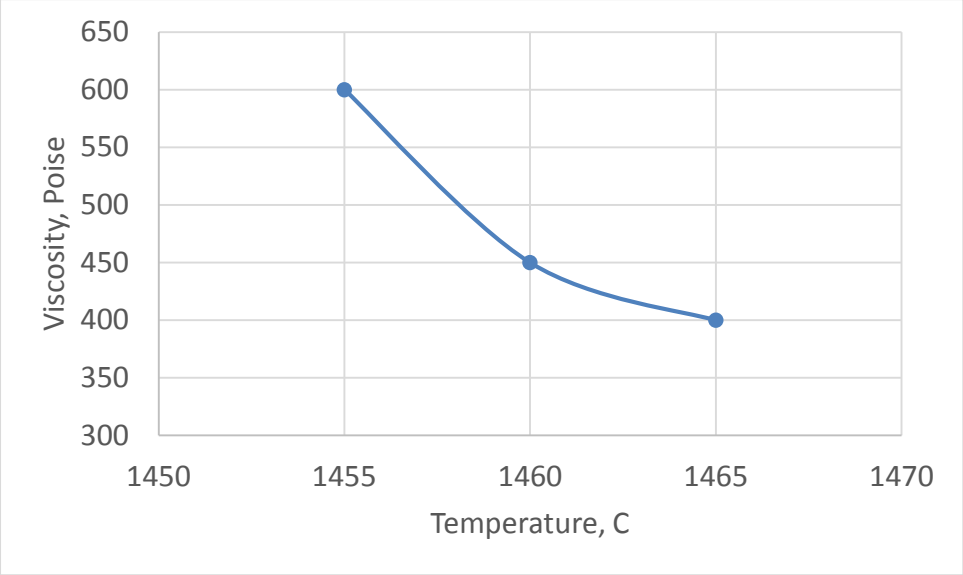


**Figure 53** Viscosity measurement on Yallourn + 4 % clay

### 7.4.4 Conclusions from the measurements using individual ash

The viscosity measurement data of Victorian brown coal ash slags indicate that all the Victorian coals require high temperatures >1450 $^{o}$C for the ash to melt.

Yallourn ash shows viscosity <250 Poise at 1440-1460 $^{o}$C. With the addition of 4% CaO flux to Yallourn ash, the temperature at which molten slag formed was slightly reduced and the viscosity of the samples was also slightly lowered. When clay was added to the ash the viscosity of the slag increased indicating a negative effect. Phase diagrams predictions on Yallourn ash suggest that the sample is mostly in a molten state at above 1400 $^{o}$C indicating it will completely melt at temperatures between 1450-1500 $^{o}$C.

Loy Yang coal on its own did not show any measurable viscosity at 1460 $^{o}$C. When 4% CaO was added as flux, measurement of viscosity was possible and a viscosity of 450-500 Poise at 1470 $^{o}$C was measured. Extrapolation of the measured data suggest that Loy Yang slag would require temperatures above 1500 $^{o}$C to have a viscosity below 250 Poise.

On the other hand, Morwell did not show any measurable viscosity on its own, or by the addition of CaO or clay as flux under 1500  C. The results indicate that Morwell ash on its own is difficult to melt.  The results of Phase diagrams indicate that the Morwell ash retains 20-30% solid component at 1600 $^{o}$C making it a very hard ash to melt with an acceptable viscosity during gasification.

## 7.5 Further measurements with Morwell and Loy Yang ash

As a result of the conclusions from the previous section further work was considered with Morwell and Loy Yang ash. These included

- Two stage gasification
- Coal or ash blending

### 7.5.1 Two stage gasification

Most coal gasifiers operate as a two-stage gasifier. Brown coal gasification with efficient slag removal can be carried out in a two-stage gasifier (similar to that designed by MHI) shown in Figure 54. The first stage of the gasifier (reduction) can be maintained at a relatively low temperature (1200 - 1300 C) for carbon conversion, whereas in the second stage (combustor) the gasifier can be maintained at higher temperature with smaller quantity of coal than the first stage. This helps in melting the slag out of the gasifier. However, the second stage still require high temperatures (~1600 $^{o}$C) resulting in high energy requirement.

**Reductor**

$Char + CO_2 \rightarrow 2CO$

$Char + H_2O \rightarrow CO + H_2$

$CO_2 + H_2O \rightarrow CO_2 + H_2$

$Coal \rightarrow VM + char$

**Combustor**

$Coal \rightarrow VM + Char$

$VM+O_2 \rightarrow CO_2+H_2O+ heat$

$Chat + CO_2 \rightarrow CO + CO_2$

$Ash + heat \rightarrow Slag$

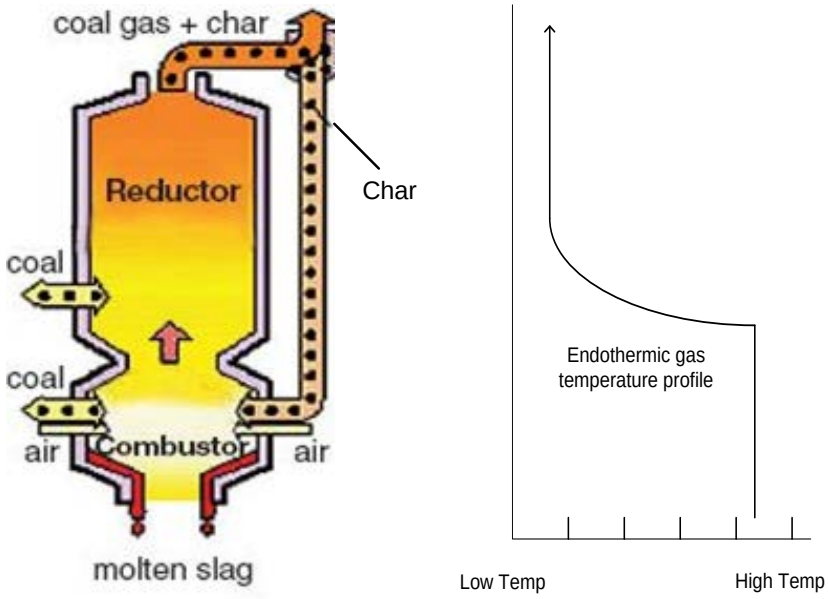


**Figure 54** A Simplified representation of the MHI Gasifier (adapted from Ishii, 2015). VM=volatile matter

### 7.5.2 Coal blending

Alternatively, we considered the possibility of blending two different coals at different proportions and test the ash samples for viscosity. This is based on the result that Yallourn ash

viscosity was within the acceptable range around 1450  C. In addition, all three coals achieved full carbon-conversion around 1300  C.

***Trial 1***

As an initial trial, we mixed Yallourn ash (which shows acceptable viscosity around 1450 ºC) and Morwell ash which did not show any sign of melting below 1550 ºC.  Different weight ratios 30:70 40:60 50:50, 60:40, and 70:30 were mixed and tested for ash fusion analysis. The results are presented in Table 18 below. All the composition tested show the temperature for initial softening temperatures to be beyond 1500 ºC suggesting the combination may not work. Table 19 shows the composition of Yallourn + Morwell mixtures. From the table, it can be observed that the mixed ash is rich in Fe, Mg and Ca.  The presence of high CaO can be adjudged as the reason for high melting point of this combination. Basing on these results the combination was not tried for Viscosity measurements.

**Table 18 Ash fusion tests (AFT) on Victorian ash mixed in different proportions**

| Sample | AFT Reducing atmosphere | | | |
|---|---|---|---|---|
| Temp ºC | Deformation | H-Spherical | Spherical | Flow |
| YL30:MW70 | >1550 | >1550 | >1550 | >1550 |
| YL40:MW60 | >1550 | >1550 | >1550 | >1550 |
| YL50:MW50 | >1550 | >1550 | >1550 | >1550 |
| YL60:MW40 | >1550 | >1550 | >1550 | >1550 |
| YL70:MW30 | >1550 | >1550 | >1550 | >1550 |
| YL70:LY30 | 1360 | >1550 | >1550 | >1550 |
| YL60:LY40 | 1310 | 1390 | 1450 | 1540 |
| YL50:LY50 | 1240 | 1320 | 1370 | 1450 |
| YL40:LY60 | 1240 | 1310 | 1350 | 1450 |
| YL30:LY70 | 1230 | 1260 | 1300 | 1360 |
| Morwell (MW) | 1320 | >1550 | >1550 | >1550 |
| Loy Yang (LY) | 1230 | 1310 | 1390 | 1470 |
| Yallourn (YL) | >1550 | >1550 | >1550 | >1550 |

**Table 19 Ash composition of Yallourn (YL)+ Morwell (MW) mixture**

| | YL30:MW70 | YL40:MW60 | YL50:MW50 | YL60:MW40 | YL70:MW30 |
|---|---|---|---|---|---|
| $SiO_2$ | 5.03 | 5.27 | 5.51 | 5.75 | 5.99 |
| $Al_20_3$ | 2.81 | 3.06 | 3.32 | 3.58 | 3.83 |
| $Fe_2O_3$ | 28.96 | 32.73 | 36.50 | 40.27 | 44.03 |
| $TiO_2$ | 0.26 | 0.26 | 0.26 | 0.26 | 0.26 |
| $K_2O$ | 0.33 | 0.32 | 0.30 | 0.28 | 0.27 |
| MgO | 27.27 | 26.44 | 25.60 | 24.77 | 23.94 |
| $Na_2O$ | 5.05 | 4.61 | 4.17 | 3.74 | 3.30 |
| CaO | **24.92** | **22.71** | **20.49** | **18.27** | **16.06** |
| $SO_3$ | 5.36 | 4.60 | 3.84 | 3.07 | 2.31 |
| $P_2O_5$ | 0.00 | 0.00 | 0.00 | 0.00 | 0.00 |

***Trial 2***

In this trial Yallourn and Loy Yang ash sample were mixed in ratios 30:70 to 70:30 and tested for ash fusion temperature. The final composition due to the mixing of Yallourn and Loy Yang ash samples is presented in Table 20. Interestingly all the samples showed relatively low melting and flow temperatures compared to the pure ash suggesting mixing of these two coals may reduce the overall flow temperatures of the mixed slag.

**Table 20 Ash composition of Yallourn (YL) + Loy Yang (LY) mixture**

| | YL70:LY30 | YL60:LY40 | YL50:LY50 | YL40:LY60 | YL30:LY70 |
|---|---|---|---|---|---|
| $SiO_2$ | 23.83 | 29.54 | 35.24 | 40.95 | 46.65 |
| $Al_20_3$ | 9.79 | 11.52 | 13.25 | 14.98 | 16.71 |
| $Fe_2O_3$ | 40.10 | 35.02 | 29.94 | 24.86 | 19.78 |
| $TiO_2$ | 0.85 | 1.04 | 1.24 | 1.43 | 1.62 |
| $K_2O$ | 0.35 | 0.39 | 0.44 | 0.48 | 0.52 |
| MgO | 16.02 | 14.21 | 12.41 | 10.60 | 8.79 |
| $Na_2O$ | 2.20 | 2.28 | 2.35 | 2.42 | 2.49 |
| CaO | **6.85** | **6.00** | **5.14** | **4.29** | **3.44** |
| $SO_3$ | 0.01 | 0.01 | 0.01 | 0.01 | 0.01 |
| $P_2O_5$ | 0.00 | 0.00 | 0.00 | 0.00 | 0.00 |

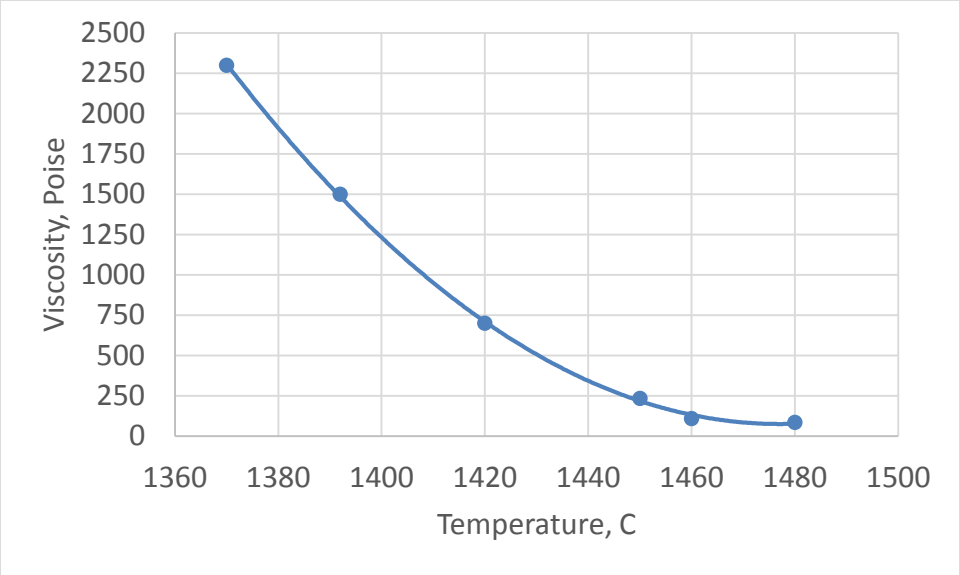


**Figure 55** Viscosity data - Yallourn + Loy Yang (30:70) mixture

The results of viscosity measurement using Yallourn and + Loy Yang (30:70) mixture are shown in Figure 55. The results indicate that the sample showed measurable viscosity at 1340-1450 $^{o}$C. However, the viscosity values are varied and change rapidly with temperature suggesting temperatures higher than 1450 $^{o}$C are required for the free flow of slag through the gasifier walls. Yallourn and Loy Yang ash samples can be mixed and can be used together in a gasifier at 70:30 ratio respectively. This mixed ash (shown in Table 18) has relatively low melting temperature of 1360 C, compared to the melting temperatures of individual ash at 1460 C and 1500 C respectively. The mixed ash YL3:LY70 is moderate in $SiO_2$, $Al_2O_3$, $Fe_2O_3$ components with alkali and alkaline earth metal components K, Mg, Na, and CaO at relatively lower concentrations. It can be concluded that moderate levels of $SiO_2$, $Al_2O_3$, and $Fe_2O_3$ in the ash is the key for relatively low melting temperatures of the ash samples.

One more combination of Yallourn + Loy Yang (50:50) mixed sample was also tested for viscosity measurements. The results are shown in Figure 56. The results indicate viscosity of 250-100 Poise is achieved at temperatures of 1400 -1460 $^{o}$C which is lower compared to Yallourn + Loy Yang (30:70) mixture. The results are in line with the ash fusion tests results presented in Table 18. However, the best composition for the combination of these two coals still needs to be optimized.

***Trial 3***

As part of further trials, Morwell + Loy Yang mixture was also tested. The samples were not tested for ash fusion to determine the flow temperatures. Alternatively, thermodynamic predictions on % molten slag formation for two combinations Morwell + Loy Yang 1:1 and 1:5 are made. As seen from the results in Figure 57, the combination of ash reached near 100%

molten slag formation between 1300-1400 ºC suggesting blending Morwell and Loy Yang coal will work for slag removal following gasification.

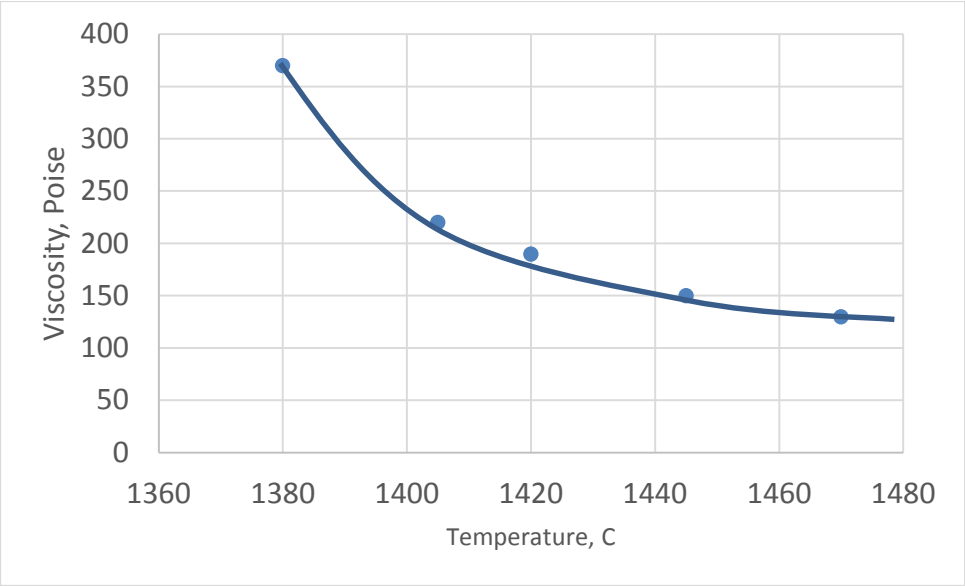


**Figure 56** Viscosity data - Yallourn + Loy Yang (50:50) mixture

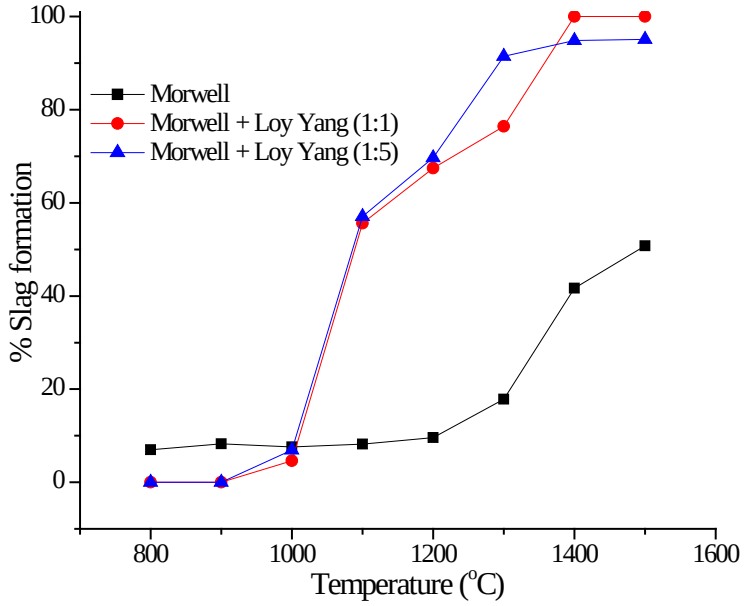


**Figure 57** Thermodynamic calculation results on % molten slag formation for the mixture of Morwell with Loy Yang ash.

**Table 21 Ash composition of Morwell (MW)+ Loy Yang (LY) mixture**

| | MW30:LY70 | MW40:LY60 | MW50:LY50 | MW60:LY40 | MW70:LY30 |
|---|---|---|---|---|---|
| $SiO_2$ | 45.93 | 39.99 | 34.04 | 28.09 | 22.15 |
| $Al_20_3$ | 15.94 | 13.96 | 11.97 | 9.98 | 8.00 |
| $Fe_2O_3$ | 8.47 | 9.78 | 11.10 | 12.41 | 13.72 |
| $TiO_2$ | 1.62 | 1.43 | 1.23 | 1.04 | 0.84 |
| $K_2O$ | 0.57 | 0.55 | 0.52 | 0.49 | 0.47 |
| MgO | 11.29 | 13.93 | 16.57 | 19.21 | 21.85 |
| $Na_2O$ | 3.80 | 4.17 | 4.53 | 4.90 | 5.26 |
| CaO | **10.09** | **13.16** | **16.23** | **19.30** | **22.37** |
| $SO_3$ | 2.30 | 3.06 | 3.83 | 4.59 | 5.36 |
| $P_2O_5$ | 0.00 | 0.00 | 0.00 | 0.00 | 0.00 |

In this trial, Loy Yang and Morwell ash samples were mixed at 50:50 ratio and tested for viscosity measurements. The results of viscosity measurements of Loy Yang and Morwell ash samples are shown in Figure 58. The final ash composition where Morwell and Loy Yang ash are mixed in different ratios is presented in Table 21.

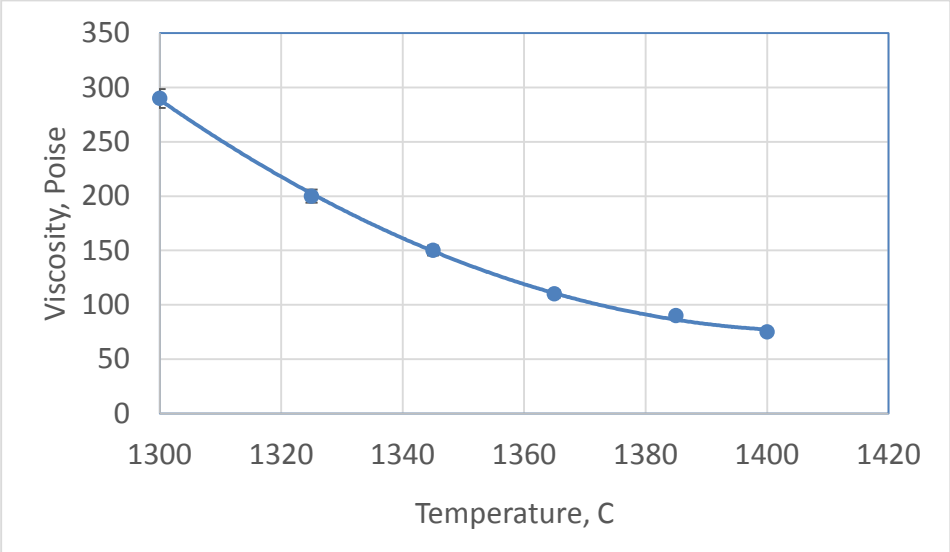


**Figure 58** Viscosity data on Morwell + Loy Yang (50:50) mixture

From the ash composition, it can be seen that Morwell + Loy Yang (50:50) mixture as shown in Table 21 will have low melting temperatures owing to moderate concentrations of the major components Al, Si, and Fe. However, Morwell and Loy Yang combination still warrant investigation in optimising the composition where low viscosity can be achieved.

### 7.5.3 Conclusions from the measurements using blended ash

It is clear form the viscosity mesurements using mixed ash that for Morwell or Loy Yang ash, a 50:50 mix with Loy Yang ash provides acceptable viscosity around 1400 $^{o}$C.

Additionally, for Loy Yang ash a 50:50 mix with Yallourn ash provides acceptable viscoisty between 1400 -1470 $^{o}$C range.

## 7.6 Comparison of viscosity models and measured viscosity data

The viscosity data on Victorian brown coals are compared against the select viscosity models $S^2$ correlation and Watt and Fereday correlation which fall in the gasification temperature range measured.

### 7.6.1 Loy Yang ash

As evident from Figure 29 in section 5.2.4, only $S^2$ correlation and Watts and Fereday correlation predicted the viscosity of Loy Yang slag to be 100-250 Poise in the temperature range of 1350-1500 $^oC$. Hence, these two models are compared with the measured viscosity data as shown in Figure 59. For Loy Yang ash itself, viscosity measurement was not possible. However, the addition of 4% CaO and clay flux reduced the slagging temperatures, which allowed the measurement of viscosity. The results suggest that the prediction from both Watts and Fereday and $S^2$ correlation are very far from the measured viscosity data. However, the measured viscosity data has similar viscosity at temperatures 150-200 $^oC$ greater than predicted from the Watt and Fereday correlation. On the other hand, $S^2$ correlation did not predict temperatures close to the experimental results. The observations suggests that neither models are suitable to predict the viscosity of Loy Yang ash and flux samples.

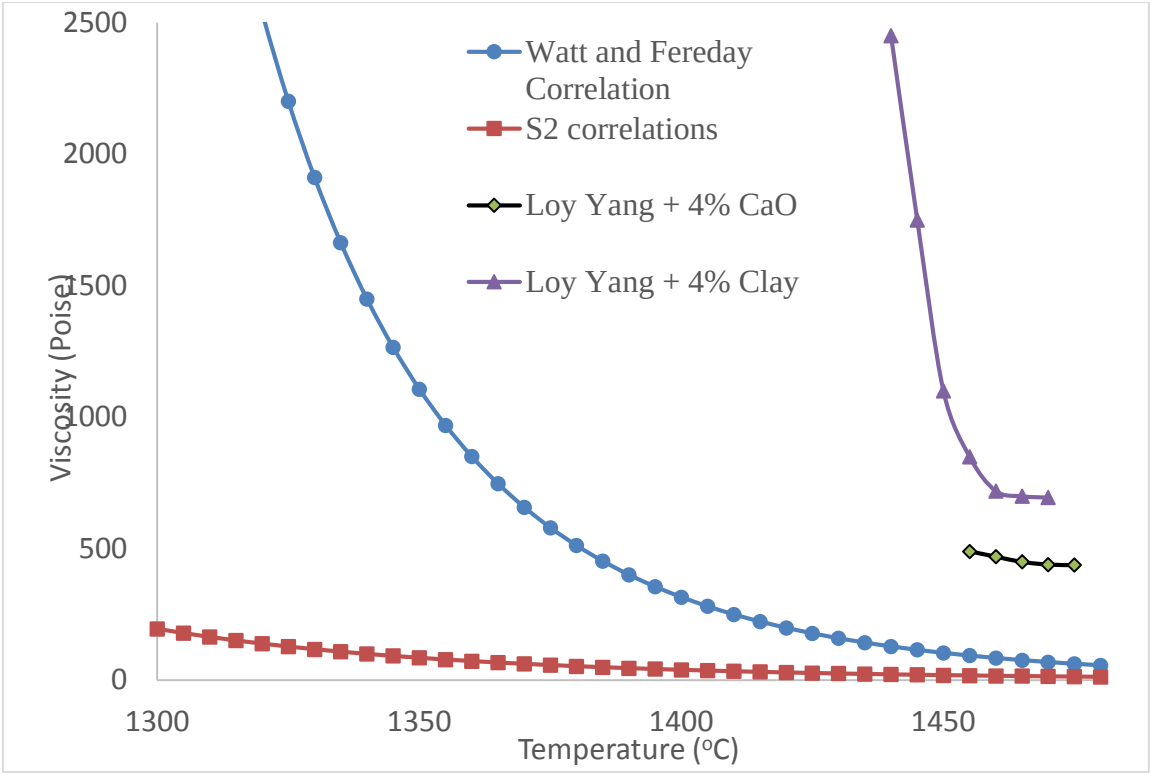


**Figure 59** Comparison of best-fit models on Loy Yang ash with experimentally measured data.

### 7.6.2 Yallourn ash

Similarly, measured viscosity of Yallourn ash was compared in Figure 60, against $S^2$ correlation, and the Watts and Fereday's correlation. These two models predict the viscosity of Yallourn slag to be 100-250 Poise in the temperature range of 1300-1350 ºC and 1420-1460 ºC respectively. The experimental data indicate a viscosity of 100-250 Poise in the temperature range of 1420-1450 ºC which is within the range of the Watt and Fereday predictions. On the other hand, $S^2$ correlations show the suitable viscosity range is achieved at temperatures >100 ºC than the experimental data. The results indicate $S^2$ correlation is not a suitable model to predict the viscosity on Yallourn ash.

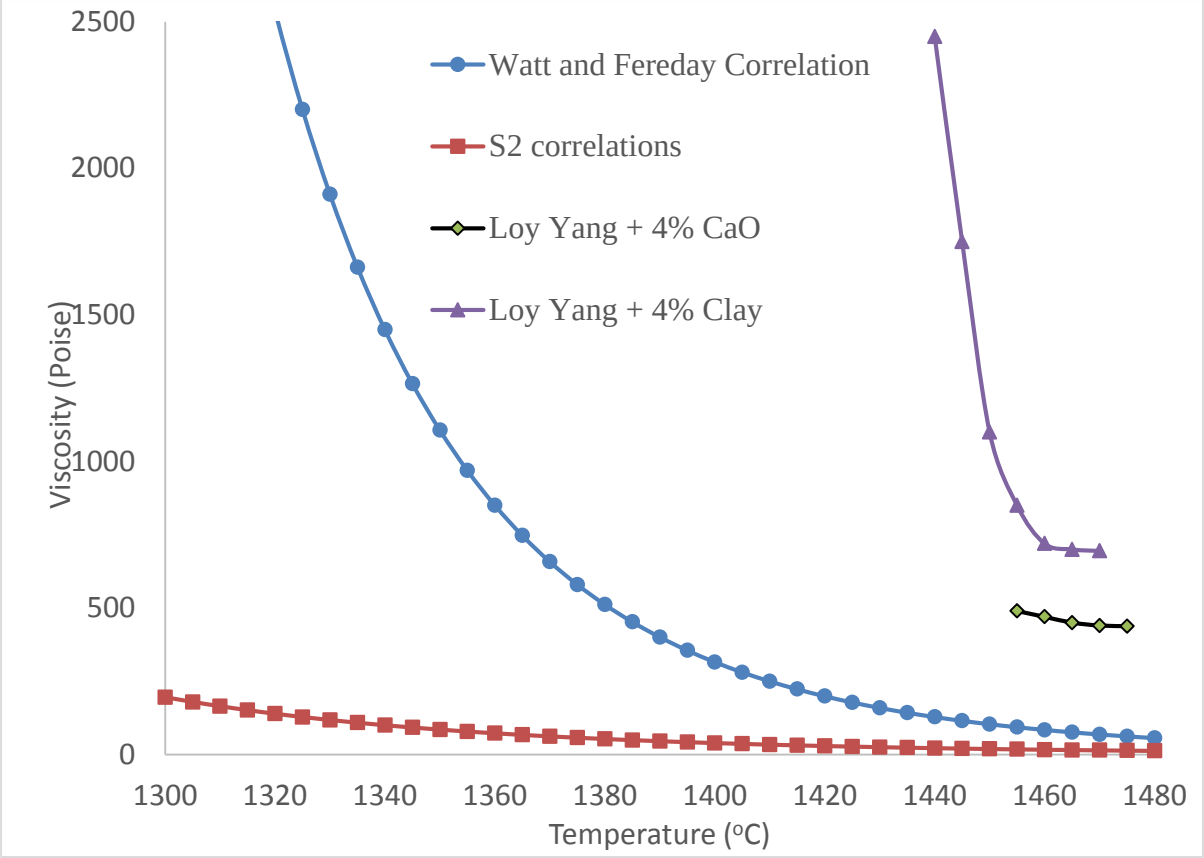


**Figure 60** Comparison of best-fit models on Yallourn ash with experimentally measured data.

### 7.6.3 Conclusions from comparison of measured viscosity and prediction from select models

The viscosity measurements on Loy Yang and Yallourn slags were compared against two models $S^2$ correlation and Watt and Fereday correlation. The prediction from Watt and Fereday correlation was very close to measured viscosity on Yallourn slag only off by 20 $^oC$ off. The comparison on Loy Yang ash the predictions are off by >150 $^oC$. On the other hand, predictions from $S^2$ correlations are not comparable to experimental data. Hence, it can be concluded that models in the literature cannot be used to predict the viscosity of Victorian brown coal slags with exception on Yallourn slag with Watt and Fereday correlation to a certain extent.

## 7.7 Overall conclusions from this project

To develop entrained flow gasification technology for use with Victorian brown coal, the problems encountered are limited data availability on the gasification performance of these coals. The unavailable data include temperature required for complete carbon conversion, trace element emission, and slag viscosity as a function of temperature.

In this project three Victorian brown coals - Loy Yang, Yallourn and Morwell - were tested for gasification performance under entrained flow condition. This was followed by thermodynamic modelling and viscosity measurements of the ash prepared from these coals that included the following:

- Gasification experiments 1000 – 1400 °C to measure carbon conversion
- Viscosity measurements in triplicate to 1550 °C
- Differential thermo-gravimetry on ash samples
- Phase diagram study of the ash systems for the three different ash types using a commercial software
- X-ray diffraction – at Monash University and the Australian Synchrotron, and
- Trace element measurements and modelling on ash and slag samples

For the batch of three Victorian coals tested extensively in this project - Loy Yang, Morwell, and Yallourn – the information generated can be summarised as follows:

<u>Carbon conversion</u>

- 106-150 µm size air-dried particles can attain over 99% Carbon conversion in twenty-one secs at 1000 °C or around eight secs at 1300 °C. There was no difference among the three different brown coals, all exhibiting a similar behaviour of Carbon conversion – temperature – residence time relationship.

<u>Viscosity</u>

- Ash fusion temperature measurement is not a reliable predictor of slag viscosity
- None of the conventional viscosity models accurately predict the viscosity of the slags from the three tested coals
- The viscosity – temperature behaviour of the three coals is different, requiring different temperatures for an acceptable range of viscosity 100-250 Poise.
- Yallourn coal can generate a slag at acceptable viscosity range around 1450 °C.
- Loy Yang and Morwell ash require in excess of 1500 °C for an acceptable viscosity range if these are to be used on their own. This is due to the very high levels of alumino-silicates in Loy Yang ash and very high level of calcium in Morwell ash.
- Addition of CaO or Clay overburden as flux material does not reduce the temperature required for an acceptable viscosity for any of the three ash types

- For Morwell ash, a 50:50 mix with Loy Yang ash reduces the temperature requirement to 1400 °C
- For Loy Yang ash, a 50:50 mix with Yallourn ash or Morwell ash reduces the temperature requirement to 1400-1470 °C

Trace element emission

- This was limited to Zn, Mn, Ba, Cr, Ni and As – as being the elements of moderate to greatest concern related to coal gasification
- Based on both thermodynamic modelling and chemical analysis following experimental work reveal that their emission in the gas phase is not significantly dependent on temperature. Over 50% of the compounds of these elements are retained in slags at gasification temperatures, and there is no systematic influence of the flux materials on their retention.

Most gasifiers operate as a two-stage gasifier, one stage being used to devolatilize the coal and convert the carbon to fuel gas, and the second stage being used to convert the ash to a molten slag. It is expected that for all three brown coals, the first stage does not need to operate above 1300 °C. The second stage requires a higher temperature between 1400 and 1550 °C depending on the coal used.

While the project has generated substantial practical information on entrained flow gasification behaviour of Victorian brown coal for the first time, some of the reasons for viscosity behaviour of the three ash types require more fundamental investigation. This is continued at Monash University using the facilities and the expertise developed.

## References


1. Woods, M. C.; Capicotto, P.; Haslbeck, J.; Kuehn, N.; Matuszewski, M.; Pinkerton, L.; Rutkowski, M.; Schoff, R.; Vaysman, V., Cost and performance baseline for fossil energy plants. *National Energy Technology Laboratory* **2007**.
2. Luxsanayotin, A.; Pipatmanomai, S.; Bhattacharya, S., Effect of mineral oxides on slag formation tendency of Mae Moh lignites. *Sonklanakarin Journal of Science and Technology* **2010,** 32, (4), 403.
3. Kong, L.; Bai, J.; Bai, Z.; Guo, Z.; Li, W., Effects of CaCO 3 on slag flow properties at high temperatures. *Fuel* **2013,** 109, 76-85.
4. F.C., K., Melting and Transformation Temperatures of Mineral and Allied Substances. In *Contributions to Geochemistry*, Interior, U. S. D. o. t., Ed. Washington, 1963.
5. Zhihui, Z.; Nan, L., Influence of Mechanical Activation of $Al_2O_3$ on Synthesis of Magnesium Aluminate Spinel. *Science of Sintering* **2004,** 36, 73-79.
6. Grasa, G. S.; Abanades, J. C., CO2 capture capacity of CaO in long series of carbonation/calcination cycles. *Industrial & Engineering Chemistry Research* **2006,** 45, (26), 8846-8851.
7. Manovic, V.; Anthony, E. J., Steam reactivation of spent CaO-based sorbent for multiple CO2 capture cycles. *Environmental science & technology* **2007,** 41, (4), 1420-1425.
8. Tanner, J.; Bläsing, M.; Müller, M.; Bhattacharya, S., The temperature-dependent release of volatile inorganic species from Victorian brown coals and German lignites under CO 2 and H 2 O gasification conditions. *Fuel* **2015,** 158, 72-80.
9. Thompson, D.; Argent, B., The mobilisation of sodium and potassium during coal combustion and gasification. *Fuel* **1999,** 78, (14), 1679-1689.
10. Sawada, Y.; Suzuki, M., Thermal change of SnI2 thin films. Part 4. TG-DTA and DSC. *Thermochimica Acta* **1995,** 254, (0), 261-266.
11. Szczerba, J.; Madej, D.; Śnieżek, E.; Prorok, R., The application of DTA and TG methods to investigate the non-crystalline hydration products of CaAl2O4 and Ca7ZrAl6O18 compounds. *Thermochimica Acta* **2013,** 567, (0), 40-45.
12. Faria, K.; Holanda, J., Thermal study of clay ceramic pastes containing sugarcane bagasse ash waste. *Journal of Thermal Analysis and Calorimetry* **2013,** 114, (1), 27-32.
13. Banjuraizah, J.; Mohamad, H.; Ahmad, Z. A., Effect of melting temperatures on the crystallization and densification of 2.8MgO·1.5Al2O3·5SiO2 glass–ceramic synthesized from mainly talc and kaolin. *Journal of Alloys and Compounds* **2011,** 509, (5), 1874-1879.
14. Vassilev, S. V.; Kitano, K.; Takeda, S.; Tsurue, T., Influence of mineral and chemical composition of coal ashes on their fusibility. *Fuel Processing Technology* **1995,** 45, (1), 27-51.
15. Vassileva, C. G.; Vassilev, S. V., Behaviour of inorganic matter during heating of Bulgarian coals: 1. Lignites. *Fuel Processing Technology* **2005,** 86, (12), 1297-1333.
16. Vejahati, F.; Xu, Z.; Gupta, R., Trace elements in coal: Associations with coal and minerals and their behavior during coal utilization–A review. *Fuel* **2010,** 89, (4), 904-911.
17. Müller, E. I.; Mesko, M. F.; Moraes, D. P.; Korn, M.; Flores, M., Wet digestion using microwave heating. In *Microwave-Assisted Sample Preparation for Trace Element Determination*, Elsevier Amsterdam: 2014; pp 99-142.
18. Hurst, H. J.; Novak, F.; Patterson, J. H., Viscosity measurements and empirical predictions for fluxed Australian bituminous coal ashes. *Fuel* **1999,** 78, (15), 1831-1840.
19. Schobert, H. H.; Streeter, R. C.; Diehl, E. K., Flow properties of low-rank coal ash slags. Implications for slagging gasification. *Fuel* **1985,** 64, (11), 1611-1617.
20. Kondratiev, A.; Jak, E., Predicting coal ash slag flow characteristics (viscosity model for the Al2O3-CaO-[`]FeO'-SiO2 system). *Fuel* **2001,** 80, (14), 1989-2000.
21. van Dyk, J. C.; Waanders, F. B.; Benson, S. A.; Laumb, M. L.; Hack, K., Viscosity predictions of the slag composition of gasified coal, utilizing FactSage equilibrium modelling. *Fuel* **2009,** 88, (1), 67-74.

22. Jensen, R. R.; Benson, S. A.; Laumb, J. D. *Subtask 3.6 - Advanced Power Systems Analysis Tools*; Energy & Environmental Research Center, Univeristy of North Dakota: 21 August 2001, 2001; p 51.
23. Browning, G. J.; Bryant, G. W.; Hurst, H. J.; Lucas, J. A.; Wall, T. F., An empirical method for the prediction of coal ash slag viscosity. *Energy and Fuels* **2003,** 17, (3), 731-737.
24. Hilary Hsiao Hui How; Bithi Roy; Bhattacharya, S., Prediction of Slag Composition and Viscosity during High Temperature Gasification of Australian Lignites In *Chemeca 2010: Engineeing at the Edge*, Hilton Adelaide, South Australia., 2010.
25. Streeter, R. C.; Diehl, E. K.; Roaldson, G. R., Measurement and Prediction of Low-Rank Coal Slag Viscosity In *The Chemistry of Low-Rank Coals*, American Chemical Society: Washington, 1984; Vol. 264.
26. Mills, K. C.; Rhine, J. M., The measurement and estimation of the physical properties of slags formed during coal gasification: 1. Properties relevant to fluid flow. *Fuel* **1989,** 68, (2), 193-200.
27. Kinaev, N. *A review of mineral matter issues in coal gasification*; RR 60; 2006.
28. Browning, G. J.; Bryant, G. W.; Hurst, H. J.; Lucas, J. A.; Wall, T. F., An Empirical Method for the Prediction of Coal Ash Slag Viscosity. *Energy & Fuels* **2003,** 17, (3), 731-737.
29. Hoy, H. R.; Roberts, A. G.; Wilkins, D. M., Behaviour of Mineral Matter in Slagging Gasification Processes. *IGE J*, 444.
30. Kondratiev, A.; Zhao, B.; Raghunath, S.; Hayes, P. C.; Jak, E. In *New tools for viscosity measurement and modelling of fully liquid and partly crystallised slags*, 2007; Die Deutsche Bibliothek: 2007.
31. Seetharaman, S.; Mukai, K.; Sichen, D., Viscosities of slags—an overview. In *VII International Conference on Molten Slags Fluxes and Salts*, The South African Institute of Mining and Metallurgy: 2004.
32. Bale, C. W.; Bélisle, E.; Chartrand, P.; Decterov, S. A.; Eriksson, G.; Hack, K.; Jung, I. H.; Kang, Y. B.; Melançon, J.; Pelton, A. D.; Robelin, C.; Petersen, S., FactSage thermochemical software and databases -- recent developments. *Calphad* **2009,** 33, (2), 295-311.
33. Song, W.; Tang, L.; Zhu, X.; Wu, Y.; Rong, Y.; Zhu, Z.; Koyama, S., Fusibility and flow properties of coal ash and slag. *Fuel* **2009,** 88, (2), 297-304.
34. The Viscosity Module. http://www.crct.polymtl.ca/factsage/fs_viscosity.php (14th December),
35. van Dyk, J. C.; Keyser, M. J.; Waanders, F. B.; Conradie, M., Manipulation of the ash flow temperature and viscosity of a carbonaceous Sasol waste stream. *Fuel* 89, (1), 229-236.
36. Cho, D.; Moon, I.; Whang, S.; Oh, M., High Temperature Slag Viscometry. *Journal of Industrial and Engineering Chemistry* **2000,** 7, 30-37.
37. Forsbacka, L.; Holappa, L.; Iida, T.; Kita, Y.; Toda, Y., Experimental study of viscosities of selected CaO–MgO–Al2O3–SiO2 slags and application of the Iida model. *Scandinavian Journal of Metallurgy* **2003,** 32, (5), 273-280.
38. Yuan, H.; Liang, Q.; Gong, X., Crystallization of Coal Ash Slags at High Temperatures and Effects on the Viscosity. *Energy and Fuels* **2012**.
39. Song, W.; Tang, L.; Zhu, X.; Wu, Y.; Zhu, Z.; Koyama, S., Flow properties and rheology of slag from coal gasification. *Fuel* **2010,** 89, (7), 1709-1715.
40. Vargas, S.; Frandsen, F. J.; Dam-Johansen, K., Rheological properties of high-temperature melts of coal ashes and other silicates. *Progress in Energy and Combustion Science* **2001,** 27, (3), 237-429.
41. Lommatzsch, T.; Megharfi, M.; Mahe, E.; Devin, E., Conceptual Study of an absolute falling-ball viscometer. *Metrologia* **2001,** 38, (6).
42. Park, N. A.; Irvine, T., Jr., The falling needle viscometer a new technique for viscosity measurements. *Wärme- und Stoffübertragung* **1984,** 18, (4), 201-206.
43. Cristescu, N. D.; Conrad, B. P.; Tran-Son-Tay, R., A closed form solution for falling cylinder viscometers. *International Journal of Engineering Science* **2002,** 40, (6), 605-620.
44. Kim, Y.; Oh, M. S., Effect of cooling rate and alumina dissolution on the determination of temperature of critical viscosity of molten slag. *Fuel Processing Technology* **2010,** 91, (8), 853-858.

45. Quon, D. H. H.; Wang, S. S. B.; Chen, T. T., Viscosity measurements of slags from pulverized western Canadian coals in a pilot-scale research boiler. *Fuel* **1984,** 63, (7), 939-942.
46. Song, W.; Sun, Y.; Wu, Y.; Zhu, Z.; Koyama, S., Measurement and simulation of flow properties of coal ash slag in coal gasification. *AIChE Journal* **2011,** 57, (3), 801-818.
47. Tonmukayakul, N.; Nguyen, Q. D., A new rheometer for direct measurement of the flow properties of coal ash at high temperatures. *Fuel* **2002,** 81, (4), 397-404.
48. Lim, S.; Oh, M., Prediction of coal slag foaming under gasification conditions by thermodynamic equilibrium calculations. *Korean J. Chem. Eng.* **2007,** 24, (5), 911-916.
49. Hurst, H. J.; Novak, F.; Patterson, J. H., Viscosity measurements and empirical predictions for some model gasifier slags. *Fuel* **1999,** 78, (4), 439-444.
50. Folkedahl, B. C.; Schobert, H. H., Effects of Atmosphere on Viscosity of Selected Bituminous and Low-Rank Coal Ash Slags. *Energy & Fuels* **2004,** 19, (1), 208-215.
51. Schobert, H. H.; Streeter, R. C.; Diehl, E. K., Flow properties of low-rank coal ash slags: Implications for slagging gasification. *Fuel* **1985,** 64, (11), 1611-1617.
52. Arvelakis, S.; Frandsen, F. J., Rheology of fly ashes from coal and biomass co-combustion. *Fuel* **2010,** 89, (10), 3132-3140.
53. Oh, M. S.; Brooker, D. D.; de Paz, E. F.; Brady, J. J.; Decker, T. R., Effect of crystalline phase formation on coal slag viscosity. *Fuel Processing Technology* **1995,** 44, (1–3), 191-199.
54. Groen, J. C.; Brooker, D. D.; Welch, P. J.; Oh, M. S., Gasification slag rheology and crystallization in titanium-rich, iron–calcium–aluminosilicate glasses. *Fuel Processing Technology* **1998,** 56, (1–2), 103-127.
55. Streeter, R. C.; Diehl, E. K.; Schobert, H. H., Measurement and Prediction of Low Rank Coal Slag Viscosity. *American Chemical Society* **1984**.
56. Brookfield DV-III Ultra Rheometers. http://www.labsource.co.uk/brookfieldengineering.html (14th June ),
57. Molybdenum. http://www.webelements.com/molybdenum/ (14th July),
58. Muhmood, L.; Seetharaman, S., Density Measurements of Low Silica CaO-SiO2-Al2O3 Slags. *Metall and Materi Trans B* **2010,** 41, (4), 833-840.
59. Browning, G.; Bryant, G.; Hurst, H.; Lucas, J.; Wall, T., An empirical method for the prediction of coal ash slag viscosity. *Energy & Fuels* **2003,** 17, (3), 731-737.
60. How, H. H. H.; Roy, B.; Bhattacharya, S., Prediction of slag composition and viscosity during high temperature gasification of Australian lignites. **2010**.
61. International, A., ASTM D1857 / D1857M-04(2010). In *Standard Test Method for Fusibility of Coal and Coke Ash*, West Conshohocken, PA, 2010.

# APPENDICES

## Appendix A: Slag Characterization-Inorganic analysis

### Summary of ash and slag characterizations

Methods of Chemical, mineralogical and microstructural analysis for slag characterization used by different research groups are summarized in Table A1.

**Table A1**: Methods of Chemical, mineralogical and microstructural analysis for slag characterization.

| Research group | Ash/Slag | Chemical composition/Elemental composition | Mineralogical composition/Microstructure | | Published article |
|---|---|---|---|---|---|
| Oh et al (1995) | synthetic slag: Alaskan Usibelli ash | | SEM/EDX | XRD | Effect of cooling rate and alumina dissolution on the determination of temperature of critical viscosity of molten slag [1] |
| Oh et al (1995) | SUFCo (Hiawatha seam, bit coal), Pittsburgh No. 8 bituminous coal, 2 Powell Mountain coals | ICP-ES | OM, SEM | XRD | Effect of crystalline phase formation on coal slag viscosity [2] |
| Oh et al (2008) | bituminous coal from Datong, China | | SEM/EDX | XRD | Changes in microstructure of a high chromium refractory due to interaction with infiltrating coal slag in a slagging gasifier environment [3] |
| Oh et al (1998) | SUFCo (Hiawatha seam, bit coal), Pittsburgh No. 8 bituminous coal, Synthetic | ICP-ES | OM, SEM/EDX | XRD, EMPA | Gasification slag rheology and crystallization in titanium-rich, iron–calcium–aluminosilicate glasses [4] |
| Song et al (2009) | Texaco gasifier slag: Shen Fu coal | XRF | SEM | XRD | Flow properties and rheology of slag from coal gasification [5] |
| Song et al (2009) | Laboratory ash and Shell gasifier slag (Chinese Huainan coal). | XRF | SEM | XRD | Fusibility and flow properties of coal ash and slag [6] |

| | | | | | |
|---|---|---|---|---|---|
| Wall et al (200) | Four coal samples with relatively high iron contents (>10 wt % Fe2O3 in ASTM ash) | | CCSEM | Mo¨ssbauer spectroscopy | An Experimental Comparison of the Ash Formed from Coals Containing Pyrite and Siderite Mineral in Oxidizing and Reducing Conditions [7] |
| Kinaev et al (2011) | Australian Bituminous coal (Blended) | | SEM | EMPA | The effect of solids and phase compositions on viscosity behavior and TCV of slags from Australian bituminous coals [8] |
| Van Dyk et. Al (2009) | Blended coal from 6 different sources of Mpumalanga area in South Africa | | SEMIC | | Viscosity predictions of the slag composition of gasified coal, utilizing FactSage equilibrium modeling [9] |
| Van Dyk et. Al (2009) | Blended coal from 6 different sources of Mpumalanga area in South Africa | | SEM, SEMPC, CCSEM | EMPA | Coal and coal ash characteristics to understand mineral transformations and slag formation [10] |
| Hurst et al (2001) | Synthetic | | SEM | XRD | Comments on the use of molybdenum components for slag viscosity measurements [11] |
| Hurst et al (1999) | fluxed slags prepared from Australian coal ash | Inductively coupled plasma excitation and a Spectro flame EOP direct reader | | | Viscosity measurements and empirical predictions for fluxed Australian bituminous coal ashes [12] |
| Nowok et al (1993) | | | IR, Raman spectroscopy s, NMR spectroscopy s, TDA, Electrical resistivity, SEM | Mossbauer spectroscopy, XRD | Structure of a Lignitic Coal Ash Slag and Its Effect on Viscosity [13] |

| | | | | | |
|---|---|---|---|---|---|
| Mattie et al (2011) | | XRF | SEM/EDX, QEMSCAN | XRD | Behavior of coal mineral matter in sintering and slagging of ash during the gasification process [14] |
| Mills et al (1989) | British Gas/Lurgi slagging gasifier slag. | | DTA | | The measurement and estimation of the physical properties of slags formed during coal gasification 1. Properties relevant to fluid flow [15] |
| Arvelakis et. Al (2010) | | | SEM/EDX, AAS | | Rheology of fly ashes from coal and biomass co-combustion [16] |
| Arvelakis et al (2006) | | | | HSXRD | Studying the Melting Behavior of Coal, Biomass, and Coal/Biomass Ash Using Viscosity and Heated Stage XRD Data [17] |
| Jak et al (2002) | | | SEM/EDS | EPMA/WDD | Prediction of coal ash fusion temperatures with the F*A*C*T thermodynamic computer package [18] |
| Wu et al (2007) | Chinese coal slag/Texaco gasifier | | SEM/EDX, Flash EA, TGA, generic oil immersion microscopy | | Characterization of residual carbon from entrained-bed coal water slurry gasifiers [19] |
| Sridhar et al (2009) | | | CSLM, SEM/EDX | | The interaction of spherical Al2O3 particles with molten Al2O3–CaO–FeOx–SiO2 slags [20] |
| Sridhar et al (20011) | | | CSLM, SEM/EDS | | Interactions of refractory materials with molten gasifier slags [21] |

| | | | | | |
|---|---|---|---|---|---|
| Huffman et al (1981) | | | SEM/AIA, | Mo¨ssbauer spectroscopy, XRD | Investigation of the high-temperature behavior of coal ash in reducing and oxidizing atmospheres [22] |
| Huffman et al (1981) | | | SEM, OM | Mo¨ssbauer spectroscopy, XRD | Correlation between ash-fusion temperatures and ternary equilibrium phase diagrams [23] |
| Mahlaba et al (2011) | | XRF | FEG-SEM | DSC, XRD | Physical, chemical and mineralogical characterization of hydraulically disposed of fine coal ash from SASOL Synfuels [24] |
| Aineto et al (2006) | ELCOGAS gasification plant slag, Spain | XRF, IR | SEM, DTA, HSM | XRD | Thermal expansion of slag and fly ash from coal gasification in IGCC power plant [25] |
| Quon et al (1984) | Canadian coal slag | EPMA | SEM | XRD | Viscosity measurements of slags from pulverized western Canadian coals in a pilot pulverized western Canadian coals in a pilot scale research boiler [26] |

| | |
|---|---|
| SEM | Scanning electron microscopy |
| OM | Optical microscopy |
| ICP-ES | inductively coupled plasma |
| emission spectroscopy | |
| XRD | X-ray diffraction |
| EPMA | Electron Probe X -ray |
| Microanalysis | |
| CCSEM | computer-controlled Scanning |
| electron microscopy | |
| SEMC | Scanning Electron Microscopy |
| Point Count | |
| TDA | Differential thermal analysis |
| IR | Infrared |
| QEMSCAN | integrated SEM and image analysis |
| system | |
| EDX | energy-dispersive X-ray |
| AAS | atomic absorption spectroscopy |
| EDS | energy-dispersive spectra analyser |
| WDD | Web length dispersive detector |
| EA | elemental analyser |
| TGA | thermogravimetric analysis |
| CSLM | Confocal Scanning Laser Microscope |
| AIA | automatic image analysis |
| DSC | Differential Scanning Calorimetry |
| FEG-SEM | Field Emission Gun Scanning Electron |
| Microscopy | |
| FE-SEM | field emission scanning electron |
| microscopy | |
| HSM | Hot stage microscopy |
| HSXRD | Heated stage XRD |
| ICP-MS | inductively coupled plasma mass |
| spectrometry | |
| ICP-AES | inductively coupled plasma atomic |
| emission spectrometry | |
| LOI | lose on ignition |
| TEM | transmitted electron microscopy |

**Reference**

[1] Kim Y, Oh MS. Effect of cooling rate and alumina dissolution on the determination of the temperature of the critical viscosity of molten slag. Fuel Processing Technology 2010; 91: 853–858

[2] Oh MS, Brooker DB, de Paz EF, Brady JJ, Decker TR. Effect of crystalline phase formation on coal slag viscosity. Fuel Process Technol 1995; 44:191–199.

[3] Kim HB, Oh MS. Changes in microstructure of a high chromia refractory due to interaction with infiltrating coal slag in a slagging gasifier environment. Ceramics International 2008; 34: 2107 – 16

[4] Groen JC, Brooker DD, Welch PJ, Oh MS. Gasification slag rheology and crystallization in titanium-rich, iron–calcium–aluminosilicate glasses. Fuel Process Technol 1998; 56:103–27.

[5] Song W, Tang L, Zhu X, Wu Y, Zhu Z, Koyama S. Flow properties and rheology of slag from coal gasification. Fuel 2010; 89: 1709 - 15

[6] Song W, Tang L, Zhu X, Wu Y, Rong Y, Zhu Z, Koyama S. Fusibility and flow properties of coal ash and slag. Fuel 2009; 88:297–304.

[7] McLennan AR, Bryant GW, Bailey CW, Stanmore BR, Wall TF. An Experimental Comparison of the Ash Formed from Coals Containing Pyrite and Siderite Mineral in Oxidizing and Reducing Conditions. Energy and Fuels 2000; 14: 308-315

[8] Ilyushechkin AY, Hla SS, Roberts DG, Kinaev NN. The effect of solids and phase compositions on viscosity behaviour and TCV of slags from Australian bituminous coals. Journal of Non-Crystalline Solids 2011; 357: 893–902

[9] Van Dyk JC, Waanders FB, Benson SA, Laumb ML, Hack K. Viscosity predictions of the slag composition of gasified coal utilizing FactSage equilibriummodelling. Fuel 2009; 88:67–74.

[10] Van Dyk JC, Benson SA, Laumb ML, Waanders FB. Coal and coal ash characteristics to understand mineral transformations and slag formation. Fuel 2009; 88: 1057-1063

[11] French D, Hurst HJ, Marvig P. Comments on the use of molybdenum components for slag viscosity measurements. Fuel Processing Technology 2001; 72: 215–225

[12] Hurst HJ, Novak F, Patterson JH. Viscosity measurements and empirical predictions for fluxed Australian bituminous coal ashes. Fuel 1999; 78: 1831–40.

[13] Nowok JW, Hurley JP, Stanley DC. Local structure of a lignitic coal ash slag and its effect on viscosity. Energy and Fuels 1993; 7: 1135–40.

[14] Matjie RH , French D, Ward CR, Pistorius PC, Li Z. Behaviour of coal mineral matter in sintering and slagging of ash during the gasification process. Fuel Process. Technol 2011; doi:10.1016/j.fuproc.2011.03.002

[15] Mills KC, Rhine JM. The measurement and estimation of the physical properties of slags formed during coal gasification – 1. Properties relevant to fluid flow. Fuel 1989; 68:193–200.

[16] Arvelakis S, Frandsen FJ. Rheology of fly ashes from coal and biomass co-combustion. Fuel 2010; 89: 3132–3140

[17] Arvelakis S, Folkedahl B, Dam-Johansen K, J. Hurley J. Studying the Melting Behavior of Coal, Biomass, and Coal/Biomass Ash Using Viscosity and Heated Stage XRD Data. *Energy & Fuels* 2006; *20:* 1329-1340

[18] Jak E. Prediction of coal ash fusion temperatures with the F*A*C*T thermodynamic computer package. Fuel 2002; 81:1655–68.

[19] Wu T, Gong M, Lester E, Wang F, Zhou Z, Yu Z. Characterisation of residual carbon from entrained-bed coal water slurry gasifiers. Fuel 2007; 86:972–982

[20] Soll-Morris H, Sawyer C, Zhang ZT, Shannon GN, Nakano J, Sridha S. The interaction of spherical $Al_2O_3$ particles with molten $Al_2O_3$–CaO–$FeO_x$–$SiO_2$ slags. Fuel 2009; 88: 670–682

[21] Nakano J, Sridhar S, Bennett J, Kwong KS, Moss T. Interactions of refractory materials with molten gasifier slags. International Journal of hydrogen energy 2011; 36: 4595 -4604

[22] Huffman GP, Huggins FE, Dunmyre GR. Investigation of the high-temperature behavior of coal ash in reducing and oxidizing atmospheres. Fuel 1981;60:585–97.

[23] Huggins FE, Kosmack DA, Huffman GP. Correlation between ash fusion temperatures and ternary equilibrium phase diagrams. Fuel 1981; 60:577–84.

[24] Mahlaba JS, Kearsley PE, Kruger RA. Physical, chemical and mineralogical characterisation of hydraulically disposed fine coal ash from SASOL Synfuel. Fuel 2011; 90: 2491–2500

[25] Aineto M, Acosta A, Rincon JM, Romero M. Thermal expansion of slag and fly ash from coal gasification in IGCC power plant. Fuel 2006; 85: 2352–2358

[26] Quon DHH, Wang SSB, Chen TT. Viscosity measurements of slags from pulverized western Canadian coals in a pilot-scale research boiler. Fuel 1984; 63: 939-942

## Appendix B: Review of viscosity models

A variety of approaches and mathematical formalisms have been used to describe the viscosities of liquid slags as a function of temperature and of the composition. Numerous viscosity models have been developed over the year for the viscosity of multi-component silicate melts. Some of these are empirical/semi empirical, whereas others have a more fundamental basis as they link the viscosity to the structure of the melt [1].

Empirical or semi-empirical models based on theoretical relations describing Newtonian fluids and relying on data regression to obtain some empirical parameters [2]. Most of these models cannot be recommended for use for compositions and temperatures even slightly different than those reported by the authors; to do so may lead to erroneous results [3]. These types of viscosity models does not take into account basic relationships between viscosity, temperature, and composition; they are limited to narrow ranges of conditions and do not have adequate predictive power outside the investigated ranges [4].

Fundamental viscosity models have been developed using thermodynamic properties of the liquid slag phase, internal structure of silicates through bridging, no bridging, and free oxygens, basicity index and corrected optical basicity [4]. These are discussed below.

### 1. Empirical viscosity models for homogeneous liquid

#### Fulcher Model (1925) [5, 6]

Fulcher proposed a relationship which used a temperature correction factor to fit viscosity data to an Arrhenius type equation

$$\eta = A + \frac{B}{T - T_0}$$

Where $A$ is a constant, $B$ is the energy of activation, and $T_0$ is the temperature correction factor.

#### Reid and Cohen (1944) [5, 6-7]

From measurements on coal-ash slags, Reid and Cohen prepared a nomogram by which the viscosity of a slag can be predicted graphically at any temperature above that of the critical viscosity. He showed that at a given temperature, the viscosity of a coal ash slag was a function of the “silica percentage”, $S$, where,

$$S = \frac{100 * SiO_2}{SiO_2 + equiv\ Fe_2O_3 + CaO + MgO}$$

Equiv $Fe_2O_3$ = $Fe_2O_3$ + 1.11Fe0 + 1.43Fe

The total alkali content in the slags never exceeded 2.5 wt%; thus, they were not considered in the modelling. It was found desirable to omit $Al_2O_3$ from the slag composition and recalculate so that

$Si0_2$ + equiv $Fe_2O_3$ + Ca0 + Mg0 = 100 Wt%

The relationship between viscosity and temperature developed was

$\eta^{-0.1614}$ = 0.000425T — C

Where *T* is in $^0$F, η in Poise, and *C* is a value dependent on the silica percentage and so must be calculated from a viscosity measurement at a given temperature.

The authors suggest that for slags containing more than 3 wt% MgO and less than 5 wt% CaO, or where the alkalies exceed 2.5 wt%, the predictions of the model should be applied with reservations [7]

**Sage-McIlroy (1959) [7]**

This model is based on experimental data. These data probably comprise both pure coal ashes and chemically altered coal ashes, all of which were probably composed chiefly of silicon, aluminium, iron and calcium, with smaller amounts of titanium, magnesium, sodium, potassium and other trace elements

A family of logarithmic curves was established by the authors showing the viscosity-temperature relationship for a range of silica ratios, The graphs are only valid for completely molten silicates, but it was explained how to calculate the viscosities of partly crystallized melts[7].

The silica ratio, S, is calculated on a weight basis

$$S = \frac{100 * SiO_2}{SiO_2 + equiv\ Fe_2O_3 + CaO + MgO}$$

**Modified silica ratio, $S^2$ (1963) [5, 6-8]**

This method was developed by BCURA. It is also based on studies of coal ash slags, containing silicon, aluminium, iron, calcium and magnesium as major components. Minor components such

as the alkali oxides were not considered in this model. The model relates the viscosity-temperature characteristics of wholly liquid slags with their chemical composition, and it is based on a recalculation of the compositional analysis of the slag in which all Fe is assumed present in the mixture as $Fe_2O_3$

$Si0_2 + Al_20_3 + equiv\ Fe_20_3 + Ca0 + Mg0 = 100\ Wt\%$

The viscosity is calculated from the following equation

$$\log \eta = 4.468\left(\frac{S}{100}\right)^2 + 1.265\left(\frac{10000}{T}\right) - 7.44$$

where η is in Poise, *T* is in K, and *S* is the silica percentage calculated by

$$S = \frac{100 * SiO_2}{SiO_2 + equiv\ Fe_2O_3 + CaO + MgO}$$

The '$S^2$ correlation', suited for slags with silica and iron oxide content less than 55% and 5% respectively.

The relationship is a mathematical reformulation of the nomogram elaborated by Reid and Cohen and all constants have been fitted from experimental data. The correlation was calculated from data from determinations on 62 samples of slags that covered the following range of chemical compositions [7]:

| | |
|---|---|
| $SiO_2$ | 31-59 wt% |
| $Al_2O_3$ | 19-37 wt% |
| Equi $Fe_2O_3$ | 0-38 wt% |
| CaO | 1-37 wt% |
| MgO | 1-12 wt% |
| $Na_2O+K_2O$ | 1-6 wt% |
| Silica ratio (S) | 45-75 |
| $SiO_2/Al_2O_3$ | 1.2-2.3 |

This model implies that the probability coefficient depends on the silica ratio, and activation energy is compositionally independent. As a result, this model is valid only for a limited compositional range [8]

**Watt-Fereday model or slope and intercept model (1963) [5, 6-8]**

The model was developed by BCURA for British coal ashes on the basis of measurements on 113 ashes of all lying within the following compositional limits [7]

| | |
|---|---|
| $SiO_2$ | 30-60 wt% |
| $Al_2O_3$ | 15-35 wt% |
| Equi $Fe_2O_3$ | 3-30 wt% |
| CaO | 2-30 wt% |
| MgO | 1-10 wt% |
| Silica ratio (S) | 40-80 |
| $SiO_2/Al_2O_3$ | 1.4-2.4 |

Initially, this model was called the “slope and intercept method” but nowadays this is more commonly known as the Watt and Fereday correlation

The ‘Watt and Fereday correlation’ is proven to yield higher accuracy for slags with high silica content (i.e. >80%) or high iron oxide content (i.e. >15%) and is represented as

$\log\eta = C + 10^7 m/(T-150)^2$

$m = 0.00835Si0_2 + 0.00601Al_20_3 — 0.109$

$c = 0.0415Si0_2 + 0.0192Al_20_3 + 0.0276 (\text{equiv } Fe_20_3) + 0.0160Ca0 — 3.92$

Where, 5 is in Poise, *T* is in $^oC$ and with the molecular formula being expressed in weight percentage

Predictive capabilities of the Watt and Fereday and *S*2 correlations were comparable, with the Watt and Fereday correlation having greater accuracy for slags with high silica content (>80%) or high iron oxide content (>15%).1 The $S^2$ method was more accurate for slags with silica percentages less than 55% and iron oxide content less than 5%.[5]

This model includes sets of individual parameters for each oxide. Again, this model is applied to a limited compositional range and generally overestimates the viscosities of multi- component slags [8]. Bottinga-Weill (1972) [7]

The Bottinga and Weill model have been developed for a wide range of silicate systems of geological interest. The authors used a linear dependence of viscosity on composition, and different coefficients are provided for each temperature range. This model differs from most empirical models in that there is an attempt to take into account aspects of the chemistry. To do this, structural complexes (associates) were introduced into the model as major components to take into account a dual behaviour of aluminum oxide in the (alkali, alkali earth) metal oxide-silica systems. The Bottinga and Weill model have been validated against experimental viscosity data for a wide range of temperatures and compositions, however, it does require a large number (470) of coefficients to do this [3].

The prediction of the viscosity of anhydrous silicate liquids is approached by means of tabulated constants, $D_i$, for each species in the melt.

$$\log \eta = \sum_i x_i D_i - 1$$

Viscosity is evaluated in Pa s, and $x_i$ indicates the individual species molar fractions.

The model performs well on some geological samples, but it is not suitable for the evaluation of melts with high contents of aluminium [7].

**Shaw (1972) [7, 8]**

Shaw introduced Arrhenius temperature behaviour into the Bottinga-Weill model and incorporated the influence of $H_2O$ content in the melt on its viscosity, which is important for geological systems. However, the compositional dependencies of the models are still fully empirical.

$$\eta = \frac{C_\eta}{C_T \alpha} \exp\left(\frac{\alpha 10^4}{T}\right)$$

Here, both the probability coefficient and activation energy depend on the same composition-derived parameter α. This parameter is calculated using the equation:

$$\alpha = \frac{x_{SiO_2} \cdot \sum x_i \alpha_i^0}{1 - x_{SiO_2}}$$

Where *xi* represents the molar fraction of oxides ($SiO_2$, $K_2O$, $Na_2O$, $Li_2O$, MgO, FeO, CaO, $TiO_2$ and '$AlO_2$') in the slag and $\alpha_i$ is an individual parameter for each oxide. Shaw's model is also applicable for a limited compositional range and usually underestimates viscosities [8].

**Lakatos (1972) [7]**

Based on viscosity-temperature measurements on 30 different laboratory-prepared compositions in the $SiO_2$-$Al_2O_3$-$Na_2O$-$K_2O$-CaO-MgO system, Lakatos et al. chose to fit the experimental data with a model based on the Vogel-Fulcher-Tamanna (VFT) equation. Compositions in the following ranges were used [7]

| | |
|---|---|
| $SiO_2$ | 0.61-0.77 mol fraction |
| $Al_2O_3$ | 0-0.05 mol fraction |
| CaO | 0.9-0.14 mol fraction |
| MgO | 0-0.10 mol fraction |
| $Na_2O$ | 0.10-0.15 mol fraction |

$K_2O$ 0-0.06 mol fraction

The VFT-equation expressed the viscosity-temperature relationship as

$$\eta = a + \frac{b}{T - c}$$

With viscosity η in Pa s, temperature T in K, and a, b, c composition-specific constants. $a = 1.5183Al_2O_3 – 1.6030CaO – 5.4936MgO + 1.4788Na_2O – 0.8350K_2O – 2.4550$

$b = 2253.4Al_2O_3 – 3919.3CaO + 6285.3MgO – 6039.7Na_2O – 1439.6K_2O + 5736.4$

$c = 294.4Al_2O_3 + 544.3CaO – 384.0MgO – 25.7Na_2O – 321.0K_2O + 471.3$

The symbols $Na_2O$, $K_2O$, CaO, MgO and $Al_2O_3$ represent the molar fraction of each species per mole $SiO_2$

**Urbain (1981) [3, 5-9]**

The Urbain formalism is one of the most widely used slag viscosity models and is based on the application of polynomial functions of slag composition to describe the pre-exponential and exponential terms in the Weymann–Frenkel equation. [10]

$\eta = AT \exp(1000B/T)$

Where a and b are compositionally dependent parameters

The silicate liquid slag components are classified into three groups: Glass formers (e.g., $SiO_2$)—g,
Amphoteric ($Al_2O_3$, $Fe_2O_3$)—am, and
Modifiers (CaO, MgO, $TiO_2$, $K_2O$, $Na_2O$)—mo

From the analysis of experimental data, Urbain postulated that the parameter **B** increases proportionally to the third power of Xg; (Xg, $X_{mo}$, and $X_{am}$ are the corresponding molar fractions of glass-forming, modifier, and amphoteric components).

$B = B_0 + B_1X_g + B_2X_g^2$

At a given Xg, the parameter B has a maximum value at the intermediate ratio of modifier to amphoteric fraction,

$$a = \frac{X_{mo}}{X_{mo} + X_{am}}$$

this latter compositional dependence can be described by the second power parabola.

$$B_{i=0...3} = b_i^0 + b_i^1 a + b_i^2 a^2$$

The parameter A is linked to B by the “compensation law”:

lnA = —mB — n

where, m and n are the model parameters. Urbain indicated that parameters m and n depended on composition, but for simplicity, recommended the average values m = 0.29 and n = 11.57 for the whole range of liquid silicate slag compositions

Urbain reported different model parameters for each ternary system $Al_2O_3$–MgO–$SiO_2$ and $Al_2O_3$–CaO–$SiO_2$ and suggested a method of extrapolating model predictions to multi-component systems. However, this method does not provide close agreement between the model predictions and experimental data in the $Al_2O_3$–CaO–MgO–$SiO_2$ systems over the whole compositional range [10]

**Riboud (1981) [7]**

Riboud *et al*. using the Urbain model with corrected compositions dependencies of *A* and *B*, successfully applied it to describe the viscosities of some industrial mould fluxes (in the $Al_2O_3$–CaO–$Na_2O$–$SiO_2$–$CaF_2$ system) [11]. They classified the slag components into five different categories, depending on their chemical nature, and attributed parameters to these categories [12]

ln A = -35.76 $Al_2O_3$ + 1.73 (FeO + CaO + MgO +MnO) + 7.02 ($Na_2O$ + $K_2O$) + 5.82$CaF_2$ – 19.81

B = 62.833 $Al_2O_3$ – 23.896 (FeO + CaO + MgO +MnO) – 39.159 ($Na_2O$ + $K_2O$) – 46.356 $CaF_2$ + 31.140

where (A in Pa s/K; B in K)

The equation was tested on continuous casting slags by the authors, and it was found to apply over the entire compositional range studied.

| | |
|---|---|
| $SiO_2$ | 26-56 wt% |
| $Al_2O_3$ | 0-12 wt % |

| | |
|---|---|
| CaO | 8-46 wt% |
| $Na_2O$ | 0-22 wt% |
| $CaF_2$ | 0-18 wt% |

It is reported that Urbain model to be marginally better for coal gasification slags [7, 8].

Riboud *et al*. considered the effects on the structure of slag melts of the acidity and basicity of the components and expressed these effects as a linear function of the concentrations of slag constituents. However, the structures of silicate melts do not always change linearly with the concentrations of the components. Their models cannot be applied over a wide composition range with constant model parameters; sometimes those parameters have to be changed to fit the viscosity in each composition range within a given region [13]

**Streeter (1984) [7, 14]**

Schobert et al. revaluated the applicability of the Urbain model on low-rank coal ash slag. The original Urbain model is modified to adapt to low-rank coal slag viscosity by the addition of the term, Δ. Three separate sets of equations for parameter Δ, *m*, and *b* have been developed in order to accommodate for low-, intermediate-, and high-silica slags. In this work, parameters Δ, *m*, and *B* are evaluated based on low-silica slags modelling.

$$\ln \eta = \ln a + \ln T + \frac{1000b}{T} - \Delta$$

Where

$$\Delta = mT + C$$

$$\text{Ln a} = -0.2693b - 11.6725$$

The model parameter, *b* in Schobert-Streeter-Diehl modified Urbain model is the same as Kalmanovitch modified Urbain model with þ being replaced as α, whereby α is given as:

$$\alpha = \frac{CaO + MgO + Na_2O + K_2O + 'FeO' + 2TiO_2 + 3SO_3}{Al_2O_3 + CaO + MgO + Na_2O + K_2O + 'FeO' + 2TiO_2 + 3SO_3}$$

For High Silica slags (b>28)

c = —1.7137(1000m) + 0.0509 1000m = —1.7264F + 8.4404

$$F = \frac{SiO_2}{CaO + MgO + Na_2O + K_2O}$$

For intermediate silica slag (24<b<28)

c = —2.0356(1000m) + 1.1094 1000m = —1.3101F + 9.9279
F = b. ($Al_2O_3$ + Fe0)

For low silica slag (b<24)

c = 01.8244(1000m) + 0.9416 1000m = —55.3649F + 37.9186

$$F = \frac{CaO}{CaO + MgO + Na_2O + K_2O}$$

The model was developed based on viscosity measurements on 17 Western US lignite and subbituminous coal slags within the compositional range [7]:

| | |
|---|---|
| $SiO_2$ | 0.25-0.70 mol fraction |
| $Al_2O_3$ | 0.08-0.27 mol fraction |
| $Fe_2O_3$ | 0-0.09 mol fraction |
| CaO | 0.08-0.33 mol fraction |
| MgO | 0.04-0.13 mol fraction |
| $Na_2O$ | 0-0.11 mol fraction |
| Minor elements | (Xi<5%) $K_2O$, $TiO_2$, $P_2O_5$, $SO_3$ |

**Kalmanovitch-Frank (1988) [5, 6-8]**

In the Kalmanovich–Frank (KF) the parameters *A* and *B* of the Urbain model have been modified to describe viscosities of the particular coal ash slags.

It is believed to be well suited for coal with high $SiO_2$, low 'FeO' content [15]. The model parameters – *a* and *b* is given as

ln a = —0.2812b — 11.8279

To allow prediction of systems that also contain the oxides of iron, magnesium, sodium, potassium, and titanium,

$$\alpha = \frac{CaO + MgO + Na_2O + K_2O + 'FeO' + TiO_2}{Al_2O_3 + CaO + MgO + Na_2O + K_2O + 'FeO' + TiO_2}$$

This method assumes that all of the oxides flux the slag to the same extent and that potassium oxide behaves as a flux.

Dyk et al. [15] employed FactSage to estimate the composition of the liquid portion of heterogeneous slags and used this composition in the KF model. It was stated that this method is highly likely to be more accurate, but without providing quantitative details [2].

**Senior and Srinivasachar model (1995) [16]**

This model was developed for predicting the viscosity of individual coal ash particles in the range of $10^4$-$10^8$ Pa-s whereas previous models have been developed and validated using compositions which generally correspond to the bulk ash. The model is designed to predict viscosity of silicates containing 35 to 99% $SiO_2$ with $Al_2O_3$, $Fe_2O_3$, FeO, CaO, MgO, $Na_2O$, $K_2O$ and $TiO_2$.

The model is divided into two parts, a low-viscosity part, < $10^4$ pa.s (High temperature) and a high-viscosity part, >$10^4$ Pa.s (Low temperature. This model is a reformulation of the of the Urbain model, based on the Weymann expression

$$\log\frac{\eta}{T} = A + \frac{10^3 B}{T}$$

$$A = \alpha_0 + \alpha_1 B + \alpha_2 \frac{NBO}{T}$$

Where, T is the temperature in Kelvin and η is viscosity in Poise.
NBO/T is the ratio of non-bridging oxygens to tetrahedral oxygens, given by

$$\frac{NBO}{T} = \frac{CaO + MgO + FeO + Na_2O + K_2O - Al_2O_3 - Fe_2O_3}{\frac{1}{2}(SiO_2 + TiO_2) + Al_2O_3 + Fe_2O_3}$$

$$B = b_0 + b_1\alpha + b_2\alpha^2 + N(b_3 + b_4\alpha + b_5\alpha^2) + N^2(b_6 + b_7\alpha + b_8\alpha^2) + N^3(b_9 + b_{10}\alpha + b_{11}\alpha^2)$$

Where, N is the mole fraction of $SiO_2$ and α is the molar ratio of

$$\alpha = \frac{CaO}{Cao + Al_2O_3}$$

Fitted values of coefficients for B is

| | High temperature | Low temperature |
|---|---|---|
| b0 | -224.98 | -7563.46 |
| b1 | 636.67 | 24431.69 |
| B2 | -418.70 | -17685.4 |
| B3 | 823.89 | 32644.26 |
| B4 | -2398.32 | -103681.0 |

| | | |
|---|---|---|
| B5 | 1650.56 | 74541.33 |
| B6 | -957.94 | -46484.8 |
| B7 | 3366.61 | 146008.4 |
| B8 | -2551.71 | -104306.0 |
| B9 | 387.32 | 21904.63 |
| B10 | -1722.24 | -68194.8 |
| B11 | 1432.08 | 48429.31 |

Coefficient A is calculated by B and NBO/T
For High High temperature

$$A_H = -2.81629 - 0.46314B - 0.35342\frac{NBO}{T}$$

For Low temperature

$$A_L = -0.982 - 0.902473B, \text{ NBO/T} \geq 1.3$$
$$A_L = 2.478718 - 0.902473B - 2.662091\frac{NBO}{T}, \text{ 0.2≤NBO/T<1.3}$$
$$A_L = 9.223 - 0.902473B - 36.3835\frac{NBO}{T}, \text{ 0≤NBO/T<0.2}$$
$$A_L = 9.223 - 0.902473B, \text{ NBO/T<0}$$

the authors concluded that this model performs better than the Kalmanovitch model for viscosities in the range $10^4$ to$10^9$ Pa.s, but the Kalmanovitch model is best at viscosities less than $10^2$ Pa.s.

**Synthetic SiO2–Al2O3–CaO–FeO model (1998-1999) [17, 18]**

Hurst et al developed three separate empirical viscosity models at the 5, 10, and 15 wt% FeO levels from experimental measurements of synthetic ashes based on least squares fit the transformed Weymann-Frenkel equations. The viscosity models may be used as a guide for selecting suitable Australian bituminous coals and determining the amount of limestone flux necessary to form suitable compositions for use in slagging entrained flow gasifiers for continuous operation of the various gasifiers at the expected slag tapping temperature range of $1400^0$C–1500 $^o$C [17]

$$\eta = AT\ exp(\frac{B}{RT})$$

$$ln(\eta) = lnA + lnT + \frac{B}{RT}$$

$$ln(\eta) = a_0 + a_1 y + a_2 y^2 + a_3 x + a_4 xy + a_5 xy^2 + a_6 x^2 + a_7 x^2 y + a_8 x^2 y^2 + a_9 x^3 + a_{10} x^3 y + a_{11} x^3 y^2$$

where η is the viscosity in Pa s, *T* is the absolute temperature, *R* is the gas constant, *A* and *B* are parameters applicable to each slag and x and y are the normalized mole fraction in $SiO_2$–$Al_2O_3$–CaO–FeO system

$$x = \frac{m_s}{m_s + m_a + m_c + m_f}$$

$$y = \frac{m_c + m_f}{m_a + m_c + m_f}$$

Coal ash slag least squares model (1999) [19]

Hurst et al.[19] developed four separate empirical viscosity models at the 0–2.5, 2.5–5, 5–7.5 and 7.5–10 wt% FeO levels in a $SiO_2$–$Al_2O_3$–CaO–FeO (SACF) system from experimental measurements of 85 fluxed slags prepared from 52 Australian coal ashes based on a least squares fit to the transformed Weymann-Frenkel equations .

$$\eta = AT\ exp(\frac{B}{RT})$$

$$ln(\eta) = lnA + lnT + \frac{B}{RT}$$

$$ln(\eta) = a_0 + a_1 y + a_2 y^2 + a_3 x + a_4 xy + a_5 xy^2 + a_6 x^2 + a_7 x^2 y + a_8 x^2 y^2 + a_9 x^3 + a_{10} x^3 y + a_{11} x^3 y^2$$

where η is the viscosity in Pa s, *T* is the absolute temperature, *R* is the gas constant, *A* and *B* are parameters applicable to each slag and x and y are the normalized mole fraction in $SiO_2$–$Al_2O_3$–CaO–FeO system

$$x = \frac{m_s}{m_s + m_a + m_c + m_f}$$

$$y = \frac{m_c + m_f}{m_a + m_c + m_f}$$

**Modified Urbain Viscosity Model for Fully Liquid Slags: Kondratiev and Jak (2001) [4, 20-22]**

Kondratiev and Jak further modified the formalism developed by Urbain in order to describe viscosities of multi-component slags. This modified formalism was then used to describe the viscosity behaviour of slags over the whole composition range in the four-component system Al2O3-CaOFeO-SiO2 at iron metal saturation (i.e. reducing conditions). Their model uses one set of parameters and agrees well with more than 3,000 experimental points covering four unary, six binary, and four ternary systems, and the liquid in the whole of the quaternary system [3]
Viscosity of the liquid phase ηL of coal ash slag is given as:

$$\eta_L = AT \exp\left(\frac{1000B}{T}\right)$$

Where, T is the temperature in Kelvin, and A and B are the model parameters, which depend only on liquid composition. Parameter A and B are linked by the following equation.
— ln A = mB + n
Where, m and m are model parameters. The parameter B expressed as follows

$$B = \sum_{i=0}^{3} b_i^0 X_s^i + \sum_{i=0}^{3}\sum_{j=1}^{2}\left(b_i^{c,j}\frac{X_c}{X_c+X_F} + b_i^{F,j}\frac{X_F}{X_C+X_F}\right) \times \left(\frac{X_C+X_F}{X_C+X_F+X_A}\right)^j X_S^i$$

Where XA, XC, XF and Xs are mole fractions of Al2O3, CaO, 'FeO' and SiO2 respectively and $b_i^o$ are parameters for the Al2O3-SiO2 system $b_i^{c,j}$ and $b_i^{F,j}$ are sets of parameters for CaO and FeO respectively which are determined by optimization.

The parameter m is expressed by the following equation

$$m = m_A X_A + m_C X_C + m_F X_F + m_S X_s$$

$m_A$, $m_C$, $m_F$ and $m_S$ are adjustable parameters.
The major advantage of this modified Urbain model is that it enables the differences in chemistry of individual components to be taken into account while retaining the strength of the Urbain assumptions, i.e. the silicate slag viscosity increases with the third power of the glass former concentration and exhibits parabolic behaviour with varying proportions of amphoteric and network modifiers. [12]

**T Shift method or BBHLW method (2002) [5]**

Browning et al. [5] developed a semi-empirical model (BBHLW model) for Newtonian fluids in which it is assumed that at a given viscosity the gradient of the viscosity–temperature curve

is the same for all coal slags. This model was developed based on the ash sample viscosity data for 117 compositions. The T-shift model is based on the theory that, if all viscosity-temperature curves for different ash samples are translated along the temperature axis, they will overlay. Thus, if a standard viscosity-temperature curve is selected, the distance that the viscosity curve of any slag must be shifted along the temperature axis to overlay the standard curve can be quantified using the following equation [23]

This semi-empirical model for Newtonian fluids is based on the Nicholls and Reid observation that, at a given viscosity, the gradient of the viscosity-temperature curve is the same for all coal ash slags in the Newtonian region, i.e

$$\frac{d\eta}{dT} = f(\eta) \neq f(T)$$

A linear regression was performed to obtain an equation relating viscosity to a modified temperature. The modified temperature is the difference between the actual temperature and a shift temperature, which is in turn correlated to composition by an empirical equation

$$\log\left(\frac{\eta}{T - T_s}\right) = \frac{14788}{T - T_s} - 10.931$$

Where T is the experimental temperature and $T_S$ is the temperature shift.

$T_S = 306.63 \ln(A) — 574.31$

The molar ratio, *A*, is given by the following expression:

$$A = \frac{3.19\,Si^{4+} + 0.855\,Al^{3+} + 1.6\,K^{+}}{0.93\,Ca^{2+} + 1.50\,Fe^{n+} + 1.21\,Mg^{2+} + 0.69\,Na^{+} + 1.35\,Mn^{n+} + 1.47\,Ti^{4+} + 1.91\,S^{2-}}$$

The above equation is a simple expression that separates species found in the slag into those that increase the viscosity (network formers) in the numerator and those that decrease viscosity (network modifiers or fluxes) in the denominator. This ratio can also give an indication of the fluxing capability of the species in the denominator from the magnitude of its coefficient. The higher its coefficient, the more effective a flux it is. The relative fluxing ability can be related to the action diameter. Smaller cations such as Fe2+ and Ti4+ are strong fluxes, and larger cations such as Na+ and Ca2+ are relatively weak fluxes.

Where the quantities of each component are in terms of mole fraction, where

$$Si^{4+} + Al^{3+} + Ca^{2+} + Fe^{n+} + Mg^{2+} + Na^{+} + K^{+} + Mn^{n+} + Ti^{4+} + S^{2-} = 1$$

Unlike the Kalmanovich-Urbain method, the proposed method shows that potassium oxide acts as a network former, that is, it increases viscosity and titanium act as a network modifier in coal

ash slags. For coal and synthetic slags with viscosities less than 1000 Pa s, their model outperformed the S2, KF and WF models, which are based on simplified oxide melts or British coal ash slags. This method also provides an indication of the relative fluxing strength of the basic oxides usually found in coal ash slags.

The proposed method is a new technique for determining the viscosity of slags in the Newtonian region below 1000 Pa s. The method was found to be the most accurate of the methods in the comparison for use with fluxed and refluxed coal ash slags, but can also be used with reasonable accuracy over a wide range of compositions. However, for SiO2- Al2O3-CaO-MgO quaternary slags, the Kalmanovitch-Urbain method proved to be most accurate [23].

The model showed satisfactory agreement for some synthetic slags, but cannot be recommended for using in the whole compositional range reported. [11]

**Modified Urbain Viscosity Model for Fully Liquid Slags: Song (2010) [9]**

Wenjia Song, Yimin Sun, Yongqiang Wu, Zibin Zhu and Shuntarou Koyama have modified Urbain formalism to describe the viscosities of fully liquid slag and homogeneous remaining liquid phase in coal ash slag samples. The modified Einstein equation and Einstein–Roscoe equation have been used to describe the viscosities of heterogeneous coal ash slag samples of $\Phi$ <10.00 vol% and $\Phi$>10.00 vol%, respectively. Viscosity of the liquid phase of coal ash slag is given as:

$$\eta_l = AT \exp\left(\frac{1000B}{T}\right)$$

$$-\ln A = 0.29B + 11.57$$

Where B is

$$B = \sum_{i=0}^{3} b_i^0 X_g^i + \sum_{i=0}^{3}\sum_{j=1}^{2} \left(b_i^{C,j}\frac{X_C}{X} + b_i^{M,j}\frac{X_M}{X} + b_i^{K,j}\frac{X_K}{X} + b_i^{N,j}\frac{X_N}{X} + b_i^{T,j}\frac{X_T}{X}\right) * \left(\frac{X}{X+X_A}\right)^j X_S^i$$

Where,

$X = X_C + X_M + X_K + X_N + X_T$

where XA, XC, XM, XK, XN, XT, XS are mole fractions of $Al_2O_3$, CaO, $SiO_2$, MgO, $K_2O$, $Na_2O$, $TiO_2$, and $SiO_2$, respectively; $b_i^{C,j}$, $b_i^{M,j}$, $b_i^{K,j}$, $b_i^{N,j}$, $b_i^{T,j}$ are empirical parameters determined through optimization—fitting the model predictions to the experimental data.

**3. Structural Viscosity Models homogeneous liquid**

The viscosity of molten slag is related to internal structure of oxide melt, and very sensitive to the changes of temperature and slag composition. Generally, slag viscosity has difficulty in being precisely measured and predicted by empirical methods. Therefore, the development of a reliable viscosity model has been required to accurately and reasonably estimate slag viscosities over

whole composition range for multicomponent oxide systems through the structural features of oxide melts [24].

A number of structurally based viscosity models have also been developed for multi-component slag using structural information. These viscosity models have been developed using a number of very different approaches to linking the viscosity of the slag to the internal structures such as thermodynamic properties of the liquid slag phase, internal structure of silicates through bridging, non-bridging, and free oxygens extracted from sophisticated thermodynamic models, basicity index and corrected optical basicity etc.

**Iida model and the modified Iida model (2002) [25-29]**

Iida's viscosity model is based on the Arrhenius-type equation, where network structure of the slag is taken into account by using the so-called modified basicity index $Bi^{(j)}$. The original Iida model which divided all the oxides into basic and acid oxides has been modified to take into account the amphoteric behaviour of certain oxides. This improved model is commonly known as the modified Iida model. Modified basicity index is similar to the basicity index *Bi*, but the amphoteric oxides $\alpha_i$ are replaced with $\alpha^*$. Basic–acid behaviour of amphoteric oxides changes according to the overall basicity of the slag.

$$\mu = A\mu_0 \exp\left(\frac{E}{Bi^{(j)}}\right)$$

$$A = 1.029 - 2.078 * 10^{-3}T + 1.050 * 10^{-6}T^2$$

$$E = 28.46 - 2.0884 * 10^{-2}T + 4.000 * 10^{-6}T^2$$

$$\mu_0 = \sum \mu_{0i} X_i$$

$$\mu_{0i} = 1.8 * 10^{-7} \frac{[M_i(T_m)_i]^{\frac{1}{2}} \exp\left({}^{H_i}/_{RT}\right)}{(V_m)_i^{\frac{2}{3}} \exp\left[\frac{H_i}{R(T_m)_i}\right]}$$

$$H_i = 5.1(T_m)_i^{\frac{1}{2}}$$

$$Bi^{(j)} = \frac{\sum(\alpha_i W_i)_B + \sum(\alpha_i^* W_i)_{Am2}}{\sum(\alpha_i W_i)_A + \sum(\alpha_i^* W_i)_{Am1}}$$

$$Bi = \frac{\sum(\alpha_i W_i)_B}{\sum(\alpha_i W_i)_A}$$

Where A and E are parameters determined to fit large a number of experimental data, μ = viscosity, $T$ = absolute temperature, $\mu_0$ = hypothetical viscosity of pure oxide, $X_i$ = mole fraction,

$Tm$ = melting temperature, $R$ = universal gas constant, $Vm$ = molar volume at melting point, $Bi^{(j)}$ = modified basicity index, $\alpha i$ specific coefficient and $W_i$ = weight percentage.

For quaternary CaO-MgO-Al2O3-SiO2 melts, $Bi^{(j)}$ is written as

$$Bi^{(j)} = \frac{\alpha_{CaO} W_{CaO} + \alpha_{MgO} W_{MgO}}{\alpha_{SiO_2} W_{SiO_2} + \alpha^{*}_{Al_2O_3} W_{Al_2O_3}}$$

$$\alpha^{*}_{Al_2O_3} = aBi + bW_{Al_2O_3} + c$$

The high accuracy claimed with this model comes from its calibration with experimental data for each family of slags The advantage of Iida model is that it covers most slag compositions and performed well (within the range of experimental error) for mold fluxes, coal slags, and blast furnace slags [25, 30]. However, one disadvantage of using Iida model is that it is difficult to apply the Iida model to systems where there is no experimental data since $\alpha i^{i}$ values are determined for each system/family and there is no general overall value for $\alpha i^{*}$.For example, one can calculate $\alpha i^{*}$from a, b, and c values for $CaO$ -$MgO$ -$Al_2O_3$ -$SiO_2$ but other a, b, c values (leading to a different $\alpha i^{*} Al_2O_3$) are for another system [29]

**KTH model [30]**

The KTH viscosity model was developed by The KTH viscosity model at the Royal Institute of Technology. For estimating the viscosities of ionic melts this model adopts the Arrhenius/Eyring equation for the description of viscosities. The activation energy for viscous flow was modelled in analogy with the modelling of Gibbs energy in thermodynamics [22] i.e the compositional dependence of the model is expressed as a function of the Gibbs free energy of solution [3]

Viscosity n is expressed by the Arrhenius equation

$$\eta = A \exp\left(\frac{\Delta G^{*}}{RT}\right)$$

where A is a constant, Ris the gas constant, T is the temperature and ΔG*is the Gibbs energy of activation for viscosity. Constant A is described by the Eyring theory

$$A = \frac{hN}{V_m} = \frac{hN\rho}{M}$$

where h is the Planck's constant, N is the Avogadro's number and $V_m$ the molar volume of the liquid. ρ stands for density and M for molecular weight.

For a multi-component system

$$\Delta G^* = \sum X_i \Delta G_i^* + \Delta G_{Mix}^*$$

Where $\Delta G_i^*$ is the Gibbs energy of activation of the pure component I in a liquid state and $\Delta G^*_{Mix}$ is for the contribution due to the mutual interaction between different species due to the mixing of the components and is a function of composition.

Although the use of thermodynamic data allows for the calculation of viscosities applicable to a wide composition range, the features of the silicate melts are not directly considered in their model [13]. The model can readily explain the viscosity of multicomponent silicate slag, but has a limitation in describing the viscosity of aluminosilicate melts, which results from using oversimplified structural units in the model [31]

**Models based on optical basicity (NPL) [29]**

NPL model developed by Mills and Sridhar uses the Arrhenius equation for the temperature dependence of slag viscosity, relates the viscosity of slags to the structure through the optical basicity corrected for the cations used for charge balancing ($\Lambda^{corr}$), which in turn can be obtained from experimental data or estimated.

The method used to account for the temperature dependence was to assume the Arrhenius behavior

$$ln\,\eta = lnA + \frac{B}{T}$$

where η is viscosity in Pa.s T is temperature and A and B are, constants with respect to temperature, A and B are functions of $\Lambda^{corr}$

$$\Lambda^{corr} = \frac{\sum x_i n_i \Lambda_i}{\sum x_i n_i}$$

where x is the mole fraction and n refers to the number of oxygen atoms in the molecule $\Lambda_i$ is optical basicity. The parameters B and ln A can be derived from the

$$\frac{ln\,B}{1000} = -1.77 + \frac{2.88}{\Lambda^{corr}}$$

$$ln\,A = -232.69(\Lambda^{corr})^2 + 357.32\Lambda^{corr} - 144.17$$

The NPL model provides a good estimation of the viscosities of iron blast furnace slag [32] Coal slags have high $SiO_2$ and $Al_2O_3$ contents and are consequently highly polymerized. It should be noted that coal slags have high activation energies because of their highly polymeric nature and tend to have high melting temperatures which restrict the measurement range and, in turn, results in uncertainties in the activation energy. These uncertainties in the activation energy lead to significant errors in the predicted viscosities [33]

**CSIRO model [33-34]**

Zhang and Jahanshahi **[34-35]** developed a model (CSIRO Model) for the estimation of viscosities of multicomponent slags. The Zhang model is based on the Weymann-Frenkel equation and links the slag viscosity to the internal structure of the slag expressed through the concentrations of bridging, non-bridging and free oxygens derived from the cell thermodynamic model. To obtain a better fit of the viscosity data, the model uses the square and the cube of the bridged oxygen concentration, multiplied by optimized viscosity parameters. It should be noted that their model for aluminosilicate systems considers the amphoteric behavior of $Al_2O_3$ using the so-called charge-compensation concept.

The temperature dependence of viscosity is calculated using the Weymann equation [26] or Frenkel equation

$$\eta = A^W T \exp\left(\frac{E_\eta^W}{RT}\right)$$

where η is viscosity, *T* is the temperature in kelvin, R is the gas constant, and $A^W$ and $E\eta^W$ are the pre-exponential terms and the activation energy, respectively. The values of *AW* and $E_y{}^W$ can be calculated by fitting experimental data for a given melt

$$E_\eta^W = a + b(N_{O^0})^3 + b(N_{O^0})^2 + d(N_{O^{2-}})$$

where *a*, *b*, *c*, and *d* are fitting parameters to be optimized for experimental data and $NO^o$,NO-, and $NO^{2-}$ are the fraction bridging, non-bridging and free oxygen respectively were obtained using the cell model.

The pre-exponential term *AW* is calculated using the equation

$$\ln(A^W) = a' + b' E^W_y$$

Where *an*' and *b*' are fitting parameters

This model correlates the viscosity as a function of the composition to the concentration of bridging, non-bridging and free oxygen. However, the correlation between the concentration of the three types of oxygen and the viscosity is not simple, it require a large number of parameters that need to be optimized [36]

**Nakamoto - Tanaka model [13, 37-38]**

Nakamoto et al. [13] have also developed a model that uses the fractions of bridging, non-bridging and free oxygen. Their model is based on the idea that viscous flow is caused by the motion of "cutting off points" that they define as the sum of non-bridging and free oxygen through the network structure. They find that the activation energy for viscous flow is inversely proportional to the distance the "cutting off points" move when shear stress is applied to the liquid. This distance is essentially the parameter of their model [36].

On the basis of the above idea the viscosity model for silicate, slag was developed based on the Arrhenius type equation

$$\eta = A \exp\left(\frac{E_V}{RT}\right)$$

$$E_V = \frac{E}{1 + \sqrt{\alpha.(N_{O^-} + N_{O^{2-}})}}$$

where $A$ ($4.80*10^{-8}$) is a constant, $E$V is the activation energy for viscosity, $R$ is the gas constant, and $T$ is the temperature. $E$ ($5.21*10^5$ (J)) is the activation energy for the viscosity of pure $SiO_2$, and α is the parameter relating to the weakness of the bonding between the cation and oxygen ion at the "cutting-off " point, which depends on the oxide component. $N_0$- and $N_02$- are fractions of the non-bridging oxygen ion and free oxygen ion, respectively, evaluated by the IRSID 'cell model.

This viscosity model can represent the composition dependence of viscosity in a wide composition range in the multi-component silicate system $SiO_2$–CaO– MgO–FeO–$Al_2O_3$ in blast furnace process. The amphoteric behavior of $Al_2O_3$ can be explained by this model. However, the IRSID "cell model" is not applicable to slag containing alkali oxides, which cannot be ignored in the slag. Therefore, to consider the effect of alkali oxides the authors modified the present model to the viscosity of aluminosilicate melts containing alkali oxides in melting furnaces, $SiO_2$–CaO–MgO–FeO–$K_2O$–$Na_2O$–$Al_2O_3$ system, by applying the method of Susa et al to evaluate the bonding states of oxygen in the molten silicate instead of thermodynamic models.

Susa *et al* described that the structure of aluminosilicate melts consists of only three kinds of chemical bonds, *i.e.* Si–BO (bridging oxygen in Si tetrahedral unit), Al–BO (bridging oxygen in Al tetrahedral unit with a charge-compensating cation), and Si–NBO (NBO: non- bridging oxygen connected with Si) with a charge-compensating cation, Accor to their assumption results in the calculation of chemical bonds of oxygen solely by the concentration of slag components. In addition, by considering the Al–BO bond in their equation, the oxygen states can be estimated in case that aluminum oxide works as network former. In the modified model, the parameter EV is calculated by

$$E_V = \frac{E}{1 + \sqrt{\sum_i \alpha_i (N_{BO+FO})_i + \sum_j \alpha_{j\ in\ Al} (N_{Al-BO})_j}}$$

where the activation energy *E*V is a function of the sum of the fractions of non-bridging oxygen ion (NBO) and free oxygen ion (FO) *N*(NBO+FO)*i* and the fraction of the bridging oxygen (BO) in the Al tetrahedral unit *N*(Al–BO)*j*. *N*(NBO+FO)i is the same as the ($N0— + N02— ) . \alpha i$ *and* $\alpha j$ in Al are parameters. *i* is the component of melt except SiO2, *i.e.* CaO, MgO, FeO, K2O, Na2O, Al2O3, and *j* is the charge-compensating ion from component *i* except Al2O3, *i.e.* $Ca^{2+}$, $Mg^{2+}$, $Fe^{2+}$, $K^{+}$ and $Na^{+}$. *A* and *E* have the same values in the original equation, *i.e.* $4.80*10^{-8}$ and $5.21*10^{5}$ (J) respectively.

It is assumed that there are no differences between non-bridging oxygen ions and free oxygen ions in the respect of the influence of those ions on viscosity. The effect of the bridging oxygen in the Al tetrahedral unit on the activation energy is treated in the same manner as the effect of the non-bridging oxygen by assuming that the bridging oxygen in the Al tetrahedral unit has a somewhat different mobility from that of the bridging oxygen in the Si tetrahedral unit.
While this model requires very few optimized parameters, the reproduction of the experimental data is considerably less accurate [31, 36]

**Pyrosearch quasi-chemical viscosity model [10, 11, 39-41]**

The model links the slag viscosities to the internal structures of the melts through the concentrations of various $Si_{0.5}O$, $Me_{2/n^{n+}}O$ and $Me_{1/n^{n+}}Si_{0.5}0$ viscous flow structural units. The concentrations of these structural units are derived from a quasi-chemical thermodynamic model of the system [41]. The quasi-chemical viscosity model, initially being optimised for the Al2O3 -CaO-'FeO'- a SiO2 system in equilibrium with metallic iron has recently been extended to MgO, K2O, and Na2O-containing slag systems. The model enables slag viscosities to be predicted with the overall accuracy 30 pct over the whole compositional range in the Al2O3-CaO-'FeO'-K2O-MgO-Na2O-SiO2 in equilibrium with metallic iron [32]. In order to reproduce the experimental viscosity data for the Al2O3-CaO-'FeO'-K2O-MgO-Na2O- SiO2 system, however, this model requires quite a large number of binary and ternary parameters

This viscosity model is based on the Eyring viscosity equation

$$\eta = \frac{2RT}{\Delta E_v} \frac{(2\pi m_{SU} KT)^{\frac{1}{2}}}{v_{SU}^{\frac{2}{3}}} \exp\left(\frac{E_a}{RT}\right)$$

where R is the gas constant, k is the Boltzmann constant, T is the absolute temperature, Ev is the energy of vaporization, Ea is the activation energy, and mSU and vSU are the weight and volume of the structural unit. The activation energy Ea is related to the potential barrier that has to be overcome by a structural unit to move to the available hole. The energy of vaporization ΔEv, which was also called by Bockris'work of hole formation', is closely related to the probability of the formation of a hole, or a free volume in the liquid. Both $\Delta E_v$ and the activation energy *Ea* was expressed as a function of various SU concentrations.

**Grundy model (FactSage)**

Recently, Grundy et al. [1, 36] developed a structural viscosity model based on the structural unit calculations from the Modified Quasichemical Model parameters optimized for the FACT oxide database for silicate melts. The structure of the silicate melt is characterised based on the concept of Q-species. The concentrations of Q-species are calculated using the concentration of bridging oxygen calculated from the Quasichemical model, thus linking the thermodynamic description of the liquid to its structure. The polymerization of the melt is then characterized by calculating the degree of connectivity of the Q-species. Viscosity is correlated to the connectivity of the silicate melt, and the resulting model requires very few optimized parameters [38]

**8 Viscosity Models heterogeneous liquid**

Both Newtonian and non-Newtonian behavior has been observed in slag systems. Non-Newtonian behavior is complex and can involve the pseudo-plastic flow of the fluids. Newtonian behavior has been reported to occur in slag systems containing less than 10–40 vol. % solids [3]. For silicate melts, non-Newtonian behavior can be caused by the appearance of crystals in the melt or the separation of immiscible liquids. Most non-Newtonian models require knowledge of the crystal fraction and sometimes crystal shape or size. There are relatively few mathematical models available to describe the behavior of multiphase slag systems.

**Annen model [42, 43]**

Annen et al. proposed a model to incorporate the effect of crystalline phases on the slag viscosity. They treated the slag as a mixture of the melt and crystalline phases, and modelled the viscosity of the mixture (μmixture) as a function of liquid's viscosity (μliq)) and the solid content:

$$\mu_{mixture} = \mu_{liq}(1 + 2.5C + 9.15C^2)$$

where C is the volume fraction of solids. For the viscosity of liquid phase, they employed the Watt-Fereday model. The solid's concentration and the liquid composition in the mixture were calculated using a chemical equilibrium code. The above equation is valid for solids present in the shape of spheres at low concentrations.

For those slags that contained elongated crystals of mullites and corundum, the above equation may not be appropriate. The model also does not describe the effect of the particle size observed in large crystals of spine vs. dendritic spinels. However, the above model or variations of the above may still provide an improved first approximation to model the effect of crystalline phase formation on slag viscosity. The success of the model by Annen et al. also depends on the accuracy of the solid's concentration predicted as a function of temperature. [43]

Oh, et al [43] made thermodynamic equilibrium calculations for the four coal slags using normalized compositions of the five major components (Si02, A1203, CaO, FeO, and MgO assuming that the liquid phase as an ideal mixture of various silicate species. The predicted crystalline phases at 900℃ agreed well with the observation However, the concentration of solids predicted as a function of temperature did not improve the viscosity predictions for Pittsburgh No. 8 and PMA [43]

Oh, et al.[44] believed these models were valid only for very small concentrations of crystallized particles but could not describe the effect of shear rate on the viscosity.[9]

**Kondratiev and Jak (2001) [4, 20-22]**

Kondratiev and Jak optimized the Urbain model the system Al2O3-CaO- 'FeO'-SiO2 with experimental data of homogeneous melts as determined by F*A*C*T. To calculate the viscosity of a heterogeneous slag, the proportion of solids and the composition of the remaining liquid phase were first estimated using F*A*C*T, then the liquid phase viscosity was calculated from the optimized Urbain model, and finally, this viscosity was adjusted depending on the volume fraction of solid particles, according to the Roscoe equation. The model enables the viscosities of homogeneous (completely molten) liquid slag systems, as well as heterogeneous (partially crystallized) slag systems, to be predicted as a function of the bulk slag composition and operating temperature over the complete range of conditions at iron saturation. It was stated that good agreement was achieved between the model and over 4000 experimental points [2]

Viscosity of slurry $5_S$ is given by:

$\eta_S = \eta_L(1 — V_S)^{-2.5}$

Where, $V_S$ being the solid volume fraction

The assumed that the slurry exhibits Newtonian behaviour, but the absolute viscosity increased due to the presence of solids. No account was taken off other factors such as particle size, shape etc[20]

**Song Model (2010) [9]**

Wenjia Song, Yimin Sun, Yongqiang Wu, Zibin Zhu and Shuntarou Koyama have measured the viscosities of 45 Chinese coal ash slag samples under different temperatures and shear rates. The computer thermodynamic software package FactSage has been used to predict liquidus temperatures, volume fractions of crystallized solid particles (Φ), and the compositions of remaining liquid phase for 45 coal ash slag samples. The flow properties of completely liquid and partly crystallized coal ash slag samples have been predicted by three viscosity models. The Urbain formalism has been modified to describe the viscosities of fully liquid slag and homogeneous remaining liquid phase in coal ash slag samples. The modified Einstein equation and Einstein–Roscoe equation have been used to describe the viscosities of heterogeneous vol % and Φ> 10.00 vol %, respectively. It can be noted that Φ<10.00 the coal ash slag samples behavior of the heterogeneous coal ash slag samples is that of the Newtonian fluid at these temperatures. To find the critical values of solid content that mark the transition from Newtonian to non-Newtonian behavior; they used FactSage to calculate the volume fraction of crystallized solid particles for the 45 coal ash slag samples as a function of temperature.

The viscosity of heterogeneous coal ash slag $\eta_S$ was calculated by the following equations.

$$\frac{\eta_S}{\eta_l} = 1 + 1.158\phi, \qquad for\ \phi < 10.0\ vol\%$$

$$\frac{\eta_S}{\eta_l} = \left(1 - \frac{\phi}{\phi_m}\right)^{-4.62r^{-0.572}}, for\ \phi > 10.0\ vol\%$$

Where Φ is the volume fraction of crystallized solid particles and $\Phi_m$ is the maximum amount of crystallized particles that the slag could accommodate before the viscosity becomes ‘‘infinite.’’

**9 Artificial neural network model [2]**

An artificial neural network (ANN) model was developed by Duchesne et al [2] to predict slag viscosity over a broad range of temperatures and slag compositions. This model outperforms other slag viscosity models, resulting in an average error factor of 5.05 which is lower than the best obtained with other available models. Slag viscosity predictions for Genesee coal ash were evaluated to determine the effect of various fluxing agents. Of the fluxing agents studied, the one with high magnesium content has the greatest effect when it comes to minimizing the required temperature for slag removal. It was stated that since the ANN does not rely upon theoretical relations, it can easily be expanded to include other factors such as atmosphere composition and new components.

## 10 Conclusion

The viscosity behaviour of the slags is determined by key process parameters, including the bulk composition of the slag, the effective oxygen partial pressure in the slag phase, and the temperature. It is related to internal structure of oxide melt, and very sensitive to the changes of temperature and slag composition. Generally, slag viscosity has difficulty in being precisely measured and predicted by empirical methods. Since operating conditions and slag compositions can vary significantly not only between processes but also within a given process, an accurate viscosity model with a wide range of applicability is desired.

Analysis of the various viscosity models for coal ash slags it can be pointed out that there are no a-priori models available that can cover the entire slag area. Most of the existing models are based on different mathematical expressions, based on semi-empirical approaches and they do not have adequate predictive power outside the investigated ranges. It is suggested that in the case of unknown slag great care should be taken for any comparison of the different models with respect to their performance, and it is not certain whether the predictions can be reliable [12].

As there is no experimental information on the slag viscosities is available for the particular composition and conditions of Victorian brown coal. Therefore, it is essential to develop a general, self-consistent and reliable viscosity model from the experimental data that can be applied over the whole compositional range.

## References

1 Grundy AN, Jung IH, Pelton AD, Decterov SA, A model to calculate the viscosity of silicate melts, part II: the $NaO_{0.5}$-MgO-CaO-$AlO_{1.5}$-$SiO_2$ system. Inter. J. Materials Research 2008; 99: 1195-1209.

2 Duchesne MA, Macchi Aa, Lu DY, Hughes RW, McCalden D, Anthony EJ. Artificial neural network model to predict slag viscosity over a broad range of temperatures and slag compositions. Fuel Processing Technology 2010;91: 831–836
3 Kondratiev A, Jak E, Hayes PC. Predicting Slag Viscosities in Metallurgical Systems. JOM Journal of the Minerals, Metals and Materials Society 2002; 54: 41-45
4 Kondratiev A, Jak E. Review of experimental data and modeling of the viscosities of fully liquid slags in the Al2O3–CaO–'FeO'–SiO2 system. Metal Mater Trans B 2001;32B:1015–25
5 Browning GJ, Bryant GW, Hurst HJ, Lucas JA, Wall TF. An empirical method for the prediction of coal ash slag viscosity. Energy Fuel 2003; 17:731–7.
6 Lucas JA, Browning GJ, Bryant GW, Hurst HJ, Wall TF. DEVELOPMENT OF THE THERMOMECHANICAL ANALYSIS TECHNIQUE FOR COAL ASH AND SLAG APPLICATIONS. 2001 CRC FOR BLACK COAL UTILISATION report 18
7 Vargas S, Frandsen FJ, Dam-Johansen K. Rheological properties of high temperature melts of coal ashes and other silicates. Prog Energy Combust Sci 2001;27: 237–429.
8 Kinaev N. A review of mineral matter issues in coal gasification. CCSD report RR 60, 2006
9 Song W, Sun Y, Wu Y, Zhu Z, Koyama S. Measurement and Simulation of Flow Properties of Coal Ash Slag in Coal Gasification. AIChE Journal 2011; 57: 801-818
10 Kondratiev A, hayes PC, Jak E. Development of a Quasi-chemical Viscosity Model for Fully Liquid Slags in the Al2O3–CaO–'FeO'–MgO–SiO2 System. Part 1. Description of the Model and Its Application to the MgO, MgO–SiO2, Al2O3–MgO and CaO–MgO Sub- systems. ISIJ International 2006; 46: 359–367.
11 Kondratiev A, hayes PC, Jak E. Development of a Quasi-chemical Viscosity Model for Fully Liquid Slags in the Al2O3–CaO–'FeO'–MgO–SiO2 System. Part 3. Summary of the Model Predictions for the Al2O3–CaO–MgO–SiO2 System and Its Sub-systems. ISIJ International 2006; 46: 375–384
12 Seetharaman S, Mukai K, and Sichen D. Viscosities of slags—an overview. VII International Conference on Molten Slags Fluxes and Salts, The South African Institute of Mining and Metallurgy, 2004.
13 Nakamoto M, Lee J, Tanaka T. A Model for Estimation of Viscosity of Molten Silicate Slag. ISIJ International 2005; 47: 651–656
14 Schobert HH, Streeter RC, Diehl EK. Flow properties of low-rank coal ash slags implications for slagging gasification. Fuel 1985; 64:1611–7.
15 Van Dyk JC, Waanders FB, Benson SA, Laumb ML, Hack K. Viscosity predictions of the slag composition of gasified coal utilizing FactSage equilibrium modelling. Fuel 2009; 88:67– 74.
16 Senior CL, Srinivasachar S. Viscosity of Ash Particles in Combustion Systems for Prediction of Particle Sticking. *Energy* & *Fuels* 1995; 9: 277-283
17 Hurst HJ, Novak F, Patterson JH. Viscosity measurements and empirical predictions for some model gasifier slags. Fuel 1999; 78: 439–44.
18 Hurst HJ, Novak F, Patterson JH. Viscosity measurements and empirical predictions for some model gasifier slags - II. Fuel 2000; 79: 1797-99.
19 Hurst HJ, Novak F, Patterson JH. Viscosity measurements and empirical predictions for fluxed Australian bituminous coal ashes. Fuel 1999; 78: 1831–40.
20 Kondratiev A, Jak E. Predicting coal ash slag flow characteristics. Fuel 2001;80:1989– 2000
21 Jak E, Christie S, Hayes PC. The Prediction and Representation of Phase Equilibria and Physicochemical Properties in Complex Slag Systems. Metal Mater Trans B 2003; 34B:595-603

22 Cormos CC, Starr F, Tzimas E. Use of lower grade coals in IGCC plants with carbon capture for the co-production of hydrogen and electricity. International Journal of Hydrogen Energy 2010; 35: 556 – 567
23 Buhre BJP, Browning GJ, Gupta RP, Wall TF. Measurement of the viscosity of coal- derived slag using thermomechanical analysis. Energy Fuel 2005; 19: 1078–83.
24 Suzuki M, Jak E. Revision of Quasi-chemical Viscosity Model to Predict Viscosity of Molten Slag in Multicomponent Oxide Systems related to Metallurgical Processes. High Temperature Processing Symposium, Swinburne University of Technology, 2011.
25 Forsbacka L, Holappa L, Iida T, Kita Y and Toda Y. Experimental study of viscosities of selected CaO–MgO–Al2O3–SiO2 slags and application of the Iida model. Scandinavian Journal of Metallurgy 2003; 32: 273–280
26 Forsbacka L, Holappa L. Viscosity of CaO–CrOx–SiO2 slags in a relatively high oxygen partial pressure atmosphere. Scandinavian Journal of Metallurgy 2004; 33: 261–268
27 lida T, Sakal H, Kita Y, Shigeno K. An Equation for Accurate Furnace Type Slags from Prediction of the Viscosities Chemical Composition. ISIJ International 2000; 40: S110-S114
*28* Xu J, Zhang J, Jie C, Liu G, Ruan F. Measuring and Modelling of viscosities of selected CaO-MgO-Al2O3-SiO2 slags. *Advanced Materials Research 2011; 152-153: 782-790*
*29* Mills KC*, Yuan L, Jones RT. Estimating the physical properties of slags. *The Journal of the Southern African Institute of Mining and Metallurgy 2011; 111: 649-658*
30 Seetharaman S, Sichen D. Viscosities of high temperature systems: a modelling approach. ISIJ Int 1997; 37: 109–118.
31 Jung IH. Overview of the applications of thermodynamic databases to steelmaking processes. Calphad 2010; 34: 332-362
32 Kondratiev A, Zhao B, Raghunath S, Hayes PC, and Jak E. New tools for viscosity measurement and model-ling of fully liquid and partly crystallised slags. Proceedings of EMC 2007
33 Mills KC, Sridhar S. Viscosities of ironmaking and steelmaking slags. Ironmaking and Steelmaking 1999; 26:262-268
34 Zhang L, Jahanshahi S. Review and modelling of viscosity of silicate melts: Part I viscosity of binary and ternary silicates containing CaO, MgO, and MnO. Metallurgy Metal Mater Trans B 1998 ; 29B: 177–186.
35 Zhang L, Jahanshahi S. Review and modelling of viscosity of silicate melts: Part II. Viscosity of melts containing iron oxide in the CaO– MgO–MnO–FeO–Fe2O3–SiO2 system. Metal Mater Trans B. 1998; 29B: 187–195.
36 Grundy AN, Liu H, Jung IH, Decterov S, Pelton AD. A model to calculate the viscosity of silicate melts, part I: viscosity of binary $SiO_2$-$MeO_x$ systems (Me = Na, K, Ca, Mg, Al). Inter. J. Materials Research 2008; 99: 1185-1194.
37 Nakamoto M, Miyabayashi Y, Lauri Holappa L, Tanaka T. A Model for Estimating Viscosities of Aluminosilicate Melts Containing Alkali Oxides. ISIJ International 2007; 47: 1409–1415
38 Miyabayashi Y, Nakamoto M Tanaka T, Yamamoto T. A Model for Estimating the Viscosity of Molten Aluminosilicate Containing Calcium Fluoride. ISIJ International 2009;49: 343–348
39 Kondratiev A. and Jan E. Quasi-chemical viscosity model for fully liquid slags in the Al2O3-CaO-'FeO'-SiO2 system. *VII International Conference on Molten Slags Fluxes and Salts,* the South African Institute of Mining and Metallurgy, 2004.

40 Kondratiev A, Hayes PC, Jak E. Development of a Quasi-chemical Viscosity Model for Fully Liquid Slags in the $Al_2O_3$–CaO–'FeO'–MgO–$SiO_2$ System. Part 2. A Review of the Experimental Data and the Model Predictions for the $Al_2O_3$–CaO-MgO, CaO–MgO–$SiO_2$ and $Al_2O_3$–MgO–$SiO_2$ Systems. ISIJ International 2006; 46: 368–374

41 Kondratiev A, Jak E. A Quasi-Chemical Viscosity Model for Fully Liquid Slags in the $Al_2O_3$-CaO-'FeO'-$SiO_2$ System. Metal Mater Trans B 2005; 36B:623-38

42 Ilyushechkin AY, Hla SS, Roberts DG, Kinaev NN. The effect of solids and phase compositions on viscosity behaviour and TCV of slags from Australian bituminous coals. Journal of Non-Crystalline Solids 2011; 357: 893–902

43 Oh MS, Brooker DB, de Paz EF, Brady JJ, Decker TR. Effect of crystalline phase formation on coal slag viscosity. Fuel Process Technol 1995; 44:191–199.

44 Tonmukayakul N, Nguyen QD. A new rheometer for direct of measurement of the flow properties of coal ash at high temperatures. Fuel 2002;81: 397–404.

## Appendix C: Viscometer designs

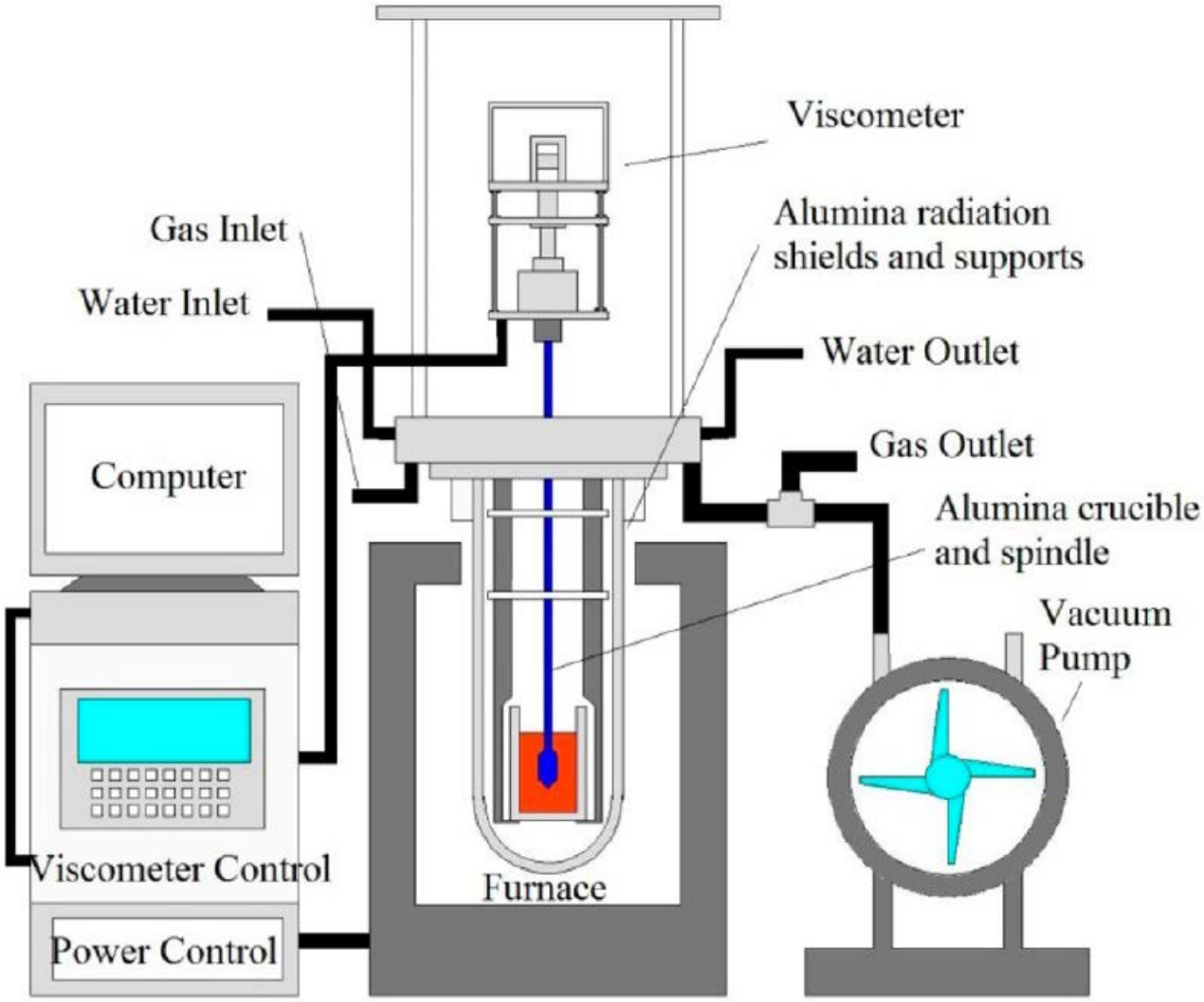


**Figure C1**: A schematic diagram of the viscosity measuring assembly Type: Rotation bob viscometer

[1]Shen Z, Liang Q, Zhang B, Xu J, and Liu H, Effect of Continuous Cooling on the Crystallization Process and Crystal Compositions of Iron-Rich Coal Slag. Energy Fuels 2015, 29, 3640−3648

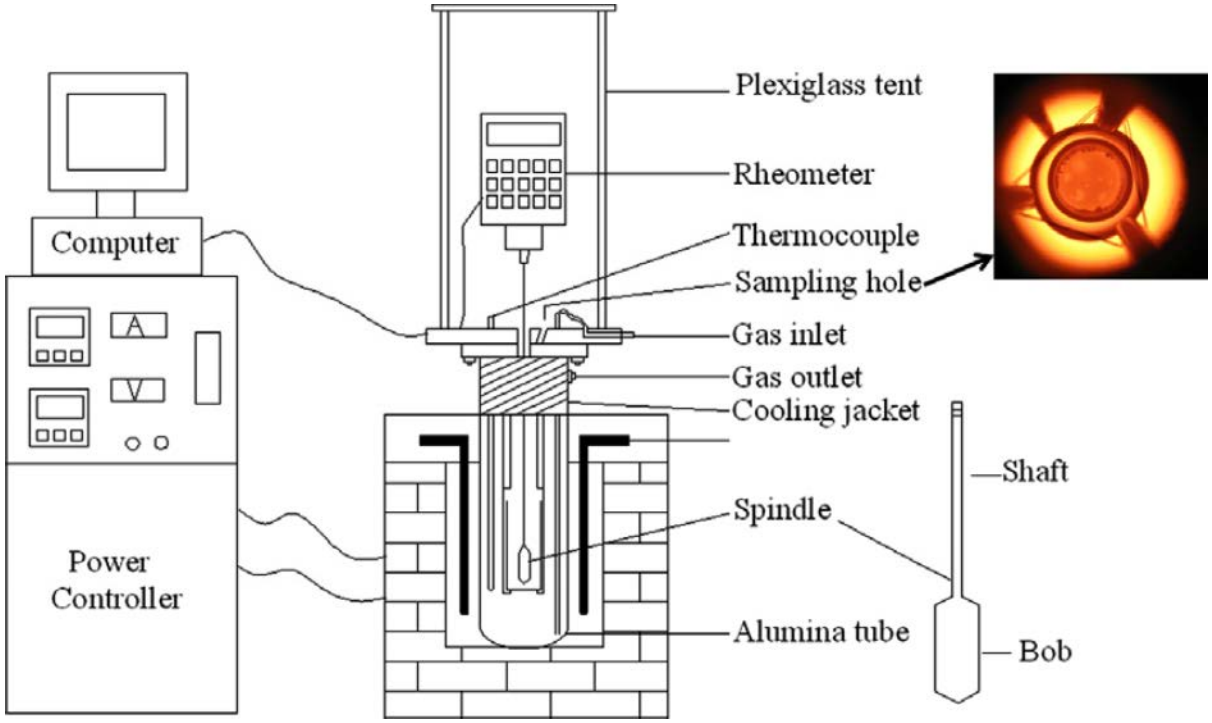


**Figure C2**: A schematic of the viscosity measuring assembly Type: Rotational bob viscometer
Viscometer: Brookfield Furnace Type: Not reported
Gas measurement: Not reported

[1] Song W, Tang L, Zhu X, Wu Y, Zhu Z, Koyama S. Flow properties and rheology of slag from coal gasification. Fuel 2010; 89: 1709 - 15

[2] Song W, Tang L, Zhu X, Wu Y, Rong Y, Zhu Z, Koyama S. Fusibility and flow properties of coal ash and slag. Fuel 2009; 88:297–304.

[3] Song W, Sun Y, Wu Y, Zhu Z, Koyama S. Measurement and Simulation of Flow Properties of Coal Ash Slag in Coal Gasification. AIChE Journal 2011; 57: 801-818.

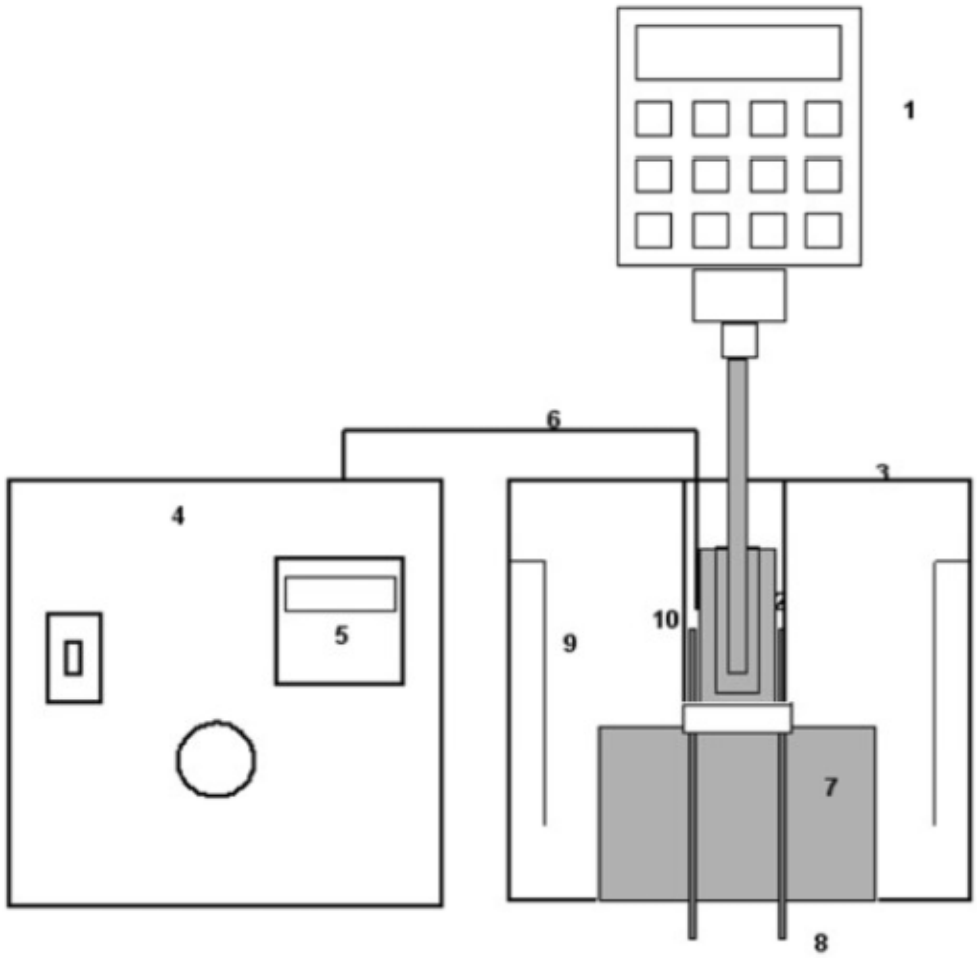


**Figure C3**: Fig1: A schematic of the viscosity measuring assembly

Type: Rotational bob Viscometer: (Brookfield HB-DVIII
Furnace: Lindberg blue/M furnace Gas measurement: Not reported

[1] Kim Y, Oh MS. Effect of cooling rate and alumina dissolution on the determination of temperature of the critical viscosity of molten slag. Fuel Processing Technology 2010; 91: 853–858

[2] Lim S, Oh MS. Prediction of coal slag foaming under gasification conditions by thermodynamic equilibrium calculations. Korean J. Chem. Eng. 2007; 24: 911-916

**Figure C4**: Viscosity measuring assembly

Product specification: Viscometer: Rotovisco RV20 Controller: Rheocontroller RC20
Furnace: ME 1700

[1] Vargas S, Frandsen FJ, Dam-Johansen K. Rheological properties of high-temperature melts of coal ashes and other silicates. Prog Energy Combust Sci 2001; 27: 237–429.

## Appendix D: Summary of viscometers used by different research group

In entrained flow gasifiers, ash in coals forms a molten slag under high temperature and flows down along the wall to the bottom of the gasifier, where it quenches and collects. To ensure a continuous flow and removal of slag, it is necessary to determine the viscosity of the coal slags as a function of the gasifier temperature. Slag viscosity measurement requires a specially designed high-temperature viscometer Most of the coal slag viscometers in the literature is rotational bob viscometer [1-7, 10-17], consist of the viscosity measuring head which is placed in the high-temperature furnace and is connected to a torque measuring device. A summary of the types viscometers used by different research group is given in table D1.

**Table D1**: Types of viscometer by different research group

| Research Group | Type | Viscometer | Furnace | Slag type | Temperature | Study |
|---|---|---|---|---|---|---|
| Oh et al (2010) | Rotational bob | Brookfield HB-DVIII | - | Synthetic slag: Alaskan Usibelli ash | 1600 | Effect of cooling rate and alumina dissolution on the determination of temperature of critical viscosity of molten slag [1] |
| Oh et al (1995) | Rotational bob | Haake Rotovisco RV-100 | heating elements (Kanthal Super ST), isolated by mullite tube | SUFCo (Hiawatha seam, bit coal), Pittsburgh No. 8 bituminous coal, 2 Powell Mountain coals | 1430 | Effect of crystalline phase formation on coal slag viscosity [2] |
| Oh et al (2005) | Rotational bob | Brookfield HB-DVIII | Lindberg blue/M furnace | synthetic Denisovsky (Russian sub-bituminous coal) slag | - | Prediction of coal slag foaming under gasification conditions by thermodynamic equilibrium calculations [3] |

| | | | | | | |
|---|---|---|---|---|---|---|
| Oh et al (1998) | Rotational bob | Haake Rotovisc o RV-100 | heating elements (Kanthal Super ST), isolated by mullite tube | SUFCo (Hiawatha seam, bit coal), Pittsburgh No. 8 bituminous coal, Synthetic | - | Gasification slag rheology and crystallization in titanium-rich, iron–calcium–aluminosilicate glasses [4] |
| Song et al (2010) | Rotational bob | Brookfield DV-III | Vertical-tube alumina furnace | Texaco gasifier slag: Shen Fu coal | 500-1550 | Flow properties and rheology of slag from coal gasification[5] |
| Song et al (2009) | Rotational bob | Brookfield DV-III | - | Laboratory ash and Shell gasifier slag (Chinese Huainan coal). | 1550 | Fusibility and flow properties of coal ash and slag [6] |
| Song et al (2011) | Rotational bob | Brookfield DV-III | - | 45 Chinese coal samples | 500-1570 | Measurement and Simulation of Flow Properties of Coal Ash Slag in Coal Gasification [7] |
| Tonmukayaku l et al (2002) | Cone and plate | | Vertical tube | - | 600-1300 | A new rheometer for direct measurement of flow properties of coal ash at high temperature. [8] |
| Buhre et al (2005) | TMA Rotational bob | Haake model 1700 | - | - | 2400 | Measurement of the Viscosity of Coal-Derived Slag Using Thermomechanical Analysis [9] |
| Hurst et al (1999) | Rotational bob | Haake model 1700 | - | Synthetic | 1300 | Viscosity measurements and empirical predictions for some model gasifier slags [10] |

| | | | | | | |
|---|---|---|---|---|---|---|
| Hurst et al (2001) | Rotational bob | Haake model 1700 | - | Synthetic | - | Comments on the use of molybdenum components for slag viscosity measurements [11] |

1. Kim Y, Oh MS. Effect of cooling rate and alumina dissolution on the determination of temperature of critical viscosity of molten slag. Fuel Processing Technology 2010; 91: 853–858
2. Oh MS, Brooker DB, de Paz EF, Brady JJ, Decker TR. Effect of crystalline phase formation on coal slag viscosity. Fuel Process Technol 1995; 44:191–199.
3. Lim S, Oh MS. Prediction of coal slag foaming under gasification conditions by thermodynamic equilibrium calculations. Korean J. Chem. Eng 2007; 24: 911-916
4. Groen JC, Brooker DD, Welch PJ, Oh MS. Gasification slag rheology and crystallization in titanium-rich, iron–calcium–aluminosilicate glasses. Fuel Process Technol 1998;56:103–27.
5. Song W, Tang L, Zhu X, Wu Y, Zhu Z, Koyama S. Flow properties and rheology of slag from coal gasification. Fuel 2010; 89: 1709 - 15
6. Song W, Tang L, Zhu X, Wu Y, Rong Y, Zhu Z, Koyama S. Fusibility and flow properties of coal ash and slag. Fuel 2009; 88:297–304.
7. Song W, Sun Y, Wu Y, Zhu Z, Koyama S. Measurement and Simulation of Flow Properties of Coal Ash Slag in Coal Gasification. AIChE Journal 2011; 57: 801-818
8. Tonmukayakul N, Nguyen QD. A new rheometer for direct of measurement of the flow properties of coal ash at high temperatures. Fuel 2002;81: 397–404.
9. Buhre BJP, Browning GJ, Gupta RP, Wall TF. Measurement of the viscosity of coal-derived slag using thermomechanical analysis. Energy Fuel 2005; 19: 1078–83.
10. Hurst HJ, Novak F, Patterson JH. Viscosity measurements and empirical predictions for some model gasifier slags. Fuel 1999; 78: 439–44.
11. French D, Hurst HJ, Marvig P. Comments on the use of molybdenum components for slag viscosity measurements. Fuel Processing Technology 2001; 72: 215–225